

Hydrological responses of critical aquatic habitat in Wood Buffalo National Park for the world's only naturally reproducing migratory population of whooping crane to past climate variation

by

Laura Anderson

A thesis
presented to the University of Waterloo
in fulfilment of the
thesis requirement for the degree of
Master of Science
in
Biology

Waterloo, Ontario, Canada, 2025

© Laura Anderson 2025

Author's Declaration

I hereby declare that I am the sole author of this thesis. This is a true copy of the thesis, including any required final revisions, as accepted by my examiners.

I understand that my thesis may be made electronically available to the public.

Abstract

The only wild, self-sustaining population of endangered whooping crane (*Grus americana*) breeds within a remote, pond-rich, groundwater discharge region in and adjacent to Wood Buffalo National Park where there is concern for habitat degradation by climate change. Due to their small area and volume, shallow ponds respond rapidly to changes in climate and are vulnerable to desiccation, which can reduce breeding success by altering food availability and encounters with predators. Hydrological information is scant in this remote region, and longer time-series of data are needed to anticipate how shallow water breeding habitat will respond to future climate warming. Here, contemporary measurements (2022-2023) at three shallow ponds that range from weakly to strongly connected to groundwater are integrated with paleolimnological analyses, which span the past ~300-400 years and capture the cold, arid Little Ice Age and subsequent warming, to improve understanding of hydrological responses to climate variation. Correspondence of pond water $\delta^{18}\text{O}$ inferred from sediment carbonate (carbonate-inferred $\delta^{18}\text{O}_{\text{pw}}$) with contemporary measurements of pond water $\delta^{18}\text{O}$ indicates that carbonate-inferred $\delta^{18}\text{O}_{\text{pw}}$ provides a reliable methodology to reconstruct past variation in pond water $\delta^{18}\text{O}$. Evidence suggests two of the three ponds desiccated during the mid- and late 1700s when the climate of the Little Ice Age was arid. At pond SK 31, where connectivity to groundwater is weak, carbonate-inferred $\delta^{18}\text{O}_{\text{pw}}$ increased during this interval and exceeded the contemporary estimate of the terminal basin steady-state isotope composition, indicating strongly negative water balance prevailed due to evaporation. Similar strong net evaporation and near-desiccation has been detected during the same time interval from a record of cellulose-inferred lake water $\delta^{18}\text{O}$ at a shallow upland lake located ~175 km to the south (Wolfe et al., 2005), which provides confidence in the interpretations based on carbonate-inferred $\delta^{18}\text{O}_{\text{pw}}$ at SK 31. At pond SK 58, where connectivity to groundwater is strong but desiccation occurred in 2023 and 2024 likely by vertical seepage, the stratigraphic record of carbonate-inferred $\delta^{18}\text{O}_{\text{pw}}$ reveals no evidence of enrichment by evaporation during the mid- and late 1700s. A distinctive peak in C/N ratios in sediment deposited ~1790 suggests, however, that an apparently rare desiccation, or near-desiccation, event may have occurred by vertical seepage when SK 31 and PAD 5 also nearly desiccated by evaporation. Smaller C/N-ratio peaks in ~1908 and ~1998 may capture two other short-lived near-desiccation events at SK 58. Recent observed desiccation at SK 58 in 2023-2024 occurred when unusually arid climate conditions resulted in a decline in water level of 60 cm in Great Slave Lake

to the lowest levels recorded by the 84-year-long record. At pond SK 26, low carbonate-inferred $\delta^{18}\text{O}_{\text{pw}}$ values throughout the ~280-year record provide no evidence of drawdown by evaporation and suggest there may have been shifting sources and discharge of groundwater, which may be indicative of the spatial and temporal variability of past hydrological conditions across this complex landscape. Overall, pond desiccation, including the recent drying of SK 58, appears to be a largely rare occurrence since 1800 but may become increasingly common with ongoing climate change.

Acknowledgements

Dr. Brent Wolfe and Dr. Roland Hall, thank you for your guidance, motivation and support you have given me throughout my degree. Through the countless opportunities, including sending me to conferences and to the field, you have helped bring me out of my comfort zone and provided me with a wealth of experience.

Dr. Rebecca Rooney and Dr. Kirsten Muller, thank you for all the thoughtful commentary and guidance you have provided for this project. Your contributions have helped strengthen this thesis and challenged me to delve deeper in producing a better final result.

Laura Neary, without you this project would not have been the same, thank you for paving the way for the whooping crane projects and for such a memorable time in the field. Your enthusiasm and devotion to your work is inspiring.

Johan Wiklund, thank you for teaching me how to collect sediment cores from the pontoon of a helicopter, a unique experience I will never forget. And thank you for your hard work dating all the sediment cores.

Sheridan Hill, thank you for all your hard work in the lab and in the field, you have contributed greatly to this project. Your kindness and generosity have been missed in the lab.

Eva Wolfe, thank you for dedicating countless hard-working hours producing valuable data for this project.

Amy Lacey, thank you for all your help in and out of the field and for always being willing to grab a coffee and chat.

Arisha Imran, thank you for your kindness and support, your leadership and determination inspires me.

Meredith Watson, thank you for being a great office mate and for always letting me distract you, I am so glad to have started my master's alongside you.

Mitch Kay, thank you for always being willing to chat and always being available to answers my questions.

Alicia Pouw, thank you for always being a source of support and for letting me crash with you and Dakota during my travels to and from the field.

Emma and Josh, thank you for always being a phone call away, I know you'd be on the next plane over if I needed you.

Katie, thank you for always being so willing to help, whatever the problem may be, I know you do everything you can to help me solve it.

Mom and dad thank you for always standing by me, and for always supporting and encouraging me in pursuing my goals.

Iain Thomson, thank you for your unwavering love and support every step of the way, and for always being there with a listening ear and helping hand.

Table of Contents

Author’s Declaration.....	ii
Abstract.....	iii
Acknowledgements.....	v
List of Figures.....	ix
List of Tables.....	xi
Chapter 1: Introduction.....	1
Chapter 2: Methods.....	5
Site selection.....	5
Fieldwork.....	8
Laboratory analysis.....	9
Contemporary hydrological measurements.....	9
Water isotope composition.....	9
Water depth variation.....	9
Paleolimnological analyses.....	10
Radiometric dating.....	10
Loss-on-ignition.....	10
Carbonate oxygen isotope composition.....	11
Organic carbon and nitrogen elemental content and isotope composition.....	12
Chapter 3: Results and Discussion.....	13
Contemporary hydrology.....	13
Paleolimnological results.....	15
Do the ponds contain datable stratigraphic records?.....	15
Does $\delta^{18}\text{O}_{\text{carb}}$ provide a means to reconstruct $\delta^{18}\text{O}_{\text{pw}}$?.....	18
What do stratigraphic records of carbonate-inferred $\delta^{18}\text{O}_{\text{pw}}$ reveal about past changes in pond hydrology?.....	19
Is there evidence of prior desiccation via vertical seepage at SK 58 based on paleolimnological measurement of the C/N ratio?.....	24
How unusual were the meteorological conditions that led to the rare 2023-2024 desiccation event at SK 58?.....	26
Chapter 4: Conclusions and Recommendations.....	30
Conclusions.....	30

Recommendations	31
References	34
Appendices.....	46
Appendix A – Contemporary water isotope compositions.....	46
Appendix B – Radiometric dating of sediment cores	47
Appendix C – Sediment core loss-on-ignition	57
Appendix D – Standard Operating Procedure (SOP).....	64
Appendix E – Sediment core carbonate isotope composition.....	69
Appendix F – Sediment core organic carbon and nitrogen elemental and isotope composition	74
Appendix G – Sediment core dominant diatom species enumeration	76

List of Figures

- Figure 1. Map of the Sass and Klewi Nesting Areas (SKNA; light green) located within the Whooping Crane Summer Range. Among the 63 seasonally sampled ponds (black-filled circles), sediment cores were collected from six ponds in September 2022 (labelled). Ponds SK 26, SK 31 and SK 58 are the focus of this project. Inset map shows the location of the SKNA (light green) within WBNP (dark green). Map created by Laura Neary..... 6
- Figure 2. Scatterplot showing the water isotope composition ($\delta^2\text{H}$, $\delta^{18}\text{O}$) of 63 ponds (grey, red) measured in August 2022 in relation to the Local Meteoric Water Line (LMWL) derived from measured isotope composition in precipitation collected at Fort Smith (NT) during 1960-1969 ($\delta^2\text{H} = 6.7 \delta^{18}\text{O} - 19.2$) by the Global Network for Isotopes in Precipitation (IAEA/WMO n.d.). The predicted Local Evaporation Line (LEL) represents the expected trajectory of isotope composition in a waterbody fed by local amount-weighted mean annual isotope composition of precipitation (δ_p) as it undergoes evaporation (from Neary, 2025). The LEL extends to δ^* , the limiting isotope composition of a desiccating waterbody, and δ_{SSL} represents the isotope composition of a terminal waterbody when evaporation is equal to inflow. Ponds SK 26, SK 31 and SK 58 (red) span much of the range of water isotope composition captured by the 63 ponds..... 7
- Figure 3. Aerial photos of ponds where the sediment cores analyzed in this study were obtained. The photos were taken in September 2022. 8
- Figure 4. Scatterplots showing seasonal variation of water isotope composition at ponds SK 31, SK 26 and SK 58 in May, August, and September 2022 and May 2023 in relation to the Local Evaporation Line (LEL) and the Local Meteoric Water Line (LMWL) (as also reported in Figure 2). SK 31 is weakly connected to groundwater while SK 26 and SK 58 are classified as strongly connected to groundwater (Neary, 2025)..... 13
- Figure 5. Time series of hourly water depth measurements from ponds SK 31, SK 26, and SK 58 during the open water seasons (June 1 – September 15) of 2022 (light blue line) and 2023 (dark blue line). Aerial photos are presented at each pond in summer 2022 and spring 2024. The percent values identify the water-level drawdown relative to the starting depths recorded on June 1, 2022 and June 1, 2023. 14
- Figure 6. Stratigraphic variation of radioisotope activities (total ^{210}Pb (red line), ^{226}Ra (blue line), and ^{137}Cs (purple line)) and modelled age-depth relations (black, grey) and associated errors bars (± 2 standard deviation units) in sediment cores from ponds SK 31, SK 26 and SK 58. The grey data points represent sediment ages that were extrapolated below the depth of supported ^{210}Pb activity. Temporal variation of dry mass sedimentation rates of SK 31, SK 26 and SK 58 is shown in the second row of graphs. 16
- Figure 7. Stratigraphic variation in $\delta^{18}\text{O}_{\text{pw}}$ inferred from sediment carbonate $\delta^{18}\text{O}$ (using Equation 2 and pond water temperature values from Table 1) at ponds SK 31, SK 26 and SK 58. Results are shown as individual measurements (grey points and dashed line) and as a 3-point running mean (solid black line). Estimates of uncertainty are based on temperature variation of $\pm 5^\circ\text{C}$ are shown

for individual measurements (grey ribbon). Also shown are $\delta^{18}\text{O}_{\text{pw}}$ values measured in water obtained in August 2022 (red filled circles) and $\delta^{18}\text{O}_{\text{pw}}$ inferred from carbonate $\delta^{18}\text{O}$ extracted from surface sediment collected in May 2024 (light blue filled circles). Contemporary estimates of δ_{SSL} (vertical blue dashed line) and δ^* (vertical red dashed line) are shown for reference (values are from Neary, 2025). 20

Figure 8. Temporal variation of paleolimnological measurements at pond SK 58, including carbonate-inferred $\delta^{18}\text{O}_{\text{pw}}$ (individual values and three-point running mean), organic carbon to nitrogen (C/N) ratios, and dry mass sedimentation rate (± 1 standard deviation). Carbonate-inferred $\delta^{18}\text{O}_{\text{pw}}$ for SK 58 is shown in reference to contemporary estimates of δ_{SSL} (blue dashed line) and δ^* (red dashed line) (from Neary, 2025). Also shown, for comparison, is the carbonate-inferred $\delta^{18}\text{O}_{\text{pw}}$ for SK 31 and the cellulose-inferred lake water $\delta^{18}\text{O}$ record for PAD 5, a shallow upland lake in the Peace-Athabasca Delta, located ~ 175 km south of SK 58 (Wolfe et al., 2005). A distinctive peak in the C/N ratio, possibly reflecting increased deposition of terrestrial organic matter, occurs at ~ 1793 CE (C/N = 13.2), and smaller peaks are evident at ~ 1906 CE (11.3) and ~ 1998 CE (10.7) (identified with an asterisk). 25

Figure 9. Cumulative precipitation (mm) during the hydrologic year (Oct 1 – Sep 30; upper graph) and open water season (May 1 – Sep 30; lower graph) for 2022 (yellow line), 2023 (red line) and 2024 (blue line) at Fort Smith (Climate station ID: 2202200 (1990-2014); 2202202 (2015-2024)). One standard deviation unit is applied to mean cumulative precipitation (black line) spanning the 30-year climate normal period (1991-2020) to display the range of normal variation (grey ribbon). The maximum and minimum cumulative precipitation spanning the 30-year climate normal period (1991-2020) is shown as reference of extreme variation (light grey ribbon). 27

Figure 10. Hourly lake water level measurements (in masl) from Great Slave Lake at Yellowknife Bay (NT) spanning 2022 (yellow solid line) and 2023 (red solid line). Standard deviation of daily average water level for the 84-year record (1938-2022) is shown for reference as a range of normal variation (dark grey ribbon). Maximum and minimum water level spanning the 84-year record (1938-2022) is shown for reference as a range of extreme variation (light grey ribbon). Daily water level data for Great Slave Lake at Yellowknife Bay (07SB001) was accessed from https://wateroffice.ec.gc.ca/mainmenu/real_time_data_index_e.html on May 9, 2025. 29

List of Tables

Table 1. Carbonate-inferred $\delta^{18}\text{O}_{\text{pw}}$ (derived using Equation 2) from the uppermost sediments of cores obtained from SK 31, SK 26 and SK 58 in comparison to $\delta^{18}\text{O}_{\text{pw}}$ measured directly from pond water obtained in August 2022. Pond water temperature is an average of hourly measurements between June 1 and September 15, 2022.	19
Table 2. Ponds recommended for paleolimnological study based on observations of desiccation during 2023 and spring 2024 (Neary, 2025). Ponds that desiccated during 2023-2024 were also observed to be desiccated in August 2025 (Arisha Imran, personal communication 2025). Also included are ponds where sediment cores were collected during September 2022 but have not been analyzed for carbonate-inferred $\delta^{18}\text{O}_{\text{pw}}$ (SK 15, SK 43, SK 51).	33

Chapter 1: Introduction

A remote wetland-rich region spanning northern Alberta and southern Northwest Territories supports critical breeding habitat for the last remaining self-sustaining, migratory population (Aransas-Wood Buffalo) of whooping crane (*Grus americana*). Whooping crane is North America's tallest bird and amongst the rarest, and it has been on the endangered species list for decades since reaching near-extinction in the 1940s when just 16 individuals remained due to overhunting and habitat loss (Chavez-Ramirez and Wehtje, 2012). Whooping cranes remain vulnerable to extinction because of their small population size, slow reproductive rate (mating pairs typically rear a single chick per year; Boyce et al., 2005), limited distribution, and 4,000-km-long migration between winter habitat in Texas and summer breeding area in and adjacent to Wood Buffalo National Park (WBNP) (Timoney et al., 1997; Chavez-Ramirez and Wehtje, 2012). Their breeding habitat is listed as a Ramsar Wetland of International Importance (Ramsar site 240 – Whooping Crane Summer Range (WCSR)), and about 80% of it is protected within WBNP. Abundant wetland breeding habitat within the karst terrane of the WCSR contributes to WBNP's designation as a UNESCO World Heritage site. In 2014, Mikisew Cree First Nations (MCFN) petitioned UNESCO for WBNP to become listed as "World Heritage in Danger", in part because of concern for the vulnerability of whooping crane habitat to climate change (MCFN, 2014). In response, a report from the WHC/IUCN Reactive Monitoring Mission listed 17 recommendations to avoid a downgrade in status and maintain the ecological integrity of the park. Recommendation #16 advocates for continued monitoring of "the entire used and potential nesting area of the whooping crane within the Greater WBNP Ecosystem so as to be able to respond to possibly changing management requirements" (WHC/IUCN, 2017; pg. 5).

Whooping cranes are highly dependent on shallow (typically <50 cm) wetland habitat (open-water wetlands (hereafter referred to as ponds) and emergent marshes with open water and adjacent shrubby fen) where they obtain preferred food (e.g., aquatic invertebrates, amphibians) and nest material (e.g., bullrush). The cranes build their nests near the shorelines where they benefit from long sight lines for predator detection (Chavez-Ramirez and Wehtje, 2012; Timoney et al., 1997; Timoney, 1999). Despite conservation successes, which have assisted growth of the Aransas-Wood Buffalo population to about 500 individuals, climate-driven changes to water levels remain a threat

to their reproductive success (Kuyt et al., 1992; Timoney et al., 1997; Timoney, 1999). Rise of water levels can inundate the nests and drown fledglings, whereas decline of water levels may increase access to nests by predators, leading to increased mortality of eggs and fledglings. Indirectly, there is also evidence that changes in water levels alter the abundance of aquatic invertebrates and vertebrates that form their diet (Kuyt and Barrie, 1992; Timoney, 1999). Studies by Timoney et al. (1997) and Timoney (1999) revealed that pond water levels fluctuate annually, with maxima after the freshet and minima in late summer, and that some ponds may dry up completely by late summer. Hydrological investigations by McNaughton (1991) at nine ponds in the Sass and Klewi Nesting Areas (SKNA) of the WCSR, where known breeding has occurred for the longest duration and nest density is greatest (Allen, 1956; Kuyt, 1981, 1993; Timoney, 1999), document that the ponds occupy areas of groundwater discharge in the karst terrane but groundwater discharge was insufficient to maintain pond water levels during years with low rainfall. Water isotope and chemistry measurements at six ponds in the Nyarling area of the WCSR by Déri-Takács et al. (2022) identified influence of groundwater that interacts with gypsum-rich substrate of the Muskeg Formation. Most recently, integrated measurements of water isotope composition, depth and chemistry by Neary (2025) at 63 well dispersed ponds and wetlands across the SKNA in 2022, when above-average snowpack was followed by below-average rainfall, revealed that peak pond water levels occurred in the spring due to input of snowmelt runoff. Spatial variability of the measurements increased during summer and fall as influence of groundwater waned and influence of evaporation on water isotope composition increased at some, but not all, of the waterbodies. Using geospatial interpolation of a multi-metric ‘Vulnerability Index’, Neary (2025) revealed that whooping crane nest locations in 2022 cluster within areas where waterbodies retained strong connectivity to groundwater and risk of desiccation is lower. While the above studies were instructive to elucidate important hydrological processes that operate at seasonal time scales, there is no knowledge of how pond hydrology responds to longer-term climate variation (e.g., decades to centuries). Such knowledge would, however, help anticipate responses of critical whooping crane breeding habitat to ongoing climate change and variability.

Paleolimnological analyses of sediment cores provide longer time series of measurements than can typically be generated by contemporary studies and may provide important insights into the hydrological responses of the shallow waterbodies to changes in climate (Smol et al., 2001; Cohen, 2003; Smol, 2008, 2010). Here, contemporary measurements of water isotope composition

(seasonal) and depth (hourly) during open-water seasons of 2022-2023 from three ponds within SKNA that range from weakly to strongly connected to groundwater are integrated with paleolimnological analyses to improve understanding of hydrological responses to climate variation. The paleolimnological records span the past ~300-400 years and capture the cold, arid Little Ice Age and subsequent warming. Oxygen isotope composition in water and components of sediment can be used to track changes over time in hydrological processes which influence pond water balance and depth, such as input by groundwater or precipitation and loss via evaporation (e.g. Wolfe et al., 2005; Li et al., 2020; Zabel et al., 2022; Wagner et al., 2025). A focus of this study is measurement of the oxygen isotope composition of carbonate (carbonate $\delta^{18}\text{O}$) in the sediment. Carbonate $\delta^{18}\text{O}$ can be used to infer past changes in oxygen isotope composition of pond water if the carbonate has precipitated in the water column and water temperature can be constrained (Kim and O'Neil, 1997; Leng and Marshall, 2004; Li et al., 2020; Wagner et al., 2025). Some shallow ponds in SKNA may be prone to desiccation (Timoney et al., 1997; Neary, 2025), which may cause a hiatus of sediment deposition and complicate inferences derived from stratigraphic analyses of paleolimnological measurements, including radiometric dating of sediment cores. Thus, contemporary water isotope measurements obtained in August 2022 were used to select three ponds for paleolimnological investigation that span a range of connectivity to groundwater and, hence, vulnerability to desiccation. Due to the possibility that the sediment cores captured past intervals of pond desiccation, this study addresses whether the stratigraphic records are datable by ^{210}Pb methods (Objective 1). Also, assumptions are tested that the carbonate is endogenic (i.e., precipitated directly from the water column), and that the carbonate $\delta^{18}\text{O}$ and an estimate of water temperature can be used to reasonably estimate pond water $\delta^{18}\text{O}$ (Objective 2). To do this, the carbonate-inferred pond-water oxygen isotope composition in surface sediment obtained in 2022, constrained by measurements of water temperature, is compared to the oxygen isotope composition of pond water measured in summer of 2022. Then, stratigraphic records of carbonate-inferred pond-water $\delta^{18}\text{O}$ at each pond are evaluated and compared among the ponds to reconstruct past changes in hydrological processes influencing pond water balance (Objective 3). Observation in 2024 that one of the three ponds desiccated after two successive arid summers likely by vertical seepage, a process of water loss that does not fractionate water isotopes, prompted assessment of additional paleolimnological measurements (i.e., carbon-to-nitrogen ratios) on the core from that pond to determine the frequency of episodes of desiccation by vertical

seepage during the past ~350 years (Objective 4). The knowledge gained from this research is intended to help anticipate how future climate change may influence shallow waterbodies in the critical nesting habitat used by Aransas-Wood Buffalo whooping crane and inform ongoing monitoring efforts addressing Recommendation #16 from the WHC/IUCN Reactive Monitoring Mission.

Chapter 2: Methods

Site selection

The WCSR spans from northern Alberta to just south of Great Slave Lake in NWT where six pond- and wetland-rich nesting areas have been identified (Lobstick, Alberta, Sass, Klewi, Nyarling and North Nyarling) in north-central Wood Buffalo National Park (WBNP) (Environment Canada, 2007). In these areas, the whooping cranes build nests, lay eggs, and raise fledglings. Seasonal measurements of water isotope composition and chemistry (May, August, September) and hourly measurements of water depth were obtained in 2022 from 63 well-dispersed ponds (one per 3x3-km grid cell) across SKNA (Figure 1; Neary, 2025). The ponds were placed into three categories of groundwater connectivity defined based on isotope mass-balance modelling of evaporation-to-inflow (E/I) ratios. Ponds with E/I ratio <0.5 in August 2022 were classified as strongly connected to groundwater; ponds with E/I ratio >1 in September 2022 were classified as weakly connected to groundwater; and ponds that did not place into either category were classified as moderately connected to groundwater. Neary (2025) demonstrated that water levels drew down in all three categories, but the drawdown was less in the waterbodies with strong (median = 23.3% of initial depth) versus weak (median = 43.8%) connectivity to groundwater. The ponds with weak connectivity lost water mainly by evaporation, whereas the ponds with strong connectivity lost water mainly by vertical seepage. Vertical seepage occurs when the water table drops enough to allow water to seep out of the sides and bottom of ponds due to insufficient recharge of groundwater from precipitation.

Based on water isotope and depth measurements in August 2022, six of the ponds were selected for sediment core collection (SK 15, SK 26, SK 31, SK 51, SK 58, SK 43; Figure 1) and three of these ponds (SK 31, SK 26, SK 58; Figure 1) were selected for paleolimnological analysis. These ponds were selected because they span the range of water isotope composition (Figure 2) and their water depth exceeded 0.5 m in June 2022, which reduces risk of prior desiccation. SK 31 (September 2022 E/I ratio = 1.49) was categorized as weakly connected to groundwater by Neary (2025), whereas SK 26 (August 2022 E/I ratio = 0.22) and SK 58 (August 2022 E/I ratio = 0.33) were categorized as strongly connected. SK 31 was 0.84 m deep in June 2022 and had relatively high water isotope composition, close to δ_{SSL} (the isotope composition of a terminal waterbody when evaporation is equal to inflow), due to enrichment by evaporative water loss, suggesting its

water levels may be strongly responsive to variation over time in precipitation and evaporation. This feature, however, may predispose SK 31 to desiccation during arid intervals, which could result in discontinuous sedimentation and an incomplete stratigraphic record with poor chronological control. In contrast, SK 26 (0.82 m deep) and SK 58 (0.58 m deep) had relatively low water isotope compositions in August 2022, reflecting strong influence of inflow of isotopically depleted groundwater (Neary, 2025) that offset enrichment by evaporation. As a consequence, they may be less prone to desiccation than SK 31, which increases the probability of obtaining continuous, datable sediment records.

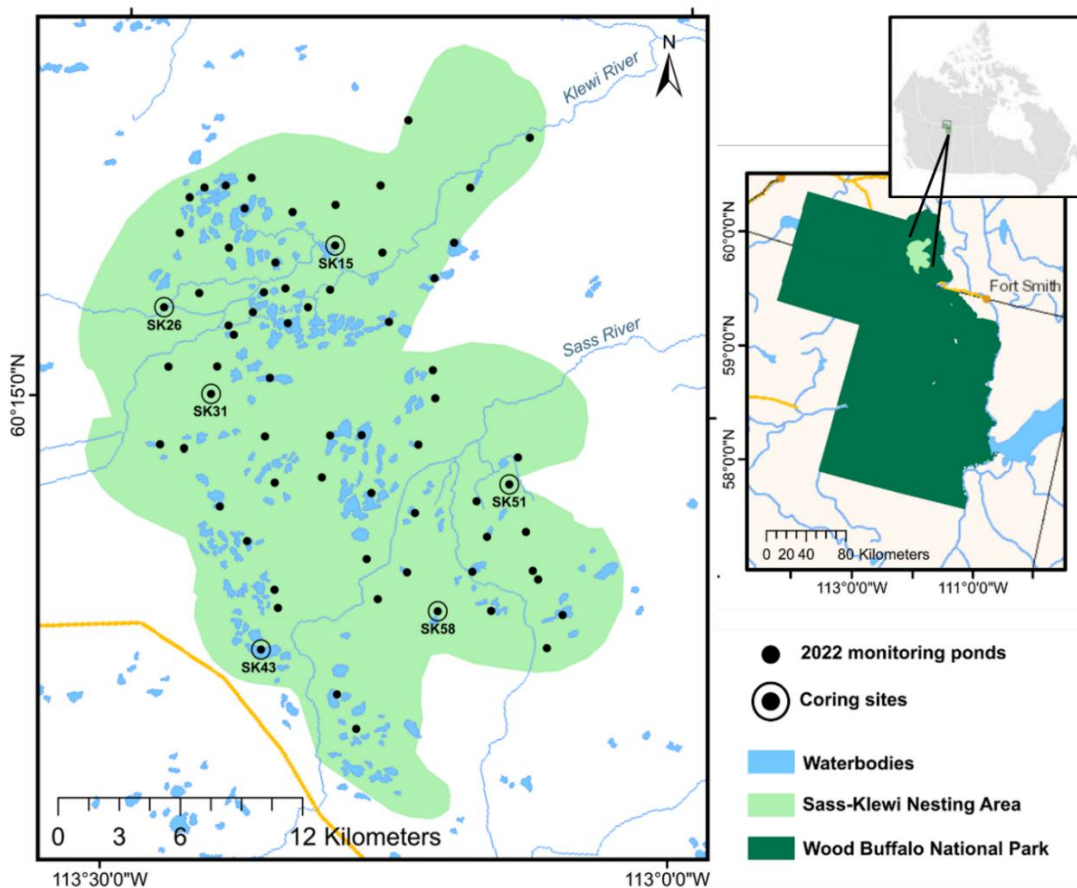


Figure 1. Map of the Sass and Klewi Nesting Areas (SKNA; light green) located within the Whooping Crane Summer Range. Among the 63 seasonally sampled ponds (black-filled circles), sediment cores were collected from six ponds in September 2022 (labelled). Ponds SK 26, SK 31 and SK 58 are the focus of this project. Inset map shows the location of the SKNA (light green) within WBNP (dark green). Map created by Laura Neary.

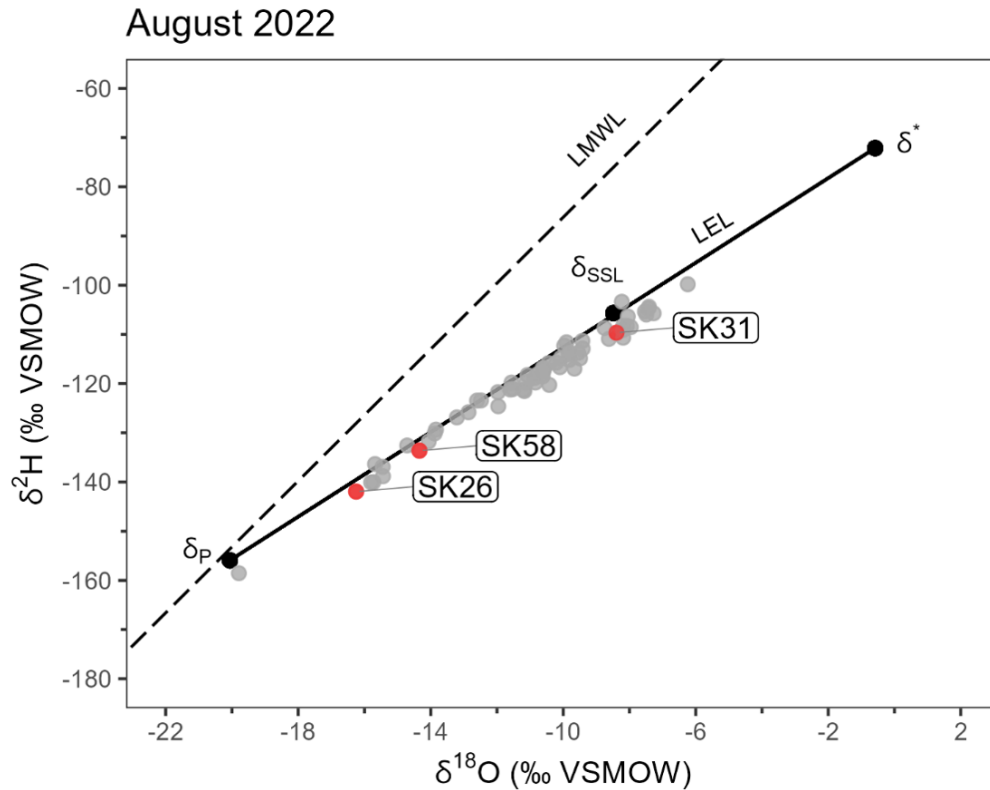


Figure 2. Scatterplot showing the water isotope composition ($\delta^2\text{H}$, $\delta^{18}\text{O}$) of 63 ponds (grey, red) measured in August 2022 in relation to the Local Meteoric Water Line (LMWL) derived from measured isotope composition in precipitation collected at Fort Smith (NT) during 1960-1969 ($\delta^2\text{H} = 6.7 \delta^{18}\text{O} - 19.2$) by the Global Network for Isotopes in Precipitation (IAEA/WMO n.d.). The predicted Local Evaporation Line (LEL) represents the expected trajectory of isotope composition in a waterbody fed by local amount-weighted mean annual isotope composition of precipitation (δ_{P}) as it undergoes evaporation (from Neary, 2025). The LEL extends to δ^* , the limiting isotope composition of a desiccating waterbody, and δ_{SSL} represents the isotope composition of a terminal waterbody when evaporation is equal to inflow. Ponds SK 26, SK 31 and SK 58 (red) span much of the range of water isotope composition captured by the 63 ponds.

The three ponds selected for paleolimnological analyses span the latitudinal range of SKNA (Figure 1), and they possess some unique morphological features (Figure 3). SK 26, the northernmost pond, is located north of Klewi River. Its water-saturated catchment supports dwarf shrubs and discontinuous forest. The catchment of SK 31, located south of Klewi River (Figure 1), supports dense growth of trees and shrubs. In August and September 2022, exposed shoreline

and desiccated small, hydrologically connected adjacent basins provide evidence of recent water-level drawdown. SK 58, the southernmost pond, is located south of Sass River. Its catchment has a well-defined border of large, mature trees, and emergent vegetation occurs within the central region of the pond. The trees likely identify the shoreline when former water levels were highest, whereas the emergent plants standing in water likely reflect their encroachment into the basin when water levels were lower in recent years compared to summer of 2022.



Figure 3. Aerial photos of ponds where the sediment cores analyzed in this study were obtained. The photos were taken in September 2022.

Fieldwork

Spatial surveys of 63 ponds were conducted in May (spring), August (summer) and September (fall) of 2022, and the results are reported in Neary (2025). A survey was also conducted in spring 2023, but sampling campaigns in summer and fall 2023 were cancelled due to nearby extensive wildfires. Seasonal sampling resumed in 2024. Data loggers (Onset HOBO pressure transducers; Model U20–001–01, 4-m range, 0.3-cm accuracy) were deployed at each pond in the spring (recording began June 1) and collected in the fall (September 15) of 2022. In 2023, loggers were deployed in spring (recording began June 1) and remained in the ponds during the next winter until collection in spring 2024 (May 24-26). The loggers recorded hourly measurements of temperature and pressure. Loggers were attached to the base of a rope connecting an anchor (rock-filled sock) to a wooden float and deployed at the sediment-water interface in a central region of each pond. One 30 ml water sample was collected at a depth of ~10 cm from each pond for measurement of water isotope composition on May 28-29, August 9-10, and September 15-17 in 2022 and May 23-24 in 2023.

Sediment cores were collected from a central location of ponds SK 26, SK 31 and SK 58 on September 16 and 17, 2022, using a hammer-assisted gravity corer (Telford et al., 2021) operated from the pontoon of a helicopter. Within 24 hours of collection, sediment cores were sectioned vertically into 0.5-cm intervals, individually sealed in Whirl-Pak bags, and stored in a refrigerator until further analyses. Two cores were collected from SK 26 and SK 31, and the longer core was designated as the primary core for analysis. A single core was collected from SK 58. Sediment cores were collected at pond depths of ~0.40 m, ~0.38 m, and ~0.22 m at SK 26, SK 31 and SK 58, respectively. Primary (and secondary) core lengths are 70.5 cm (51.0 cm) at SK 26, 77.0 cm (68.5 cm) at SK 31, and 32 cm at SK 58. Recently deposited surface sediments (uppermost ~1 cm) were collected from a central deepwater region of SK 26, SK 31 and SK 58 on May 27 and 28, 2024, using a Mini-Glew gravity corer (Glew, 1991).

Laboratory analysis

Contemporary hydrological measurements

Water isotope composition

Water samples were analyzed for water isotope composition at the University of Waterloo – Environmental Isotope Laboratory (UW-EIL) using a Los Gatos Research Liquid Water Isotope Analyser (model T-LWIA-45-EP). Samples were run in duplicates at a minimum of every tenth sample and a suite of water standards (Vienna Standard Mean Ocean Water (VSMOW), Standard Light Antarctic Precipitation (SLAP)) from the International Atomic Energy Agency (IAEA) were used as reference materials. Isotope compositions were reported as $\delta^{18}\text{O}$ (‰ VSMOW ± 0.2 ‰) and $\delta^2\text{H}$ (‰ VSMOW ± 0.8 ‰), where $\delta_{\text{Sample}} = [(R_{\text{sample}}/R_{\text{VSMOW}}) - 1]$, and R is the sample and VSMOW ratio of $^{18}\text{O}/^{16}\text{O}$ or $^2\text{H}/^1\text{H}$. Results of $\delta^{18}\text{O}$ and $\delta^2\text{H}$ are normalized to -55.5 ‰ and -428 ‰, respectively, for SLAP (Coplen, 1996). Data from this analysis are reported in Tables A1-A3 of Appendix A.

Water depth variation

Water depth was calculated from hourly measurements of absolute pressure (psi) and temperature recorded by the data loggers in each pond and measurements of air pressure and temperature by a logger suspended in the air in Fort Smith (NT), using the Barometric Compensation Assistant in HOBOWare Pro software. The water depth measurements spanning the 2022 open water season are from Neary (2025). For each year (2022, 2023), the magnitude of

drawdown at each pond between June 1 and September 15 is expressed as a year-specific percentage of the initial water depth recorded on June 1st.

Paleolimnological analyses

Radiometric dating

Age-depth relations of the sediment cores were determined using ^{210}Pb and ^{137}Cs methodologies (Appleby and Oldfield, 1978; Appleby, 2001). For cores from all three ponds, subsamples of sediment were taken from each well-mixed 0.5-cm interval through the upper 15 cm, from every second 0.5-cm interval between 16 and 20 cm, and every fourth 0.5-cm interval below 20 cm. For each sample, a measured mass of freeze-dried sediment was tightly packed into pre-weighed polycarbonate tubes up to an approximate height of 3.5 cm. The sediment was sealed with a silicone septum and 1 cm² of epoxy resin and left undisturbed for a minimum of 21 days to allow for equilibration of parent (^{222}Rn) and daughter (^{226}Ra) radioisotopes. An Ortec HPGe Digital Gamma Ray Spectrometer and Maestro 32 software were used to measure activity of radioisotopes ^{210}Pb , ^{226}Ra (via the weighted mean of daughter radioisotopes ^{214}Pb and ^{214}Bi) and ^{137}Cs . ^{226}Ra , the parent isotope of ^{210}Pb , was used to determine supported ^{210}Pb activity, while unsupported ^{210}Pb activity (i.e., excess ^{210}Pb derived from the decay of atmospheric ^{222}Rn), was determined by subtracting supported ^{210}Pb activity from total ^{210}Pb activity. The Constant Rate of Supply (CRS) model was used in conjunction with estimated unsupported ^{210}Pb activity to determine age-depth relations and rates of sedimentation. Estimated ages below background depth (estimated as the depth where total ^{210}Pb activity equals ^{226}Ra activity) were linearly extrapolated using dry mass of sediment. ^{137}Cs activity profiles were assessed for a peak associated with an increase in atmospheric concentrations of ^{137}Cs in 1963 caused by above-ground nuclear weapons testing. Data generated from this analysis are reported in Tables B1-B6 of Appendix B.

Loss-on-ignition

Loss-on-ignition analysis was performed to determine stratigraphic variation in bulk sediment composition, including organic matter, mineral matter and carbonate content (Heiri et al., 2001). A measured mass (approximately 0.5 g, and up to 1.0 g) of wet sediment was subsampled from each well-mixed 0.5-cm interval and placed into pre-weighed crucibles. The sediment was heated sequentially at a series of three different temperatures and placed into a desiccator to cool for two hours before recording the loss in mass following each temperature

treatment. Dried sediment (at 90°C for 24 hours) was heated in a muffle furnace at 550°C for two hours to determine organic matter content (as the mass lost) and mineral matter content (as the mass remaining). Then, the remaining mineral sediment was combusted at 950°C for two hours to remove carbonates. The loss of mass following this combustion was then multiplied by 1.36 to determine the carbonate content (Dean, 1974). Data generated from this analysis are reported in Tables C1-C3 of Appendix C.

Carbonate oxygen isotope composition

The oxygen isotope composition of sediment carbonate was measured to reconstruct the oxygen isotope composition of pond water. Details of sample preparation and analysis are provided in Appendix D. Briefly, a subsample of approximately 0.2-0.5 mg of well-mixed, finely ground, freeze-dried sediment was taken from every second 0.5-cm interval of the sediment core from each pond and from surface sediments collected in 2024. Subsamples were placed into a 5 ml exetainer glass vial and sealed with a septum (pre-baked for 24 hours to remove impurities) and a rubber cap. The exetainer glass vials were connected to a dual needle system attached through the septum and flushed with helium for 5 minutes at a target flow rate of 100-200 ml/min to remove all carbon dioxide and oxygen in the vials' headspace. Subsamples were then acidified with approximately 100 µl of purified phosphoric acid to evolve CO₂ from carbonates, which was then analyzed at the UW-EIL using a dual inlet isotope ratio mass spectrometer (Thermo Delta V Plus). Results are reported as δ¹⁸O_{carb} values (‰) relative to the VPDB standard with analytical uncertainty of ± 0.2‰. Data generated from this analysis (also including δ¹³C_{carb}) are reported in Tables E1-E3 of Appendix E.

The oxygen isotope composition of pond water (δ¹⁸O_{pw}) was inferred from the oxygen isotope composition of sediment carbonate (δ¹⁸O_{carb}) using the calcite-water equilibrium equation from Leng and Marshall (2004):

$$T = 13.8 - 4.58(\delta^{18}O_{carb} - \delta^{18}O_{pw}) + 0.08(\delta^{18}O_{carb} - \delta^{18}O_{pw})^2 \quad (1)$$

where T represents the temperature (°C) at which carbonate forms within the pond water column. This equation was rearranged to solve for δ¹⁸O_{pw}:

$$\delta^{18}O_{pw} = 8 * \delta^{18}O_{carb} - \frac{229 + \sqrt{800T + 41401}}{8} \quad (2)$$

where T was calculated using the mean hourly pond water temperature during the open water season of 2022, as recorded by the water-depth loggers (June 1 – September 15), and applied to each stratigraphic interval. Pond-specific mean water temperatures were 17.87°C, 17.59°C and 20.09°C for SK 26, SK 31 and SK 58, respectively. For carbonates formed at equilibrium with pond water, the oxygen isotope composition decreases by ~0.24‰ for each 1°C increase in temperature (Craig, 1965). To account for potential water temperature variation during the time intervals captured by the sediment cores, an uncertainty of ±5°C was applied to the estimated $\delta^{18}\text{O}_{\text{pw}}$ values for each stratigraphic interval. Because average air temperature at Fort Smith (NT) between May 1 and September 30 (representing the open-water season) varied by ±1.3 °C (standard deviation) during the 1991-2020 climate normal period, a ± 5°C variation is considered reasonable to incorporate potential pond water temperature variation during the past ~300-400 years captured by the sediment cores.

Organic carbon and nitrogen elemental content and isotope composition

Ratios of organic carbon to nitrogen content (C/N) were used to track variation in the source of sediment organic matter at SK 58, following standard methods (Wolfe et al., 2002). The analysis of organic carbon and nitrogen content was performed only on the sediment core from SK 58 to help determine if this pond may have desiccated in the past, because we observed it to dry out completely in 2023 and 2024 but did not capture this event in the $\delta^{18}\text{O}_{\text{pw}}$ inferred from surface sediment carbonate $\delta^{18}\text{O}$ (collected in 2024), presumably because the pond desiccated due to vertical seepage which does not lead to oxygen isotope fractionation of pond water. Subsamples of wet sediment from each well-mixed 0.5-cm interval of the core from SK 58 were treated with 10% (by volume) hydrochloric acid (HCl) at 60°C for 2 hours to remove inorganic carbon (i.e., carbonate). Samples were then rinsed with deionized water to remove acid residues, freeze-dried, weighed and submitted for analysis at the UW-EIL. Measurements were made after combustion conversion from solid to gas using a 4010 Elemental Analyzer coupled to a Delta Plus XL continuous flow isotope ratio mass spectrometer (CFIRMS). Samples were run in duplicates at a minimum of every tenth sample. Results are reported as weight ratios of organic %C to %N. The results from this analysis, including measurements of organic carbon and nitrogen isotope composition, are reported in Table F1 of Appendix F.

Chapter 3: Results and Discussion

Contemporary hydrology

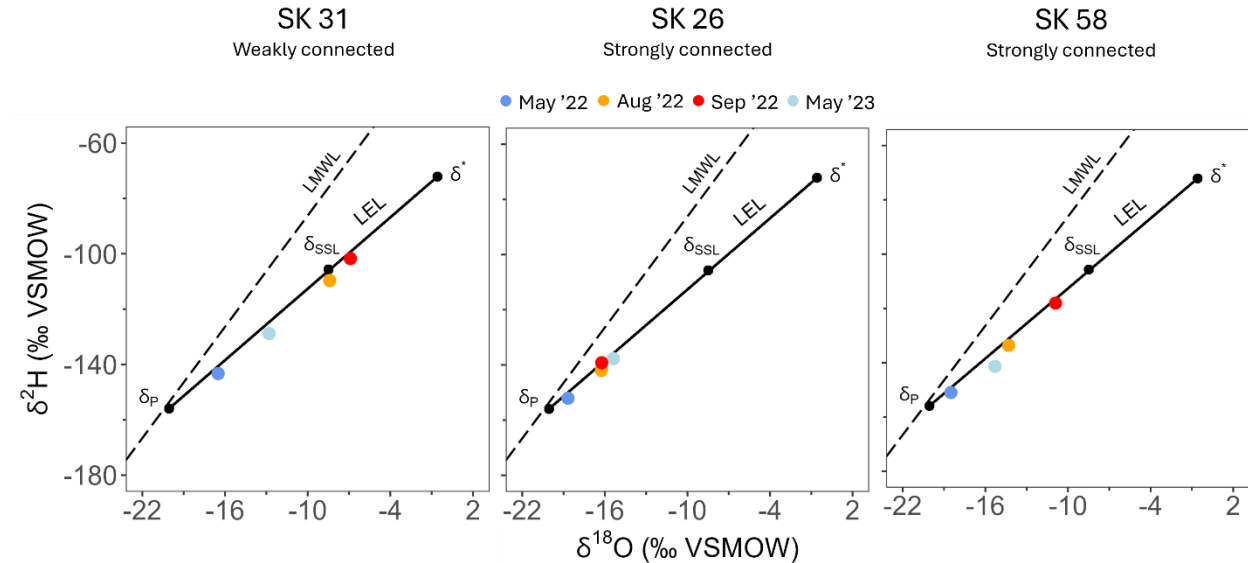


Figure 4. Scatterplots showing seasonal variation of water isotope composition at ponds SK 31, SK 26 and SK 58 in May, August, and September 2022 and May 2023 in relation to the Local Evaporation Line (LEL) and the Local Meteoric Water Line (LMWL) (as also reported in Figure 2). SK 31 is weakly connected to groundwater while SK 26 and SK 58 are classified as strongly connected to groundwater (Neary, 2025).

Water isotope compositions at SK 31, SK 26 and SK 58 plot closely along the LEL, but they differ in position and temporal variation. At all three ponds, water is most isotopically depleted (near δ_p) in May 2022 ($\delta^{18}\text{O}$: -18.7 to -16.5 ‰; $\delta^2\text{H}$: -152.1 to -143.3 ‰) due to substantial inflow of isotopically depleted snowmelt and possibly groundwater discharge (Neary, 2025). In all three ponds, values are lower in May 2022 than in May 2023, likely due to greater inflow of snowmelt after an unusually thick snowpack and delayed freshet in 2022 (Neary, 2025). Pond water isotope composition increases in August and September 2022 in response to very little rainfall and low relative humidity, which increased rates of evaporation. The greatest isotopic enrichment occurred at SK 31 in August 2022 ($\delta^{18}\text{O}$: -8.4 ‰; $\delta^2\text{H}$: -109.7 ‰) when the composition approached δ_{SSL} , and in September 2022 ($\delta^{18}\text{O}$: -6.9 ‰; $\delta^2\text{H}$: -101.7 ‰) when it exceeded δ_{SSL} . This suggests evaporative water loss exerts strongest influence on water balance at

SK 31. In contrast, water isotope composition remained low at SK 26 in August ($\delta^{18}\text{O}$: -16.3 ‰; $\delta^2\text{H}$: -142.0 ‰) and September 2022 ($\delta^{18}\text{O}$: -16.2 ‰; $\delta^2\text{H}$: -139.2 ‰), identifying strong influence of isotopically depleted input waters that offset enrichment by evaporation. Water isotope composition in August and September 2022 is comparable to the May 2023 value, consequently, SK 26 is interpreted to maintain strong influence of an isotopically depleted input source (i.e., groundwater discharge) throughout the open water season even when summer rainfall is low (Neary, 2025). Water isotope composition in August ($\delta^{18}\text{O}$: -14.3 ‰; $\delta^2\text{H}$: -133.6 ‰) and September ($\delta^{18}\text{O}$: -10.9 ‰; $\delta^2\text{H}$: -118.1 ‰) 2022 at SK 58 is intermediate between that of the other two ponds and remains below δ_{SSL} . Given SK 58 lacks a visible outflow channel, this suggests intermediate influence of inflow from groundwater or precipitation and loss via evaporation on water isotope composition relative to the other two ponds.

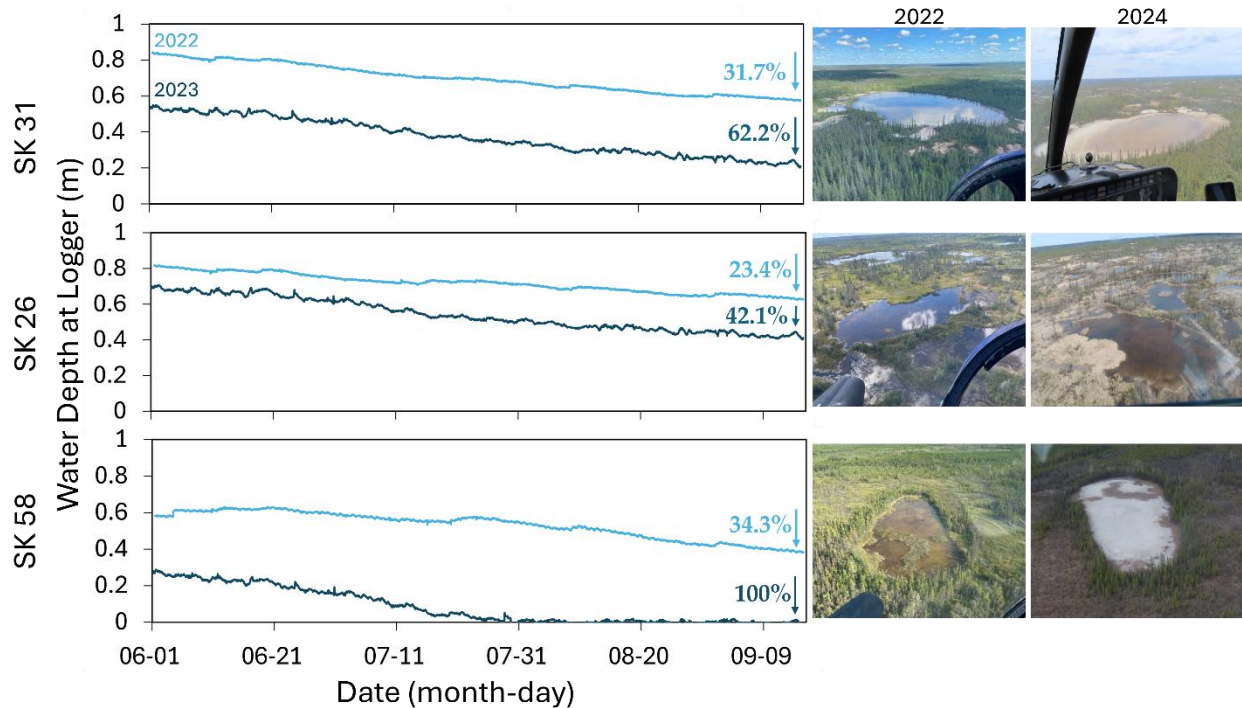


Figure 5. Time series of hourly water depth measurements from ponds SK 31, SK 26, and SK 58 during the open water seasons (June 1 – September 15) of 2022 (light blue line) and 2023 (dark blue line). Aerial photos are presented at each pond in summer 2022 and spring 2024. The percent values identify the water-level drawdown relative to the starting depths recorded on June 1, 2022 and June 1, 2023.

During the open water seasons of 2022 and 2023, water levels declined at all three ponds from their initial depth recorded on June 1 (Figure 5). Between June 1 and September 15 of 2022, the drawdown was 0.27 m, 0.19 m, and 0.20 m at SK 31, SK 26 and SK 58, respectively. When expressed as a percentage of the initial depth in 2022 the drawdown magnitude is 31.7% at SK 31, 23.4% at SK 26, and 34.3% at SK 58 (Neary, 2025). The drawdown was greater between June 1 and September 15 of 2023, with declines of 0.33 m (62.2%), 0.29 m (42.1%) and 0.28 m (100%) at SK 31, SK 26 and SK 58, respectively. Figure 5 does not show the decline of water depth that occurred after September 15, 2022 and before June 1, 2023. When these declines are factored in, the drawdown between June 1, 2022 and the end of the record in 2023 is 0.64 m (75.8%) at SK 31, 0.41 m (50.7%) at SK 26, and 0.58 m (100%) at SK 58 (Figure 5). The measurements at SK 58 identify complete desiccation occurred during the last week of July 2023, and aerial imagery reveals SK 58 was also a dry basin in spring (Figure 5) and fall of 2024. Wildfires prevented sampling in summer and fall of 2023 for analysis of water isotope composition, thus the hydrological processes responsible for the drawdown, and desiccation at SK 58, during the open water season of 2023 cannot be discerned from these data alone.

Paleolimnological results

Do the ponds contain datable stratigraphic records?

Deposition of sediment may cease or become reduced during intervals when ponds desiccate, and sediment may be lost via transport by wind and other processes, which presents challenges in obtaining a reliable ^{210}Pb -derived chronology for analysis of sediment cores. When the bottom sediment is under a thin film of water or exposed to air, there is also opportunity for redistribution of ^{210}Pb in association with mixing of near-surface sediments by physical or biological processes and post-depositional resuspension of sediment (Oldfield and Appleby, 1984). These potential unconformities and disturbances may complicate the application of the CRS model and confound estimates of sedimentation rates. The shallowest of the three ponds (SK 58), which was 0.58 m deep at the start of the study in June 2022, desiccated during the summer of 2023. Thus, it is important to evaluate if core dating could have been compromised by other prior desiccation episodes at SK 58 and the other two ponds. Due to the observed seasonal variability in water depth of SK 31, SK 26 and SK 58, it was unknown whether the ponds would contain coherent stratigraphic records. Thus, radiometric analyses were used to assess the integrity of stratigraphic

records and develop sediment core chronologies before using other analyses on the sediment cores to infer past changes in basin hydrology.

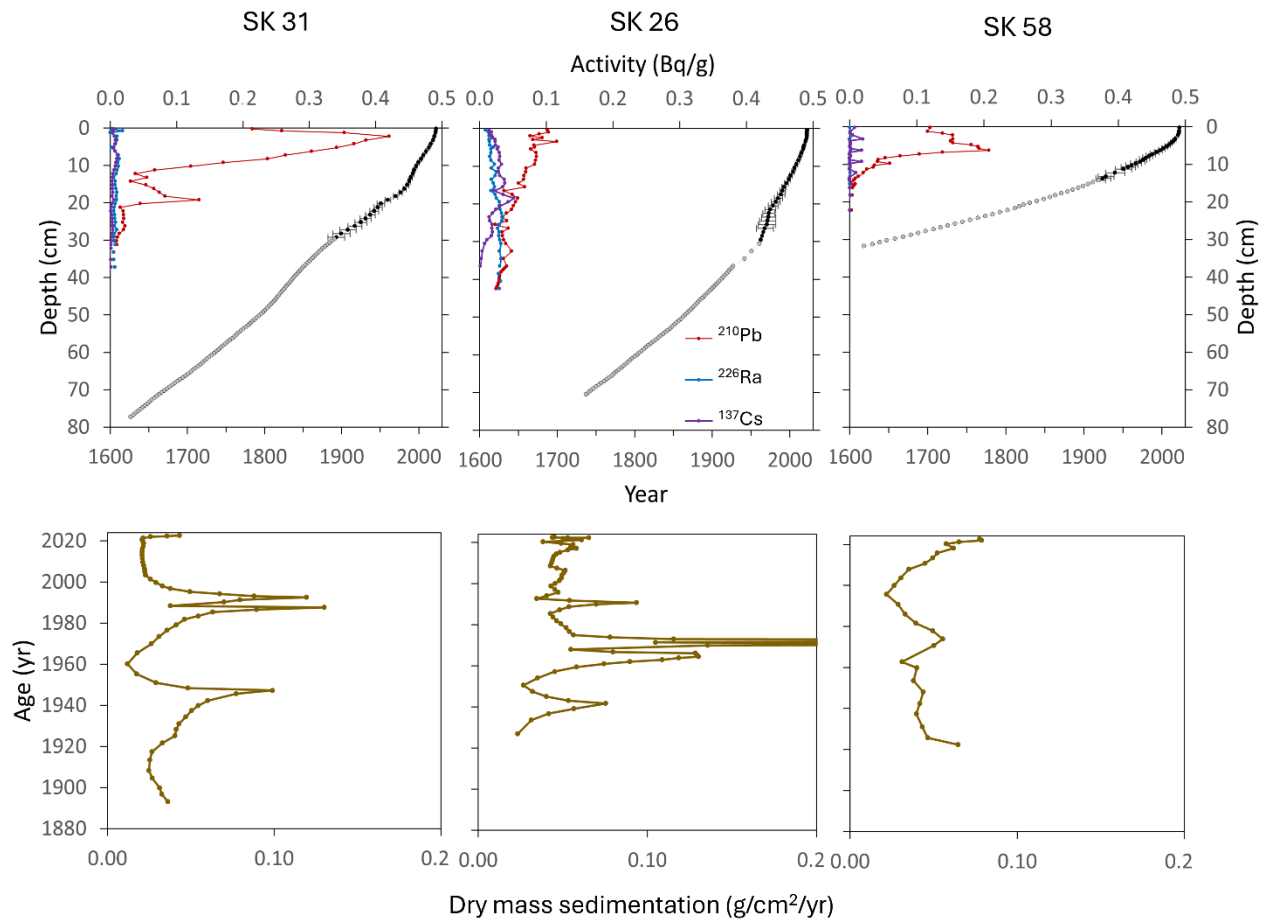


Figure 6. Stratigraphic variation of radioisotope activities (total ^{210}Pb (red line), ^{226}Ra (blue line), and ^{137}Cs (purple line)) and modelled age-depth relations (black, grey) and associated errors bars (± 2 standard deviation units) in sediment cores from ponds SK 31, SK 26 and SK 58. The grey data points represent sediment ages that were extrapolated below the depth of supported ^{210}Pb activity. Temporal variation of dry mass sedimentation rates of SK 31, SK 26 and SK 58 is shown in the second row of graphs.

At SK 31, total ^{210}Pb activity increases with depth in the uppermost sediment until a peak is reached at 2.25 cm (mid-point depth; ~ 2021 CE), which can be attributed to a recent increase in sedimentation rate (Figure 6). This subsurface peak of total ^{210}Pb activity is followed by an approximately exponential decline with depth that is interrupted by two discernible peaks at 12.25-

13.75 cm (~1993-1989 CE) and 14.25-19.25 cm (~1988-1963 CE), which reflect troughs in the sedimentation rate and coincide with rise of organic matter content (See Table C1 of Appendix C). *Chara* remains were more abundant in the sediment between 14 cm and 20 cm, and a layer of distinctly darker brown organic-rich sediment was noted in the 13.0 to 13.5 cm interval, which could reflect a very shallow water environment with slower sedimentation rates. Total ^{210}Pb activity reaches background at 29.75 cm. Linear extrapolation of the CRS modelled dates below 29.75 cm, based on cumulative dry mass, results in a basal date of ~1627 CE.

At SK 26, total ^{210}Pb activity declines approximately linearly with depth through the upper 40 cm of the sediment core (Figure 6). No visible stratigraphic changes were observed during core sectioning. Results of loss-on-ignition analysis support an unchanging record of sediment composition (See Table C2 of Appendix C) and contemporary hydrological measurements (Figure 4, 5) provide evidence of strong connectivity to groundwater. Based on these data, there is no evidence to suggest marked variation of water levels or pond desiccation occurred during the time captured by the sediment core. Sedimentation rate however reveals notable variation with higher and more variable sedimentation during the late 1950s through mid-1970s, which may reflect periods of shoreline expansion. Total ^{210}Pb activity reaches background at a depth of 36.75 cm (~1926 CE), and extrapolation of the CRS modelled dates below 36.75 cm results in a basal date of ~1738 CE.

At SK 58, total ^{210}Pb activity increases with depth through the upper 6.5 cm (~1998 CE) and declines approximately exponentially thereafter (Figure 6). Sedimentation rate rises in the upper 6.5 cm but declines between 9 cm (~1972) and 6.5 cm (~1998), when the slowest sedimentation rate occurred. These features suggest a period of shallower water and slower sedimentation occurred during ~1972-1998, which may coincide with encroachment of the emergent vegetation into the basin (Figure 3). Relatively high abundance of *Chara* remains, and distinctly different sediment colour were noted in sediment deposited after ~1998, which reflect a rise of water levels after ~1998. Background ^{210}Pb activity is reached at 14.25 cm (~1919 CE) and extrapolation of the CRS modelled dates below that results in a basal date of ~1615 CE.

The presence of a well-defined peak of ^{137}Cs activity is often used as an independent chronological marker associated with peak emissions from above-ground testing of nuclear weapons that occurred in 1963 (Appleby, 2001), but none of the cores possess a well-defined peak.

This can be common in organic-rich sediments with low clay and silt content, which are more prone to post depositional mobility of ^{137}Cs (Appleby, 2001; Wan et al., 2005). Consequently, CRS modelling of ^{210}Pb activity could not be independently verified using ^{137}Cs activity profiles. Marked stratigraphic variation in the ^{210}Pb activity profiles from all three ponds suggest there has not been substantial mixing or disturbance of the sediment, because mixing would likely result in little to no stratigraphic variation of ^{210}Pb activity (Swarzenski, 2014). The ^{210}Pb -derived chronologies at SK 31, SK 26 and SK 58, thus, suggest these shallow ponds contain datable stratigraphic records with evidence of varying sedimentation rates and possibly episodes of near-desiccation during the intervals when sedimentation rates can be determined by CRS modelling (since ~1891 at SK 31, since ~1925 at SK 26, since ~1915 at SK 58).

Does $\delta^{18}\text{O}_{\text{carb}}$ provide a means to reconstruct $\delta^{18}\text{O}_{\text{pw}}$?

Oxygen isotope composition of carbonate in lake and pond sediments can potentially be used as a tracer of lake or pond water $\delta^{18}\text{O}$ if the carbonate is endogenic and the water temperature at the time of formation can be constrained (Leng and Marshall, 2003). Records of oxygen isotope composition of carbonate, however, may be confounded by the supply and deposition of detrital carbonate. To assess the viability of carbonate $\delta^{18}\text{O}$ to reconstruct pond water $\delta^{18}\text{O}$, carbonate-inferred $\delta^{18}\text{O}_{\text{pw}}$ in the uppermost sediment from each of the three sediment cores were compared to measured $\delta^{18}\text{O}_{\text{pw}}$. In most high-latitude regions, endogenic carbonate precipitates during periods of maximum aquatic productivity (Leng and Marshall, 2004). Because light, temperature and nutrients are strong determinants of aquatic algae growth rates, pond productivity likely reaches maxima in the SKNA in the summer. Thus, water temperature was estimated using a seasonal average (Jun 1 – Sep 15, 2022) of measured hourly pond water temperatures at SK 31, SK 26 and SK 58 (Table 1). Based on $\delta^{18}\text{O}_{\text{pw}}$ measurements taken in spring (May), summer (August) and fall (September) at SK 31, SK 26 and SK 58, $\delta^{18}\text{O}_{\text{pw}}$ measured in the summer (August 2022) would be the closest estimate of peak productivity and thus the most appropriate comparison to carbonate-inferred $\delta^{18}\text{O}_{\text{pw}}$ from surface sediment (~2022).

Table 1. Carbonate-inferred $\delta^{18}\text{O}_{\text{pw}}$ (derived using Equation 2) from the uppermost sediments of cores obtained from SK 31, SK 26 and SK 58 in comparison to $\delta^{18}\text{O}_{\text{pw}}$ measured directly from pond water obtained in August 2022. Pond water temperature is an average of hourly measurements between June 1 and September 15, 2022.

	Inferred $\delta^{18}\text{O}_{\text{pw}}$ from uppermost sediments (~2022)	Measured $\delta^{18}\text{O}_{\text{pw}}$ (August 2022)	Difference (Measured – inferred $\delta^{18}\text{O}_{\text{pw}}$)	Pond water Temperature (°C)
SK 31	-10.30 ‰	-8.39 ‰	1.91‰	17.59
SK 26	-17.48 ‰	-16.25 ‰	1.23‰	17.87
SK 58	-14.34 ‰	-14.34 ‰	0.00‰	20.09

Carbonate-inferred $\delta^{18}\text{O}_{\text{pw}}$ values are in close agreement with $\delta^{18}\text{O}_{\text{pw}}$ measured in August 2022, with small to no differences of 1.91 ‰, 1.23 ‰, and 0.00 ‰ at ponds SK 31, SK 26 and SK 58, respectively (Table 1). The agreement among measured and inferred $\delta^{18}\text{O}_{\text{pw}}$ values supports down-core reconstruction of $\delta^{18}\text{O}_{\text{pw}}$ from analysis of carbonate $\delta^{18}\text{O}$ in sediment cores from these ponds. Similarly, Wagner et al. (2025) showed strong correlation between modern lake water $\delta^{18}\text{O}$ and carbonate $\delta^{18}\text{O}$ of surface sediment in Shark Lake (Alberta), a hydrologically open system predominantly fed by groundwater and snowmelt. Additionally, Li et al. (2020) examined 33 lakes in western China and similarly found that lake water $\delta^{18}\text{O}$ is a strong determinant of carbonate $\delta^{18}\text{O}$, even when isotopic equilibrium may not be achieved in natural lacustrine settings. Overall, the use of carbonate $\delta^{18}\text{O}$ provides a reasonable means to infer mid-summer pond water $\delta^{18}\text{O}$, assuming temperature can be constrained and there is minimal confounding influence of detrital carbonate down-core.

What do stratigraphic records of carbonate-inferred $\delta^{18}\text{O}_{\text{pw}}$ reveal about past changes in pond hydrology?

Close agreement between carbonate-inferred $\delta^{18}\text{O}_{\text{pw}}$ from uppermost sediment from the three sediment cores and measured $\delta^{18}\text{O}_{\text{pw}}$ validates the use of $\delta^{18}\text{O}_{\text{carb}}$ as a means to reconstruct $\delta^{18}\text{O}_{\text{pw}}$ down-core, if we can assume there is minimal confounding influence of detrital carbonate and water temperature can be constrained. Based on contemporary isotope hydrology of SK 31, SK 26 and SK 58, shifts in carbonate-inferred $\delta^{18}\text{O}_{\text{pw}}$ are likely associated with shifts along the LEL reflecting changes in evaporation relative to inflow. However, water loss by vertical seepage,

demonstrated to occur in the WCSR (Neary, 2025), cannot be detected by this method because this hydrological process does not lead to isotope fractionation.

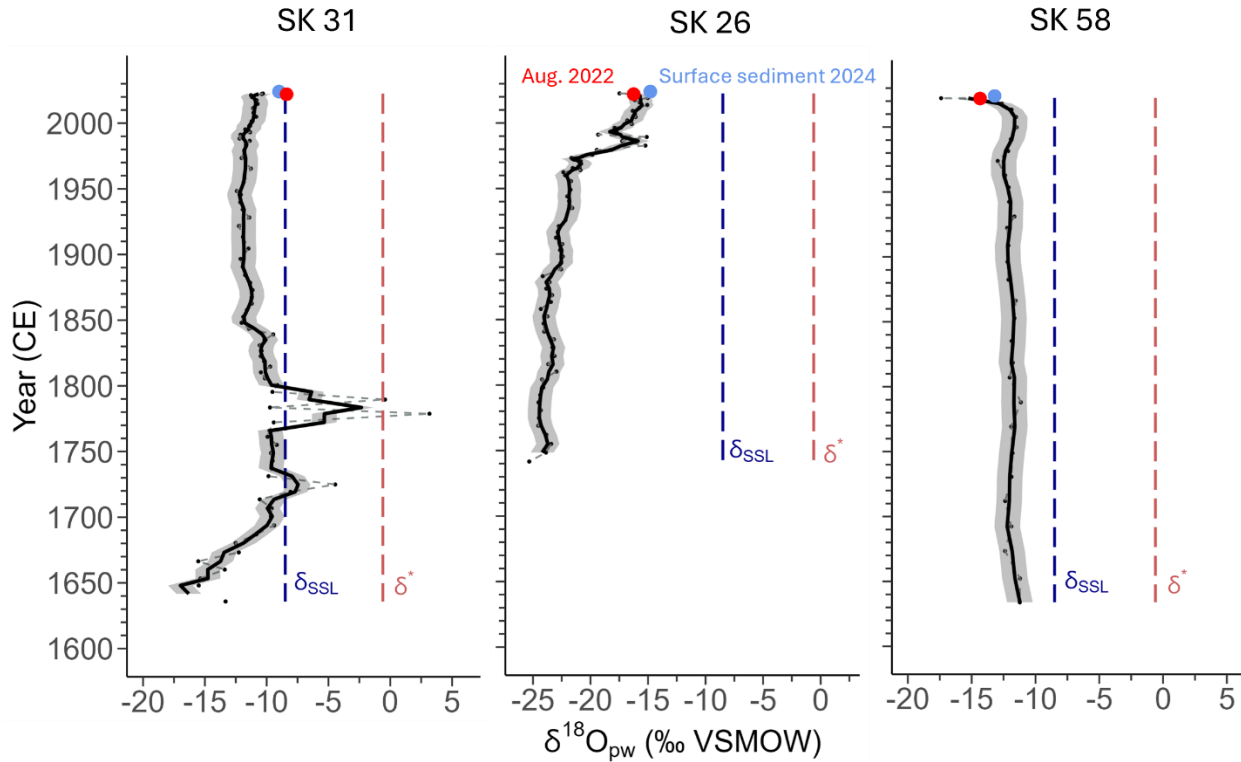


Figure 7. Stratigraphic variation in $\delta^{18}\text{O}_{\text{pw}}$ inferred from sediment carbonate $\delta^{18}\text{O}$ (using Equation 2 and pond water temperature values from Table 1) at ponds SK 31, SK 26 and SK 58. Results are shown as individual measurements (grey points and dashed line) and as a 3-point running mean (solid black line). Estimates of uncertainty are based on temperature variation of $\pm 5^\circ\text{C}$ are shown for individual measurements (grey ribbon). Also shown are $\delta^{18}\text{O}_{\text{pw}}$ values measured in water obtained in August 2022 (red filled circles) and $\delta^{18}\text{O}_{\text{pw}}$ inferred from carbonate $\delta^{18}\text{O}$ extracted from surface sediment collected in May 2024 (light blue filled circles). Contemporary estimates of δ_{SSL} (vertical blue dashed line) and δ^* (vertical red dashed line) are shown for reference (values are from Neary, 2025).

Stratigraphic variation of carbonate-inferred $\delta^{18}\text{O}_{\text{pw}}$ is substantially greater at SK 31 (-20.08 ‰ to 3.17 ‰) than at the other two ponds (Figure 7). $\delta^{18}\text{O}_{\text{pw}}$ measured on water obtained in August 2022 at SK 31 agrees well with the uppermost carbonate-inferred $\delta^{18}\text{O}_{\text{pw}}$ values in the sediment core and with carbonate-inferred $\delta^{18}\text{O}_{\text{pw}}$ in the surface sediment sample obtained in May

2024, which suggests the $\delta^{18}\text{O}$ of carbonate can be used to reconstruct $\delta^{18}\text{O}_{\text{pw}}$. At SK 31, carbonate-inferred $\delta^{18}\text{O}_{\text{pw}}$ is isotopically depleted and below the contemporary estimate of δ_{SSL} (i.e., where evaporation = inflow) in sediment deposited before ~ 1720 CE and after ~ 1800 CE, but values are more variable and exceed the contemporary estimate of δ_{SSL} in sediment deposited between ~ 1720 - 1800 . Carbonate-inferred $\delta^{18}\text{O}_{\text{pw}}$ exceeds the contemporary estimate of δ^* in sediment deposited in ~ 1779 CE and ~ 1790 CE. These findings suggest strong net evaporation was prevalent at SK 31 during much of the 1700s, when cool, arid conditions of the Little Ice Age (LIA) prevailed (Luckman and Watson, 1999; Luckman, 2000; Watson and Luckman, 2001), and shorter-lived episodes of desiccation occurred during the latter part of the 18th century. After ~ 1800 CE, carbonate-inferred $\delta^{18}\text{O}_{\text{pw}}$ values range more narrowly (-12.41 ‰ to -9.14 ‰) and remained consistently below the contemporary estimate of δ_{SSL} , suggesting positive pond water balances have prevailed since the early 1800s.

At SK 26, carbonate-inferred $\delta^{18}\text{O}_{\text{pw}}$ values (-25.32 ‰ to -15.03 ‰) remained well below the contemporary estimate of δ_{SSL} for the entire record (since ~ 1745 ; Figure 7). Also, contemporary $\delta^{18}\text{O}_{\text{pw}}$ measured in August 2022 and $\delta^{18}\text{O}_{\text{pw}}$ inferred from surface sediment obtained in May 2024 agree well with the uppermost carbonate-inferred $\delta^{18}\text{O}_{\text{pw}}$ values. Before ~ 1980 CE, mean carbonate-inferred $\delta^{18}\text{O}_{\text{pw}}$ is -22.82 ‰ (values range -25.32 ‰ to -19.45 ‰), which is below that of contemporary mean annual precipitation in the region ($\delta^{18}\text{O}$: -20.06 ‰; Neary, 2025). Consistently low carbonate-inferred $\delta^{18}\text{O}_{\text{pw}}$ values that are well below mean annual $\delta^{18}\text{O}$ of precipitation, as occurred in the samples deposited during ~ 1745 to 1980 CE (-25.32 ‰ to -19.45 ‰) are difficult to interpret. It is particularly challenging to identify a source or process that could generate these low carbonate-inferred $\delta^{18}\text{O}_{\text{pw}}$ values, based on available data alone, because the range falls below the contemporary range of $\delta^{18}\text{O}_{\text{pw}}$ values (-18.68 ‰ to -15.39 ‰) at SK 26 (Figure 4). Listed and evaluated below are four potential mechanisms that may account for low carbonate-inferred $\delta^{18}\text{O}_{\text{pw}}$ values at SK 26, followed by a sudden increase in ~ 1980 CE. 1) Thaw of permafrost underlying the pond and its contributing basin may contribute to isotopically depleted pond water. This is because permafrost has low $\delta^{18}\text{O}$, typically ranging ~ -35 to -20 ‰ (Meyer et al., 2010; Lachniet et al., 2012; Anderson et al., 2013; Lacelle et al., 2014; Wan et al., 2020). Conversely, permafrost thaw would likely result in a change in the rate of accumulation of organic matter in sediments, either increasing or decreasing the concentration of sediment organic matter (Vonk et al., 2012; Deison et al., 2012; Vonk et al., 2015; Bouchard et al., 2017). This would

result in a discernible change in sediment composition, yet loss-on-ignition analysis reveals that the sediment composition of SK 26 remains virtually unchanging throughout the sediment core (see Table C2 of Appendix C). Permafrost thaw, therefore, is unlikely to be the mechanism causing low carbonate-inferred $\delta^{18}\text{O}_{\text{pw}}$ values at SK 26. 2) Pond SK 26 is proximal to the Klewi River, raising the possibility that the pond and river were more hydrologically connected before ~1980 CE, causing lower $\delta^{18}\text{O}_{\text{pw}}$ values, and less hydrologically connected after ~1980 CE causing more positive $\delta^{18}\text{O}_{\text{pw}}$ values due to greater influence of evaporation when inflow of isotopically depleted river water declined. However, the average $\delta^{18}\text{O}$ value of the Klewi River measured in May 2022, when it is most isotopically depleted, is -18.42 ‰ (Neary, 2025), which is substantially higher than the range of carbonate-inferred $\delta^{18}\text{O}_{\text{pw}}$ in this stratigraphic interval. Early study design included analysis of diatom assemblage composition, and *Fragilaria construens* is the most commonly occurring diatom taxon in the sediment record of SK 26, among other *Fragilaria* species (see Table G2 of Appendix G), which indicates conditions of a lentic, not lotic, waterbody (Krammer and Lange-Bertalot, 1991; Reavie and Smol, 1998; Ruhland and Smol, 2002; Ruhland et al., 2003). If there had there been a connecting channel between SK 26 and the Klewi River before ~1980 CE, there would be evidence of a notable shift in diatom community composition and there would likely be high relative abundance of taxa that prefer lotic habitat. Based on contemporary $\delta^{18}\text{O}$ of the Klewi River and diatom assemblages of SK 26, it is thus unlikely that the pond and river have been hydrologically connected during the time interval represented by the sediment core. 3) Changes in local meteorological conditions, such as decreased $\delta^{18}\text{O}$ values caused by greater input of isotopically depleted snowmelt may account for low $\delta^{18}\text{O}_{\text{pw}}$ values. However, changes in local meteorological conditions would be expected to affect all three ponds. Specifically, SK 31 should show evidence of meteorological changes since it is the most weakly connected to groundwater. But SK 31 and SK 58 do not show an increase in $\delta^{18}\text{O}_{\text{pw}}$ values since ~1980. A distinct shift from very low $\delta^{18}\text{O}_{\text{pw}}$ values before ~1980 CE to more positive values thereafter is an isolated phenomena at SK 26 among the three study ponds. Therefore, it is unlikely past influence of ^{18}O -depleted snowmelt on the water balance caused the low $\delta^{18}\text{O}_{\text{pw}}$ values at SK 26 before ~1980 CE. Further, the water-saturated catchment of SK 26 does not appear to show evidence of substantial drawdown in recent years (Figure 3). Therefore, evaporative enrichment is unlikely to account for the rise in $\delta^{18}\text{O}_{\text{pw}}$ values after ~1980 CE. 4) A 4th possibility is that the source of input water at SK 26 changed at ~1980. Before 1980, there may have been an influential source of ^{18}O depleted

groundwater to the pond that may have originated from precipitation that occurred at higher elevation, such as the Caribou Hills. After 1980, the groundwater source may have shifted to a more localized source. Low carbonate $\delta^{13}\text{C}$ in sediment deposited before 1980 suggests the pre-1980 groundwater source interacted with respired organic matter, whereas higher carbonate $\delta^{13}\text{C}$ in sediment deposited after 1980 suggests the post-1980 groundwater source interacted with carbonate bedrock (see Figure E1), which is common in dolostone ($\text{CaMg}(\text{CO}_3)_2$) of the Keg River Formation and is considered an aquifer in the region (Tsui and Cruden 1984). When considered together, the contemporary and paleolimnological data therefore suggest that a sudden change from very low carbonate-inferred $\delta^{18}\text{O}_{\text{pw}}$ values before ~1980 CE to more positive values thereafter may be attributed to a shift in source and influence of groundwater.

Carbonate-inferred $\delta^{18}\text{O}_{\text{pw}}$ at SK 58 remains below δ_{SSL} for the entire record and the values span the narrowest range (-17.40 ‰ to -11.15 ‰) among the three ponds (Figure 7). Carbonate-inferred $\delta^{18}\text{O}_{\text{pw}}$ of sediment in the core and the surficial sediment collected in 2024 agree well with contemporary $\delta^{18}\text{O}_{\text{pw}}$ value measured August 2022 (Figure 7). $\delta^{18}\text{O}_{\text{pw}}$ inferred from surface sediment carbonate $\delta^{18}\text{O}$ obtained from the desiccated basin of SK 58 in May 2024 reveals the $\delta^{18}\text{O}_{\text{pw}}$ remains low and within the range of values captured by the sediment core. If the pond dried up by evaporation, it would be expected that the $\delta^{18}\text{O}_{\text{pw}}$ inferred from surface sediment carbonate $\delta^{18}\text{O}$ would have increased to a value that exceeds δ_{SSL} and falls near the contemporary estimate of δ^* . The absence of enrichment of carbonate-inferred $\delta^{18}\text{O}_{\text{pw}}$ in surface sediment collected in 2024 suggests that SK 58 desiccated during the arid summer of 2023 due to water loss by vertical seepage as the water table subsided. This aligns with contemporary measurements of water isotope composition and drawdown magnitude suggesting this pond is strongly connected to the shallow groundwater discharge zone (Figures 4, 5). Because water loss via vertical seepage does not alter the isotope composition, it is possible that SK 58 may have desiccated in the past despite consistently low values of carbonate-inferred $\delta^{18}\text{O}_{\text{pw}}$. To explore this possibility, other paleolimnological measurements were assessed for evidence of pond desiccation at SK 58.

Is there evidence of prior desiccation via vertical seepage at SK 58 based on paleolimnological measurement of the C/N ratio?

The ratio of elemental organic carbon to nitrogen (C/N) is a measurement that may be sensitive to pond desiccation. C/N ratios can reflect changes in the source of organic material preserved within pond sediment. When pond water depth is stable, organic material would be primarily derived from aquatic sources, with C/N ratios typically ranging from ~4 to 10 (Meyers, 1994; Tyson, 1995; Meyers and Teranes, 2001). Conversely, during periods of low water levels or pond desiccation, contributions of terrestrial organic matter may increase at the coring location (e.g., Wolfe et al., 2011). An influx of carbon-rich terrestrial material or preferential nitrogen decomposition can result in a higher C/N ratio, typically exceeding ~12 (Prah et al., 1980; Tyson, 1995). Also, sediment transport may be reduced during intervals of very shallow pond water (Oldfield and Appleby, 1984). Thus, dry mass sedimentation rate could provide additional insight into changes in water levels at SK 58.

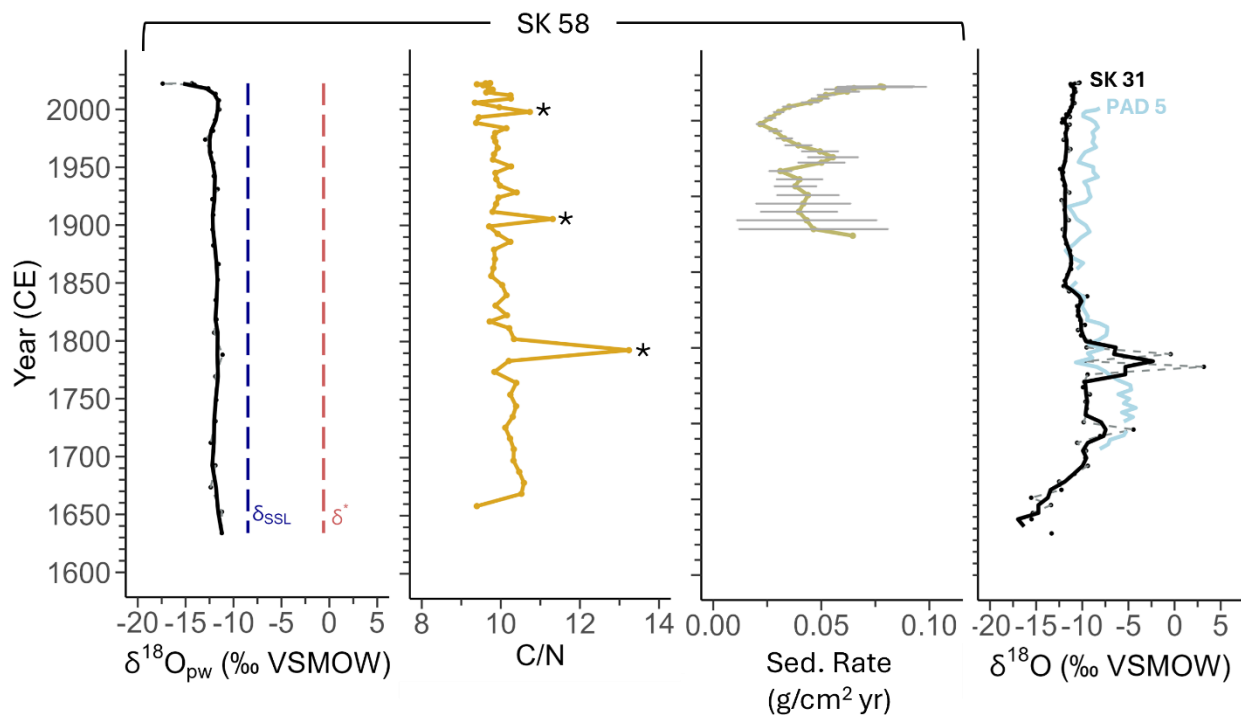


Figure 8. Temporal variation of paleolimnological measurements at pond SK 58, including carbonate-inferred $\delta^{18}\text{O}_{\text{pw}}$ (individual values and three-point running mean), organic carbon to nitrogen (C/N) ratios, and dry mass sedimentation rate (± 1 standard deviation). Carbonate-inferred $\delta^{18}\text{O}_{\text{pw}}$ for SK 58 is shown in reference to contemporary estimates of δ_{SSL} (blue dashed line) and δ^* (red dashed line) (from Neary, 2025). Also shown, for comparison, is the carbonate-inferred $\delta^{18}\text{O}_{\text{pw}}$ for SK 31 and the cellulose-inferred lake water $\delta^{18}\text{O}$ record for PAD 5, a shallow upland lake in the Peace-Athabasca Delta, located ~ 175 km south of SK 58 (Wolfe et al., 2005). A distinctive peak in the C/N ratio, possibly reflecting increased deposition of terrestrial organic matter, occurs at ~ 1793 CE (C/N = 13.2), and smaller peaks are evident at ~ 1906 CE (11.3) and ~ 1998 CE (10.7) (identified with an asterisk).

The C/N ratios are largely unvarying in the sediment core from SK 58, with a median value of ~ 9.9 which falls within the typical range of aquatic organic material (Figure 8). Exceptions include three intervals with markedly higher C/N ratios, which are dated to ~ 1793 CE (C/N = 13.2), ~ 1906 CE (11.3) and ~ 1998 CE (10.7). The C/N ratio of the most substantial peak, in ~ 1793 CE, exceeds the typical range of values for aquatic sediment and may reflect a brief rise in the contribution of terrestrial derived organic material. This may be an indication of drawdown and

desiccation at SK 58 in response to a particularly dry episode in the late 1700s during the cool and arid LIA. Periods of low precipitation and relative humidity during the LIA could have resulted in water loss via vertical seepage as the water table dropped. Notably, the carbonate-inferred $\delta^{18}\text{O}_{\text{pw}}$ record at SK 31 shows evidence of strong influence of evaporation during the same time (Figure 8). Neary (2025) showed that during the arid summer of 2022, ponds highly connected to groundwater drew down mainly by vertical seepage whereas ponds weakly connected to groundwater drew down mainly by evaporation. Therefore, it is possible that near-desiccation during the arid LIA was caused by evaporation at SK 31 and by vertical seepage at SK 58. Furthermore, at a shallow upland lake in the Peace Athabasca Delta (known informally as ‘PAD 5’), located ~175 km southeast of the SKNA, there is evidence of near desiccation by net evaporation in response to arid climate conditions and low flood frequency (Figure 8; Wolfe et al., 2005) which coincides with the lowermost C/N ratio peak at SK 58. This suggests that pond and lake drying in response to low precipitation during the LIA is a regional occurrence, further supporting the likelihood of desiccation or near-desiccation at SK 58 during the same time. In ~1906 CE, and again in ~1998 CE, smaller but discernible peaks in C/N ratios (to ~11.3 and ~10.7, respectively) at SK 58 may reflect minor increases in relative contribution of terrestrial organic matter (Figure 8). The smaller peak in C/N ratio in ~1998 aligns well with a decrease in sedimentation rate. These data suggest two other possible intervals of near-desiccation at SK 58. The most recent interval is consistent with Timoney et al. (1997) who reported more than half of the observed ponds desiccated by late summer of 1996. Overall, the evidence suggests that desiccation of SK 58, as occurred in 2023, has been rare during the past ~400 years, except for possibly one to three episodes detected during ~1793, 1906 and 1998 CE. Although SK 58 maintains strong connectivity to groundwater, periods of low precipitation and overall arid climate conditions during 2022-2023 may have contributed to a seemingly rare desiccation event.

How unusual were the meteorological conditions that led to the rare 2023-2024 desiccation event at SK 58?

Since the paleolimnological evidence suggests observed and recorded desiccation in 2023-2024 is a rare occurrence at SK 58, cumulative precipitation records from Fort Smith during 2022-2024 were compared to the 30-year climate normal (1991-2020) to further understand the role of precipitation in the preceding year and two years of the rare drying event at SK 58.

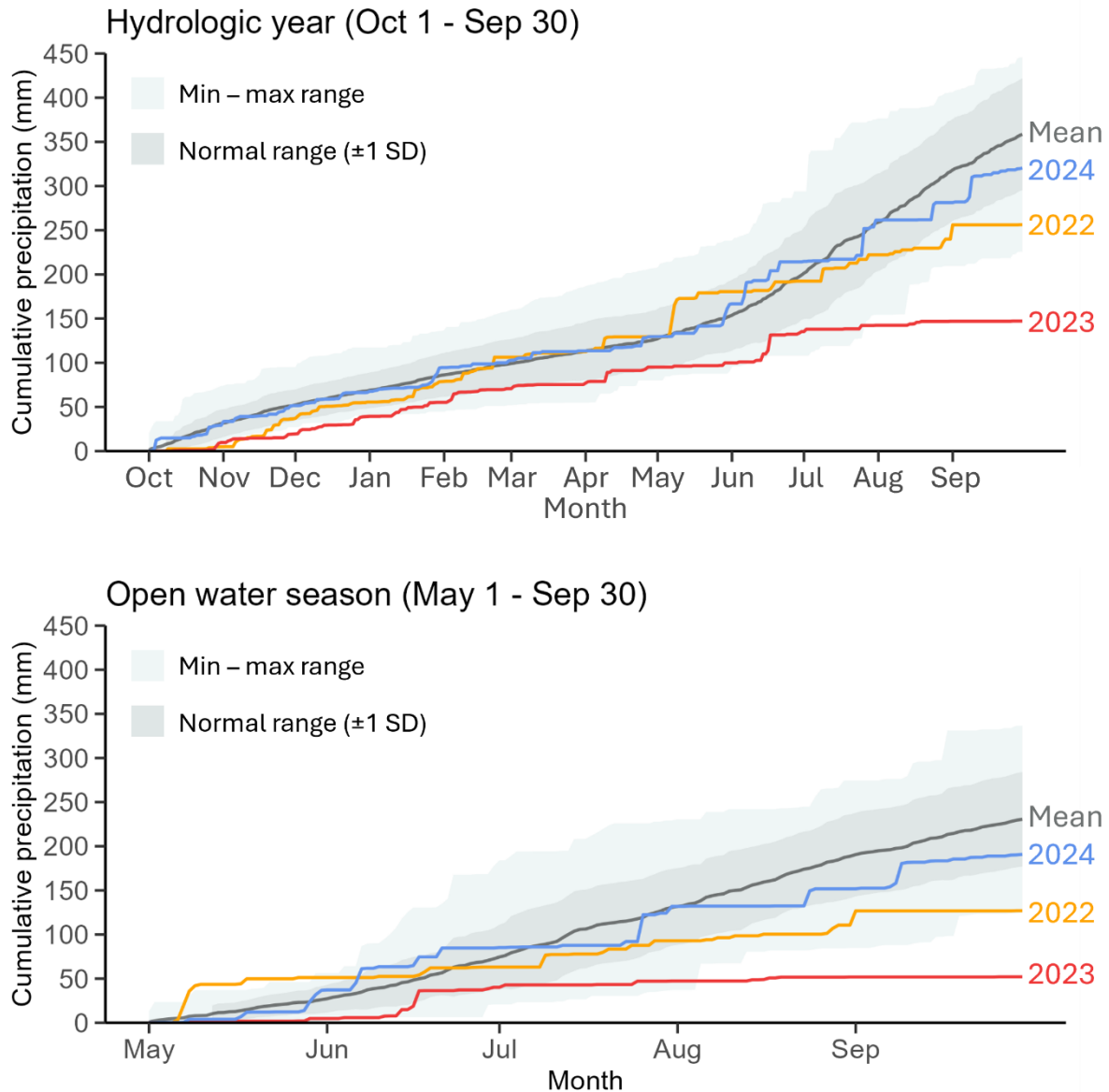


Figure 9. Cumulative precipitation (mm) during the hydrologic year (Oct 1 – Sep 30; upper graph) and open water season (May 1 – Sep 30; lower graph) for 2022 (yellow line), 2023 (red line) and 2024 (blue line) at Fort Smith (Climate station ID: 2202200 (1990-2014); 2202202 (2015-2024)). One standard deviation unit is applied to mean cumulative precipitation (black line) spanning the 30-year climate normal period (1991-2020) to display the range of normal variation (grey ribbon). The maximum and minimum cumulative precipitation spanning the 30-year climate normal period (1991-2020) is shown as reference of extreme variation (light grey ribbon).

Mean cumulative precipitation (mm) during the 1991-2020 climate normal is 359 mm for the hydrologic year and 231 mm for the open water season (Figure 9). In 2022, little rain fell between May and September, and cumulative open-water season precipitation was far below average by late summer and remained below the range of normal variation for the remaining months of the year. Below average precipitation continued into 2023, when cumulative precipitation remained well below the normal range of variation. The lowest cumulative precipitation recorded in Fort Smith since 1991 occurred in 2023 (hydrologic year = 147 mm, open water season = 52 mm). In response to well below average precipitation during 2022 and 2023, SK 58 desiccated by mid-July 2023 (Figure 5) and remained dry in spring 2024. Low water levels observed across southern NWT are the result of multi-year drought conditions driven by extremely hot and arid weather that began during summer 2022 and continued throughout 2023 (Government of the Northwest Territories, 2023). Notably, substantial decline of water levels during 2023 also occurred at Great Slave Lake (to the north of the SKNA), a much larger lake that drains a substantially larger watershed. Water levels of Great Slave Lake decreased by ~0.6 m between January 2022 and November 2023 and reached the lowest level of the 84-year-long record in 2023 (Figure 10), which is comparable to the decline recorded at SK 58 during the same interval (0.58 m). Notably, several climate-related records were broken globally in 2023, indicating exceptional conditions occurred well beyond the WCSR and Great Slave Lake's watershed (Ripple et al., 2023). This includes the highest global daily average surface air temperature (since 1850), the highest ocean surface temperature (since 1991), the lowest global and Antarctic sea ice extent (since 1991), and the greatest cumulative area of wildfire in Canada on record. Ripple et al. (2023) argue that these unprecedented conditions seen worldwide during 2023 are a result of human-caused greenhouse warming which increases the frequency and intensity of extreme events. Such extreme events are likely to exert adverse effects on critical nesting habitat that supports the Aransas-Wood Buffalo population of whooping crane. Of particular concern is greater frequency and duration of desiccation of waterbodies that the cranes use for nesting and feeding. Pond desiccation is particularly harmful when it occurs in spring and early summer, when eggs and fledglings are most vulnerable to predation and when parents need access to enough food to promote growth of their young (CWS USFWS 2007). Although past research has suggested cranes preferentially select ponds with the lowest risk of desiccation for nesting (Neary, 2025), paleolimnological data from this study suggests that even strongly connected ponds that have rarely desiccated in the past, can desiccate under extreme

drought conditions (i.e. SK 58 during 2023-2024). Increased frequency and duration of pond desiccation with ongoing climate warming may result in a loss of critical nesting habitat in the last remaining WCSR.

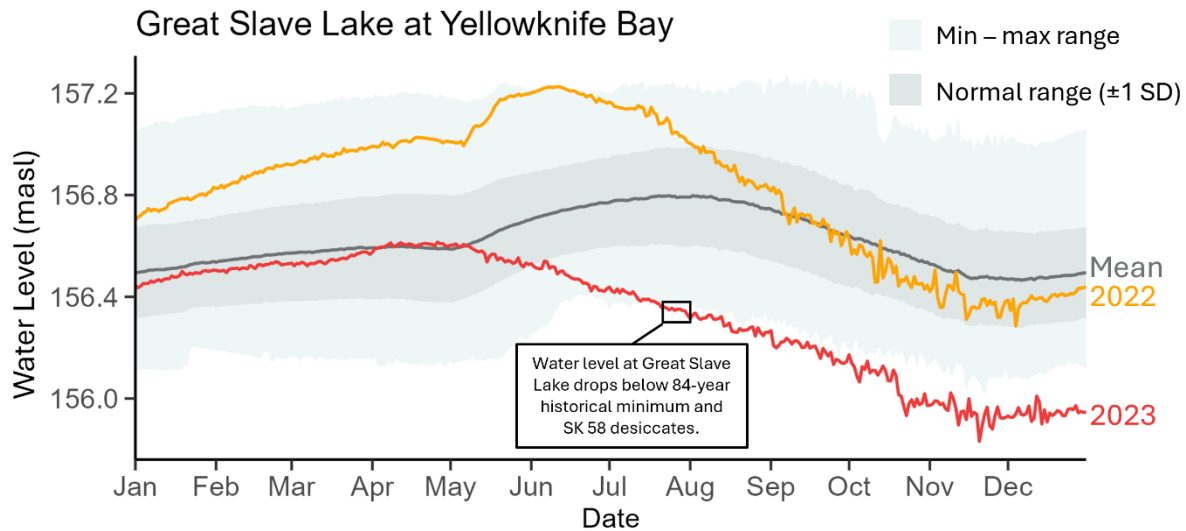


Figure 10. Hourly lake water level measurements (in masl) from Great Slave Lake at Yellowknife Bay (NT) spanning 2022 (yellow solid line) and 2023 (red solid line). Standard deviation of daily average water level for the 84-year record (1938-2022) is shown for reference as a range of normal variation (dark grey ribbon). Maximum and minimum water level spanning the 84-year record (1938-2022) is shown for reference as a range of extreme variation (light grey ribbon). Daily water level data for Great Slave Lake at Yellowknife Bay (07SB001) was accessed from https://wateroffice.ec.gc.ca/mainmenu/real_time_data_index_e.html on May 9, 2025.

Chapter 4: Conclusions and Recommendations

Conclusions

Mating pairs of the endangered Aransas-Wood Buffalo whooping crane population build nests and raise their fledglings along the shorelines of shallow waterbodies within a remote, water-rich landscape of WBNP. However, the shallow basin morphometry makes the waterbodies vulnerable to drawdown and desiccation during relatively arid years, which can reduce reproductive success by increasing access by predators and altering food supply. This research integrated contemporary measurements during 2022-2024 with paleolimnological analyses of sediment cores obtained from three ponds in the SKNA, where nest density is the greatest, to generate long temporal data on hydrological responses to past climate variation to better anticipate how breeding habitat will respond to future climate change. The landscape includes substantial areas of groundwater discharge, and the three ponds span a hydrological gradient from weakly to strongly connected to groundwater. Sediment cores from all three ponds were datable by ^{210}Pb methods despite differences in their vulnerability to desiccation, and the cores spanned the past ~280-410 years. Contemporary measurements of pond water $\delta^{18}\text{O}$ and temperature support that sediment carbonate $\delta^{18}\text{O}$ can be used to reconstruct pond water $\delta^{18}\text{O}$, which provides the basis for reconstruction of past variation of pond water $\delta^{18}\text{O}$. Water loss by vertical seepage, a previously recognized hydrological process in this landscape that occurs when the water table drops below pond water levels, likely caused the desiccation of SK 58 in 2023 and 2024. This hydrological process, however, does not lead to fractionation of water isotopes and, thus, cannot be detected using measurements of sediment carbonate $\delta^{18}\text{O}$. Elemental C/N ratios were measured in the sediment core from SK 58 to detect possible past desiccation horizons caused by vertical seepage.

Evidence at two of the three study ponds suggests desiccation occurred during the mid- to late 1700s in response to arid climate conditions that prevailed during the LIA. At SK 31, the pond where contemporary water isotope measurements identify connectivity to groundwater is weak, carbonate-inferred $\delta^{18}\text{O}_{\text{pw}}$ values exceeded contemporary estimate of δ_{SSL} and approached contemporary estimate of δ^* between the mid- and late 1700s. This finding identifies that SK 31 desiccated due to evaporation. Near-desiccation by evaporation also has been detected during the same time in a cellulose-inferred lake water $\delta^{18}\text{O}$ record from a shallow upland lake (PAD 5)

located ~175 km south of the SKNA (Wolfe et al., 2005), which provides confidence in the interpretations based on carbonate-inferred $\delta^{18}\text{O}_{\text{pw}}$ at SK 31. At SK 58, where measurements of carbonate-inferred $\delta^{18}\text{O}_{\text{pw}}$ from surface sediments in 2023 and 2024 suggest observed desiccation in 2023 and 2024 occurred by vertical seepage despite strong connectivity to groundwater, the stratigraphic record of carbonate-inferred $\delta^{18}\text{O}_{\text{pw}}$ reveals no evidence of enrichment by evaporation during the mid- and late 1700s. A distinctive peak in C/N ratios in sediment deposited ~1790 suggests, however, that an apparently rare desiccation, or near-desiccation, event may have occurred by vertical seepage when SK 31 and PAD 5 also desiccated or nearly desiccated by evaporation. Smaller C/N-ratio peaks in ~1908 and ~1998 may capture two other short-lived near-desiccation events at SK 58. Collectively, the evidence suggests desiccation events are rare at SK 31 and SK 58 since the late 1700s. The recent observed desiccation at SK 58 in 2023-2024 occurred when unusually arid climate conditions resulted in a decline in water levels of 60 cm in Great Slave Lake to the lowest levels recorded by the 84-year-long record. Although pond desiccation appears to be rare at SK 31 and SK 58, the frequency of desiccation events may increase with ongoing climate warming. Very low carbonate-inferred $\delta^{18}\text{O}_{\text{pw}}$ values in the record from SK 26 are challenging to interpret, but it is speculated that SK 26 has been variably influenced by shifting sources and discharge of groundwater. At this site, there is no evidence of desiccation via evaporation during the arid LIA, which may demonstrate the spatial and temporal variability of past hydrological conditions across this complex landscape.

Recommendations

Based on the findings of this research, five recommendations are listed below for future studies to address. 1) Obtain sediment cores from additional ponds that span the spatial extent of SKNA. Paleolimnological records from the three ponds of this study reveal that pond desiccation has occurred rarely during the past 300-400 years, but three ponds are insufficient to accurately determine the frequency of rare events across an entire landscape. Analysis of sediment from more ponds that desiccated in 2023 and 2024 (see Table 2 for specific study site recommendations) will be valuable to assess the rarity of widespread desiccation during these years and, more generally, to improve our understanding of the frequency of desiccation events in the SKNA and the climatic conditions that cause them. Ponds with moderate to strong connectivity to groundwater are not entirely resilient to climate variation because they can desiccate by vertical seepage when the climate is sufficiently arid to cause substantial lowering of the water table, as occurred at SK 58

in 2023 and 2024. However, weakly connected ponds (e.g., SK 31) are likely more responsive to past arid conditions and may provide a more fulsome record of pond hydrological response to past climate. 2) Carbonate-inferred $\delta^{18}\text{O}_{\text{pw}}$ should be measured on the sediment cores of SK 15, SK 43 and SK 51, which were collected in 2022, to further assess the rarity of desiccation across the landscape. At all three ponds, contemporary measurements of $\delta^{18}\text{O}_{\text{pw}}$ during August 2025 show strong evidence of evaporative enrichment (Arisha Imran, personal communication 2025). Contemporary data would suggest the water balance of these ponds is strongly responsive to water loss via evaporation. Thus, records of pond desiccation in response to past climate (i.e. the LIA) are likely to be captured in carbonate-inferred $\delta^{18}\text{O}_{\text{pw}}$. 3) C/N ratios should be measured on the sediment core from SK 31 to further test the utility of this approach to detect possible desiccation horizons. The carbonate-inferred $\delta^{18}\text{O}_{\text{pw}}$ record identifies this pond desiccated in the mid- to late 1700s and so this provides an opportunity to assess how reliably measurement of C/N ratios capture known episodes of pond desiccation. 4) C/N ratios should also be measured on the sediment core from SK 26 to detect possible desiccation events via vertical seepage, as was achieved at SK 58. Desiccation may have occurred in the past at SK 26 (as it did at SK 31 and SK 58 during the LIA) by vertical seepage which could not be detected using measurements of carbonate-inferred $\delta^{18}\text{O}_{\text{pw}}$. 5) Explore the use of alternative measurements to detect desiccation horizons in sediment cores, even when ponds desiccate via vertical seepage. For example, hyperspectral imaging (HIS) is a non-destructive in-situ biogeochemical analysis of sediment cores to track past environmental conditions and processes (Zander et al., 2022). Backscattered electron (BSE) imaging has been previously used as a map of porosity (Kemp et al., 2001) and may be able to detect changes in mineralogy of sediment cores. X-ray radiography and densitometry uses sediment structure and density variations to interpret changes in environmental conditions (Smol, 2001). If pond desiccation produces a distinct mineral crust, then this method may be able to detect past desiccation events. A Russian peat corer may be a useful device to collect sediment cores which better preserve the stratigraphy and allow for desiccation horizons to be visualized more readily than was possible with the gravity corer used in this study. For example, cracks and thin strata of denser sediment or strata with a crumbly texture may be detected using a Russian peat corer that indicate episodes of very shallow water or near-desiccation (e.g., Wolfe et al. 2005).

Table 2. Ponds recommended for paleolimnological study based on observations of desiccation during 2023 and spring 2024 (Neary, 2025). Ponds that desiccated during 2023-2024 were also observed to be desiccated in August 2025 (Arisha Imran, personal communication 2025). Also included are ponds where sediment cores were collected during September 2022 but have not been analyzed for carbonate-inferred $\delta^{18}\text{O}_{\text{pw}}$ (SK 15, SK 43, SK 51).

Pond ID	Hydrological classification	Starting depth in m (May 2022)	Desiccated during 2023?	May 2024 depth (m)	Sep 2024 depth (m)
SK 2	Weak	0.60	Yes	0.00	0.00
SK 15	Moderate	0.70	No	0.30	0.12
SK 19	Weak	0.40	Yes	0.02	0.00
SK 28	Weak	0.50	Yes	0.00	0.00
SK 30	Moderate	0.23	Yes	0.03	0.00
SK 32	Weak	0.60	Yes	0.00	0.00
SK 41	Moderate	0.80	No	0.00	0.00
SK 43	Moderate	0.30	No	0.28	0.20
SK 47	Moderate	0.20	Yes	0.00	0.00
SK 51	Strong	0.70	No	0.28	0.03
SK 57	Moderate	0.36	Yes	0.00	0.00
SK 58	Strong	0.58	Yes	0.00	0.00

References

- Allen, R.P. (1956). A report on the Whooping Crane's Northern Breeding Grounds, A supplement to Research Report No.3, The Whooping Crane. Edited by Robert Porter Allen. National Audubon Society, 1130 Fifth Ave., New York 28, N.Y. Vol.21(3) p. 378–379. <https://www.jstor.org/stable/3796562>.
- Anderson, L., Birks, J., Rover, J. & Guldager, N. (2013). Controls on recent Alaskan lake changes identified from water isotopes and remote sensing. *Geophysical Research Letters*, 40, 3413-3418. <https://doi.org/10.1002/grl.50672>
- Appleby, P. G., & Oldfield, F. (1978). The calculation of lead-210 dates assuming a constant rate of supply of unsupported ^{210}Pb to the sediment. *Catena*, 5(1), 1-8. [https://doi.org/10.1016/S0341-8162\(78\)80002-2](https://doi.org/10.1016/S0341-8162(78)80002-2)
- Appleby, P.G. (2001). Chronostratigraphic techniques in recent sediments. In W. M. Last & J. P. Smol (Eds.), *Tracking environmental change using lake sediments (Developments in paleoenvironmental research). Volume 1: Basin analysis, coring, and chronological techniques*. (pp. 171-203). Springer, Dordrecht.
- Austin, J.E., Hayes, M.A. & Barzen, J.A. (2019). Revisiting the historic distribution and habitats of the Whooping Crane. Chapter 3 in *Whooping Cranes: Biology and conservation. Biodiversity of the world: conservation from genes to landscapes*. (pp. 25–88). Academic Press, San Diego, California, USA. <https://doi.org/10.1016/B978-0-12-803555-9.00003-7>.
- Bethke, C.M. & Johnson, T.M. (2008). Groundwater age and groundwater age dating. *Annual Review of Earth and Planetary Sciences*, 36(1), 121-152. <https://doi.org/10.1146/annurev.earth.36.031207.124210>
- Blake, E. (2023, November 6). Great Slave Lake water levels at record low. Cabin Radio. Retrieved from <https://cabinradio.ca/160102/news/environment/great-slave-lake-water-levels-at-record-low/>

- Bouchard, F., MacDonald, L.A., Turner, K.W., Thienpont, J.R., Medeiros, A.S., Biskaborn, B.K., Korosi, J., Hall, R.I., Pienitz, R. & Wolfe, B.B. (2017). Paleolimnology of thermokarst lakes: a window into permafrost landscape evolution. *Arctic Science*, 3, 91-117. <https://doi.org/10.1139/as-2016-0022>
- Bowen, G.J. & Wilkinson, B. (2002). Spatial distribution of $\delta^{18}\text{O}$ in meteoric precipitation. *Geology*, 30(4), 315–318. [https://doi.org/10.1130/0091-7613\(2002\)0302.0.CO;2](https://doi.org/10.1130/0091-7613(2002)0302.0.CO;2)
- Boyce, M.S., Lelle, S.R. & Johns, B. (2005) Whooping Crane recruitment enhanced by egg removal. *Biological Conservation*, 126 (3), 395– 401. <https://doi.org/10.1016/j.biocon.2005.06.011>
- Canadian Wildlife Service and US Fish and Wildlife Service (CWS–USFWS). (2007). International recovery plan for the whooping crane. Ottawa: Recovery of Nationally Endangered Wildlife (RENEW), and U.S. Fish and Wildlife Service, Albuquerque, New Mexico. <https://www.nrc.gov/docs/ml1118/ml111880004.pdf>.
- Chavez-Ramirez, F. & Wehtje, W. (2012). Potential impact of climate change scenarios on whooping crane life history. *Wetlands*, 32, 11–20. <https://doi.org/10.1007/s13157-011-0250-z>
- Cohen, A.S. (2020). *Paleolimnology: The History and Evolution of Lake Systems*. Oxford University Press. <https://doi.org/10.1093/oso/9780195133530.001.0001>
- Deison, R., Smol, J.P., Kokelj, S.V., Pisaric, M.F.J., Kimpe, L.E., Poulain, A.J., Sanei, H., Thienpont, J.R. & Blais, J.M. (2012). Spatial and temporal assessment of mercury and organic matter in thermokarst affected lakes of the Mackenzie Delta Uplands, NT, Canada. *Environmental Science & Technology*, 46(16), 8748-8755. <https://doi.org/10.1021/es300798w>
- Déri-Takács, J., Rostron, B., Mendoza, C. & Mádl-Szőnyi, J. (2022). Hydrogeochemical characteristics refine the conceptual model of groundwater flow in Wood Buffalo National Park, Canada. *Water*, 14(6), 965. <https://doi.org/10.3390/w14060965>

- Edwards, T.W.D. & McAndrews, J.H. (1989). Paleohydrology of a Canadian Shield lake inferred from ^{18}O in sediment cellulose. *Canadian Journal of Earth Sciences*, 26(9), 1850-1859. <https://doi.org/10.1139/e89-158>
- Environment Canada. (2007). Recovery Strategy for the Whooping Crane (*Grus americana*) in Canada. Species at Risk Act Recovery Strategy Series. Environment Canada, Ottawa. https://www.sararegistry.gc.ca/virtual_sara/files/plans/rs_whooping_crane_final_1007_e.pdf.
- Finger-Higgins, R.A., Chipman, J.W., Lutz, D.A., Culler, L.E., Virginia, R.A. & Ogden, L.A. (2019). Changing lake dynamics indicate a drier Arctic in western Greenland. *Journal of Geophysical Research: Biogeosciences*, 124(4), 870-883. <https://doi.org/10.1029/2018JG004879>
- Gibson J.J., Eby P., Birks S.J., Twitchell C., Gray C. & Kariyeva J. (2022). Isotope-based water balance assessment of open water wetlands across Alberta: Regional trends with emphasis on the oil sands region. *Journal of Hydrology: Regional Studies*, 40. <https://doi.org/10.1016/j.ejrh.2022.101036>
- Gibson, J.J. & Reid, R. (2014). Water balance along a chain of tundra lakes: A 20-year isotopic perspective. *Journal of Hydrology* 519, 2148-2164. <https://doi.org/10.1016/j.jhydrol.2014.10.011>
- Glew, J.R. (1991). Miniature gravity corer for recovering short sediment cores. *Journal of Paleolimnology* 5, 285-287. <https://doi.org/10.1007/BF00200351>
- Government of the Northwest Territories, Department of Environment and Climate Change. (2023, November 3). NWT water monitoring bulletin. Retrieved from <https://www.gov.nt.ca/ecc/en/services/water-monitoring-bulletins>
- Heiri, O., Lotter, A. & Lemcke, G. (2001). Loss on ignition as a method for estimating organic and carbonate content in sediments: reproducibility and comparability of results. *Journal of Paleolimnology*, 25(1). <https://doi.org/10.1023/A:1008119611481>
- Heyng, A.M., Mayr, C., Lucke, A., Moschen, R., Holger, H., Striewski, B. & Bauersachs, T. (2015). Middle and Late Holocene paleotemperatures reconstructed from oxygen isotopes

and GDGTs of sediments from Lake Pupuke, New Zealand. *Quaternary International*, 374, 3-14. <https://doi.org/10.1016/j.quaint.2014.12.040>

International Crane Foundation (ICF). (2019). Species Review: Whooping Crane (*Grus americana*). Baraboo, Wisconsin, USA. https://savingcranes.org/wpcontent/uploads/2022/05/crane_conservation_strategy_whooping_crane.pdf.

Kim, S.T. & O'Neil, J.R. (1997). Equilibrium and nonequilibrium oxygen isotope effects in synthetic carbonates. *Geochimica et cosmochimica acta*, 61(16), 3461-3475. [https://doi.org/10.1016/S0016-7037\(97\)00169-5](https://doi.org/10.1016/S0016-7037(97)00169-5)

Krammer, K. & Lange-Bertalot, H. (1991). Bacillariophyceae. 3. Teil: Centrales, Fragilariaceae, Eunotiaceae. In Ettl, H., Gerloff, J., Heynig, H. & Mollenhauer, D. (Eds.). *Süßwasserflora von Mitteleuropa*. (2(3), pp. 1-576). Gustav Fisher Verlag, Stuttgart, Germany.

Kuyt, E. (1981). Population status, nest site fidelity and breeding habitat of whooping cranes. In: Lewis, J.C. and Masatomi, H. (Eds.), *Crane Research Around the World: Proceedings of the International Crane Symposium*. Sapporo, Japan, (pp. 119–125). <https://archive.org/details/populationstatus00kuyt/page/120/mode/2up>

Kuyt, E. (1992). Aerial radio-tracking of whooping cranes migrating between Wood Buffalo National Park and Aransas National Wildlife Refuge, 1981-84. Occasional Paper 74, Canadian Wildlife Service, Ottawa, Canada. <http://parkscanadahistory.com/wildlife/paper-74.pdf>.

Kuyt, E. (1993). Whooping Crane, *Grus americana*, home range and breeding range expansion in Wood Buffalo National Park, 1970-1991. *The Canadian Field-Naturalist*, 107(1), 1–12. <https://www.biodiversitylibrary.org/item/108204#page/1/mode/1up>

Kuyt, E., Barry, S.J. & Johns, B.W. (1992). Below average whooping crane production in Wood Buffalo National Park during drought years 1990 and 1991. *Blue Jay*, 50(4), 225–229. <https://doi.org/10.29173/bluejay5097>

- Lacelle, D., Fontaine, M., Forest, A.P. & Kokelj, S. (2014). High-resolution stable water isotopes as tracers of thaw unconformities in permafrost: A case study from western Arctic Canada. *Chemical Geology*, 368, 85-96. <https://doi.org/10.1016/j.chemgeo.2014.01.005>
- Lachniet, M.S., Lawson, D.E. & Sloat, A.R. (2012). Revised ¹⁴C dating of ice wedge growth in interior Alaska (USA) to MIS 2 reveals cold paleoclimate and carbon recycling in ancient permafrost terrain. *Quaternary Research*, 78(2), 217-225. <https://doi.org/10.1016/j.yqres.2012.05.007>
- Leng, M.J. & Marshall, J.D. (2003). Paleoclimate interpretation of stable isotope data from lake sediment archives. *Quaternary Science Review*, 23(7-8), 811-831. <https://doi.org/10.1016/j.quascirev.2003.06.012>
- Li, H., Liu, X., Tripathi, A., Feng, S., Elliott, B., Whicker, C., Arnold, A. & Kelley, A.M. (2020). Factors controlling the oxygen isotopic composition of lacustrine authigenic carbonates in Western China: implications for paleoclimate reconstructions. *Scientific Reports*, 10(1), 16370. <https://doi.org/10.1038/s41598-020-73422-4>
- Luckman, B.H. & Watson, E. (1999). Precipitation reconstruction in the southern Canadian Cordillera. In Preprints of the 10th Symposium on Global Change Studies, 79th Annual Meeting of the American Meteorological Society (pp. 296-299). Dallas, TX, January 10-15.
- Luckman, B.H. (2000). The Little Ice Age in the Canadian Rockies. *Geomorphology*, 32, 357-384. [https://doi.org/10.1016/S0169-555X\(99\)00104-X](https://doi.org/10.1016/S0169-555X(99)00104-X)
- McNaughton, D. (1991). Final report on hydrological investigations Wood Buffalo National Park 1985 to 1990. Wood Buffalo National Park. Ft. Smith, NT, Canada. <http://parkscanadahistory.com/publications/woodbuffalo/hydrology-1991.pdf>
- Meyer, H., Schirrmeister, L., Yoshikawa, K., Opel, T., Wetterich, S., Hubberten, H.W. & Brown, J. (2010). Permafrost evidence for severe winter cooling during the Younger Dryas in northern Alaska. *Geophysical Research Letters*, 37, L03501. <https://doi.org/10.1029/2009GL041013>, 2010

- Meyers, P. A., & Teranes, J. L. (2001). Sediment organic matter. In Last, W., & Smol, J.P. (Eds.), *Tracking Environmental Change Using Lake Sediments* (pp. 240-267). Dordrecht: Kluwer Academic Publishers.
- Meyers, P.A. (1994). Preservation of elemental and isotopic source identification of sedimentary organic matter. *Chemical Geology*, *114*(3-4), 289-302. [https://doi.org/10.1016/0009-2541\(94\)90059-0](https://doi.org/10.1016/0009-2541(94)90059-0)
- Michelutti, N. & Smol, J.P. (2016). Visible spectroscopy reliably tracks trends in paleo-production. *Journal of Paleolimnology* *56*, 253-265. <https://doi.org/10.1007/s10933-016-9921-3>
- Mikisew Cree First Nation (MCFN). (2014). Petition to the World Heritage Committee requesting inclusion of Wood Buffalo National Park on the list of World Heritage in danger. https://cpawsnab.org/wpcontent/uploads/2018/03/Mikisew_Petition_respecting_UNESCO_Site_256_-_December_8_2014.pdf
- Neary, L.K. (2025). Development and application of aquatic ecosystem monitoring approaches for the Peace-Athabasca Delta and Whooping Crane Nesting Region of Wood Buffalo National Park [Doctoral dissertation, University of Waterloo]. UW Space. <https://hdl.handle.net/10012/21659>
- Oldfield, F. & Appleby, P.G. (1984). Empirical testing of ^{210}Pb -dating models for lake sediments. Leicester University Press.
- Osborne, E., Richter-Menge, J., & Jeffries, M. (2018). Arctic Report Card 2018. <https://www.arctic.noaa.gov/Report-Card>
- Peng, X., Shi, T., Chen, Y. & Gao, W. (2014). Estimating soil organic carbon using VIS/NIR spectroscopy with SVMR and SPA methods. *Remote Sensing* *6*(4), 2699-2717. <https://doi.org/10.3390/rs6042699>
- Pham, S.V., Leavitt, P.R., McGowan, S., Wissel, B. & Wassenaar, L.I. (2009). Spatial and temporal variability of prairie lake hydrology as revealed using stable isotopes of hydrogen and oxygen. *Limnology and Oceanography*, *54*(1), 101-118. <https://doi.org/10.4319/lo.2009.54.1.0101>
- Poage, M.A. & Chamberlain, C.P. (2001). Empirical relationships between elevation and the stable isotope composition of precipitation and surface waters: considerations for studies

- of paleoelevation change. *American Journal of Science*, 301(1), 1-15. <https://doi.org/10.2475/ajs.301.1.1>
- Prahl, F.G., Bennett, J.T. & Carpenter, R. (1980). The early diagenesis of aliphatic hydrocarbons and organic matter in sedimentary particulates from Dabob Bay, Washington. *Geochimica et Cosmochimica Acta*, 44(12), 1967-1976. [https://doi.org/10.1016/0016-7037\(80\)90196-9](https://doi.org/10.1016/0016-7037(80)90196-9)
- Prowse, T.D., Beltaos, S., Gardner, J.T., Gibson, J.J., Granger, R.J., Leconte, R., Peters, D.L., Pietroniro, A., Romolo, A. & Toth, B. (2006). Climate change, flow regulation and land-use effects on the hydrology of the Peace-Athabasca-Slave System; Findings from the Northern Rivers Ecosystem Initiative. *Environmental Monitoring and Assessment*, 113, 167-197. <https://doi.org/10.1007/s10661-005-9080-x>
- Reavie, E.D. & Smol, J.P. (1998). Epilithic diatoms of the St Lawrence River and their relationships to water quality. *Canadian Journal of Botany*, 76(2). <https://doi.org/10.1139/b97-173>
- Ripple, W.J., Wolf, C., Gregg, J.W., Rockström, J., Newsome, T.M., Law, B.E., Marques, L., Lenton, T.M., Xu, C., Huq, S., Simons, L. & King, D.A. (2023). The 2023 state of the climate report: Entering uncharted territory. *BioScience*, 73 (12), 841-850. <https://doi.org/10.1093/biosci/biad080>
- Ruhland, K., Priesnitz, A. & Smol, J.P. (2003). Paleolimnological evidence from diatoms for recent environmental changes in 50 lakes across Canadian Arctic treeline. *Arctic, Antarctic and Alpine Research*, 35(1), 110-123. [https://doi.org/10.1657/1523-0430\(2003\)035\[0110:PEFDFR\]2.0.CO;2](https://doi.org/10.1657/1523-0430(2003)035[0110:PEFDFR]2.0.CO;2)
- Ruhland, K.M. & Smol, J.P. (2002). Freshwater diatoms from the Canadian Arctic treeline and development of paleolimnological inference models. *Journal of Phycology*, 38(2), 249-264. <https://doi.org/10.1046/j.1529-8817.2002.01129.x>
- Schindler D.W. & Smol J.P. (2006). Cumulative effects of climate warming and other human activities on freshwaters of Arctic and Subarctic North America. *Ambio*, 35(4): 160–168. [https://doi.org/10.1579/0044-7447\(2006\)35\[160:CEOCWA\]2.0.CO;2](https://doi.org/10.1579/0044-7447(2006)35[160:CEOCWA]2.0.CO;2)

- Schindler, D.W. & Donahue, W.F. (2006). An impending water crisis in Canada's western prairie provinces. *Proceedings of the National Academy of Sciences of the United States of America*, 103(19), 7210-7216. <https://doi.org/10.1073/pnas.0601568103>
- Smol, J.P. & Douglas, M.S.V. (2007). Crossing the final ecological threshold in high Arctic ponds. *Proceedings in the National Academy of Sciences U.S.A.*, 104(30), 1239–12397. <https://doi.org/10.1073/pnas.0702777104>
- Smol, J.P. (2010). The power of the past: using sediments to track the effects of multiple stressors on lake ecosystems. *Freshwater Biology* 55(1), 43-59. <https://doi.org/10.1111/j.1365-2427.2009.02373.x>
- Smol, J.P. (2016). Arctic and sub-Arctic shallow lakes in a multiple-stressor world: A paleoecological perspective. *Hydrobiologia*, 778, 253–272. <https://doi.org/10.1007/s10750-015-2543-3>
- Smol, J.P., (2008). Pollution of lakes and rivers: a paleoenvironmental perspective. Blackwell, Oxford.
- Smol, J.P., Birks, H.J.B., Last, W.M. (Eds.) (2001). *Tracking Environmental Change Using Lake Sediments*. Springer. <https://doi.org/10.1007/0-306-47671-1>
- Swarzenski, P.W. (2014). ²¹⁰Pb Dating. Encyclopedia of scientific dating methods (pp. 1-11). https://link.springer.com/rwe/10.1007/978-94-007-6326-5_236-1
- Telford, J.V., Kay, M.L., Heide, H.V., Wiklund, J.A., Owca, T.J., Faber J.A., Wolfe, B.B. & Hall, R.I. (2021). Building upon open-barrel corer and sectioning systems to foster the continuing legacy of John Glew. *Journal of Paleolimnology*, 65, 271-277. <https://doi.org/10.1007/s10933-020-00162-w>
- Timoney, K. (1999). The habitat of nesting whooping cranes. *Biological Conservation*, 89(2), 189–197. [https://doi.org/10.1016/S0006-3207\(98\)00121-9](https://doi.org/10.1016/S0006-3207(98)00121-9)
- Timoney, K., Zoltai, S.C. & Goldsborough, L.G. (1997). Boreal diatom ponds: A rare wetland associated with nesting whooping cranes. *Wetlands*, 17(4), 539–551. <https://doi.org/10.1007/BF03161520>

- Tondu, J.M.E., Turner, K.W., Wolfe, B.B., Hall, R.I., Edwards, T.W.D. & McDonald, I. (2013) Using water isotope tracers to develop the hydrological component of a long-term aquatic ecosystem monitoring program for a northern lake-rich landscape. *Arctic, Antarctic and Alpine Research*, 45(4), 594-614. <https://doi.org/10.1657/1938-4246-45.4.594>
- Tsui, P.C. & Cruden, D.M. (1984). Deformation associated with gypsum karst in the Salt River Escarpment, northeastern Alberta. *Canadian Journal of Earth Sciences* 21(8), 949-959. <https://doi.org/10.1139/e84-099>
- Tyson, R.V. (1995). Bulk Geochemical Characterization and Classification of Organic Matter: Carbon:Nitrogen Ratios and Lignin-Derived Phenols. (pp. 383-394). Springer, Dordrecht.
- Van Exem, A., Debret, M., Copard, Y., Vanniere, B., Sabatier, P., Marcotte, S., Laignel, B., Reyss, J.L. & Desmet, M. (2017). Hyperspectral core logging for fire reconstruction studies. *Journal of Paleolimnology* 59, 297-308. <https://doi.org/10.1007/s10933-017-0009-5>
- Vonk, J.E., Sanchez-Garcia, L., Dongen, B.E., Alling, V., Kosmach, D., Charkin, A., Semiletov, I.P., Dudarev, O.V., Shakhova, N., Roos, P., Eglinton, T.I., Andersson, A. & Gustafsson, O. (2012). Activation of old carbon by erosion of coastal and subsea permafrost in Arctic Siberia. *Nature*, 489, 137-140. <https://doi.org/10.1038/nature11392>
- Vonk, J.E., Tank, S.E., Bowden, W.B., Laurion, I., Vincent, W.F., Alekseychik, P., Amyot, M., Billet, M.F., Canario, J., Cory, R.M., Deshpande, B.N., Helbig, M., Jammet, M., Karlsson, J., Larouche, J., MacMillan, G., Rautio, M., Walter Anthony, K.M., & Wickland, K.P. (2015). Reviews and syntheses: Effects of permafrost thaw on Arctic aquatic ecosystems. *Biogeosciences*, 12(23), 7129-7167. <https://doi.org/10.5194/bg-12-7129-2015>
- Wagner, Z.C., Steinman, B.A., Finkenbinder, M.S., Abbott, M.B. & Stansell, N.D. (2025). A 10,000-year lake-sediment based reconstruction of precipitation isotope values in the Canadian Rocky Mountains. *Quaternary Science Reviews*, 356. <https://doi.org/10.1016/j.quascirev.2025.109255>
- Wan, C., Gibson, J.J. & Peters, D.L. (2020). Isotopic constraints on water balance of tundra lakes and watersheds affected by permafrost degradation, Mackenzie Delta region, Northwest

- Territories, Canada. *Science of the Total Environment*, 731. <https://doi.org/10.1016/j.scitotenv.2020.139176>
- Wan, G.J., Chen, J.A., Wu, F.C., Xu, S.Q., Bai, Z.G., Wan, E.Y., Wang, C.S., Huang, R.G., Yeager, K.M. & Santschi, P.H. (2005). Coupling between $^{210}\text{Pb}_{\text{ex}}$ and organic matter in sediments of a nutrient-enriched lake: An example from Lake Chenghai, China. *Chemical Geology*, 224(4). <https://doi.org/10.1016/j.chemgeo.2005.07.025>
- Wang, W., Lee, X., Xiao, W., Liu, S., Schultz, N., Wang, Y., Zhang, M. & Zhao, L. (2018). Global lake evaporation accelerated by changes in surface energy allocation in a warmer climate. *Nature Geoscience*, 11(6), 410-414. <https://doi.org/10.1038/s41561-018-0114-8>
- Watson, E. & Luckman, B.H. (2001). Dendroclimatic reconstruction of precipitation for sites in the southern Canadian Rockies. *The Holocene*, 11(2). <https://doi.org/10.1191/0959683016724758>
- WHC/IUCN. (2017). Reactive monitoring mission to Wood Buffalo National Park, Canada; mission report, March 2017. *United Nations Educational, Scientific and Cultural Organization*. <http://whc.unesco.org/en/documents/156893>
- Wilcox, E.J., Wolfe, B.B. & Marsh, P. (2022). Assessing the influence of lake and watershed attributes on snowmelt bypass at thermokarst lakes. *Hydrology and Earth System Sciences*, 26(23), 6185-6205. <https://doi.org/10.5194/hess-26-6185-2022>
- Williams, O. (2024, May 8). The data behind Yellowknife Bay's wild lack of water. Cabin Radio. <https://cabinradio.ca/182130/news/yellowknife/the-data-behind-yellowknife-bays-wild-lack-of-water/>
- Williamson, C.E., Saros, J.E., Warwick, V.F. & Smol, J.P. (2009). Lakes and reservoirs as sentinels, integrators, and regulators of climate change. *Limnology and Oceanography*, 54(6), 2273-2282. https://doi.org/10.4319/lo.2009.54.6_part_2.2273
- Wolfe, B.B., Edwards, T.W.D., Hall R.I. & Johnston J.W. (2011). A 5200-year record of freshwater availability for regions in western North America fed by high-elevation runoff. *Geophysical Research Letters*, 38(11): L11404. <https://doi.org/10.1029/2011GL047599>

- Wolfe, B.B., Edwards, T.W.D., Elgood, R.J. & Beuning, K.R.M. (2001). Carbon and Oxygen Isotope Analysis of Lake Sediment Cellulose: Methods and Applications. In: Last, W.M., Smol, J.P. (eds) *Tracking Environmental Change Using Lake Sediments*. Developments in Paleoenvironmental Research, vol 2. Springer, Dordrecht. https://doi.org/10.1007/0-306-47670-3_14
- Wolfe, B.B., Karst-Riddoch, T.L., Vardy, S.R., Falcone, M.D., Hall, R.I. & Edwards, T.W.D. (2005). Impacts of climate and river flooding on the hydroecology of a floodplain basin, Peace–Athabasca Delta, Canada: A.D. 1700–present. *Quaternary Research*, 64, 147–162. <https://doi.org/10.1016/j.yqres.2005.05.001>
- Wolfe, B.B., Light, E.M., Macrae, M.L., Hall, R.I., Eichel, K., Jasechko, S., White, J., Fishback, L. & Edwards, T.W.D. (2011). Divergent hydrological responses to 20th century climate change in shallow tundra ponds, western Hudson Bay Lowlands. *Geophysical Research Letters*, 38(23), L23402. <https://doi.org/10.1029/2011GL049766>
- Wood Buffalo National Park (WBNP). (2019). World Heritage Site Action Plan. Parks Canada. <https://www.pc.gc.ca/en/pn-np/nt/woodbuffalo/info/action>.
- Woolway, R.I., Sharma, S. & Smol, J.P. (2022). Lakes in hot water: the impacts of a changing climate on aquatic ecosystems. *BioScience*, 72(11), 1050–1061. <https://doi.org/10.1093/biosci/biac052>
- Yin, L., Hou, G., Su, X., Wang, D., Dong, J., Hao, Y. & Wang, X. (2010). Isotopes (δD and $\delta^{18}\text{O}$) in precipitation, groundwater and surface water in the Ordos Plateau, China: implications with respect to groundwater recharge and circulation. *Hydrogeology Journal*, 19, 429–443. <https://doi.org/10.1007/s10040-010-0671-4>
- Zabel, N.A., Soliguin, A.M., Wiklund, J.A., Birks, S.J., Gibson, J.J., Fan, X., Wolfe, B.B. & Hall, R.I. (2022). Paleolimnological assessment of past hydro-ecological variation at a shallow hardwater lake in the Athabasca Oil Sands Region before potential onset of industrial development. *Journal of Hydrology: Regional Studies*, 39. <https://doi.org/10.1016/j.ejrh.2021.100977>

Zander, P.D., Wienhues, G. & Grosjean, M. (2022). Scanning hyperspectral imaging for in situ biogeochemical analysis of lake sediment cores: review of recent developments. *Journal of Imaging* 8(3). <https://doi.org/10.3390/jimaging8030058>

Zhang, X., Vincent, L.A., Hogg, W.D. & Niitsoo, A. (2000). Temperature and precipitation trends in Canada during the 20th century. *Atmosphere-Ocean*, 38(3), 395–429. <https://doi.org/10.1080/07055900.2000.9649654>

Appendices

Appendix A – Contemporary water isotope compositions

Table A1: Measured water isotope compositions ($\delta^{18}\text{O}$, $\delta^2\text{H}$) in 2022 and spring 2023 at pond SK 31.

Date	$\delta^{18}\text{O}$ (‰ VSMOW)	$\delta^2\text{H}$ (‰ VSMOW)
May 23 2023	-12.79	-128.85
Sep 15 2022	-6.94	-101.73
Aug 9 2022	-8.39	-109.66
May 29 2022	-16.53	-143.27

Table A2: Measured water isotope compositions ($\delta^{18}\text{O}$, $\delta^2\text{H}$) in 2022 and spring 2023 at pond SK 26.

Date	$\delta^{18}\text{O}$ (‰ VSMOW)	$\delta^2\text{H}$ (‰ VSMOW)
May 23 2023	-15.39	-137.71
Sep 15 2022	-16.23	-139.21
Aug 9 2022	-16.25	-141.95
May 29 2022	-18.68	-152.06

Table A3: Measured water isotope compositions ($\delta^{18}\text{O}$, $\delta^2\text{H}$) in 2022 and spring 2023 at pond SK 58.

Date	$\delta^{18}\text{O}$ (‰ VSMOW)	$\delta^2\text{H}$ (‰ VSMOW)
May 24 2023	-15.30	-141.36
Sep 17 2022	-10.93	-118.06
Aug 10 2022	-14.34	-133.63
May 29 2022	-18.49	-151.00

Appendix B – Radiometric dating of sediment cores

Table B1: Measured ^{210}Pb , ^{137}Cs and ^{226}Ra values and CRS dates for the SK 31 sediment core.

Midpoint depth (cm)	Total ^{210}Pb (dpm/g)	^{210}Pb error (1 std. dev.)	^{137}Cs (dpm/g)	^{137}Cs error (1 std. dev.)	^{226}Ra (dpm/g)	^{226}Ra error (1 std. dev.)	Midpoint depth CRS dates with linear extrapolation
0.25	12.8488	1.4092	0.3635	0.3023	0.1604	0.1178	2022.60
0.75	15.5349	1.6764	0.2771	0.3861	1.1193	0.2173	2022.37
1.25	21.1641	1.7779	0.1891	0.4096	0.0104	0.0118	2022.04
1.75	25.1798	1.8823			0.8542	0.1965	2021.58
2.25	25.2345	1.7476	0.3840	0.3154	0.6415	0.1552	2020.91
2.75	24.1748	2.3095					2020.19
3.25	23.1452	1.5098	0.6017	0.2176	0.4649	0.2035	2019.31
3.75	22.5925	1.9120					2018.10
4.25	22.0486	1.1730	0.4477	0.1694	0.5007	0.1097	2016.73
4.75	21.2600	1.6590					2015.33
5.25	20.4904	1.1731	0.3383	0.1610	0.1116	0.0696	2013.83
5.75	19.3227	1.4626					2012.20
6.25	18.2002	0.8735	0.4331	0.1388	0.4736	0.0918	2010.45
6.75	17.0033	1.3143					2008.73
7.25	15.8601	0.9820	0.7355	0.1366	0.6542	0.1167	2007.10
7.75	15.0318	1.2440					2005.58
8.25	14.2328	0.7636	0.5889	0.1172	0.8283	0.1563	2004.09
8.75	12.1200	0.9541					2002.32
9.25	10.2274	0.5719	0.5127	0.0868	0.6779	0.0849	2000.55
9.75	8.6786	0.7309					1998.87
10.25	7.2946	0.4550	0.4644	0.0765	0.7377	0.0797	1997.35
10.75	5.4987	0.5921					1995.96
11.25	4.0249	0.3789	0.3561	0.0687	0.6239	0.0714	1994.67
11.75	3.0721	0.4972					1993.58
12.25	2.2830	0.3219	0.2514	0.0619	0.5370	0.0627	1992.74
12.75	3.0806	0.3136					1991.82
13.25	3.3104	0.2772	0.2246	0.0467	0.2895	0.0427	1990.69
13.75	5.5672	0.3500					1989.22
14.25	1.8242	0.2594	0.1588	0.0451	0.4630	0.0495	1987.95
14.75	2.4653	0.4010					1987.09
15.25	3.2415	0.3058	0.2109	0.0506	0.4443	0.0523	1985.95
15.75	3.5798	0.4336					1984.37
16.25	3.9408	0.3074	0.2033	0.0491	0.5298	0.0552	1982.55
16.75	4.1834	0.4734					1980.40
17.25	4.4356	0.3600	0.2489	0.0555	0.5931	0.0631	1977.77
17.75	4.6904	0.5015					1974.93
18.25	4.9548	0.3492	0.1672	0.0550	0.5522	0.0599	1971.64
18.75	6.3729	0.5256					1967.66
19.25	8.0387	0.3928	0.3272	0.0575	0.5763	0.0616	1962.74
19.75	4.8994	0.4612					1957.61
20.25	2.7081	0.2417	0.1712	0.0426	0.4583	0.0471	1953.07
20.75	1.6507	0.3300					1949.66
21.25	0.9125	0.2247	0.0793	0.0409	0.3520	0.0479	1947.78
21.75	1.0348	0.3116					1946.37
22.25	1.1675	0.2159	0.0539	0.0398	0.3283	0.0393	1943.92
22.75	1.1808	0.3032					1941.02
23.25	1.1941	0.2129	0.1267	0.0385	0.4141	0.0423	1938.53
23.75	1.2130	0.3206					1935.81
24.25	1.2321	0.2397	0.1743	0.0429	0.4207	0.0464	1932.64
24.75	1.1818	0.3305					1929.58

25.25	1.1329	0.2276	0.1840	0.0408	0.4797	0.0462	1926.66
25.75	1.2352	0.3204					1923.39
26.25	1.3436	0.2256	0.1939	0.0400	0.3895	0.0433	1919.47
26.75	1.2666	0.3504					1915.36
27.25	1.1926	0.2681	0.2320	0.0472	0.5946	0.0550	1910.80
27.75	0.9984	0.3610					1906.33
28.25	0.8266	0.2417	0.1550	0.0443	0.3956	0.0459	1902.12
28.75	0.7340	0.3234					1898.21
29.25	0.6486	0.2148	0.1692	0.0395	0.3568	0.0492	1894.88
29.75	0.6068	0.3090					1891.90
30.25	0.5670	0.2221	0.1417	0.0410	0.3413	0.0469	1888.92
30.75	0.5842	0.3154					1885.74
31.25	0.6018	0.2239	0.0752	0.0421	0.4772	0.0464	1882.74
31.75	0.5184	0.3862					1879.80
32.25	0.4430	0.3147	0.0696	#DIV/0!			1876.88
32.75	0.3754	0.3846					1874.11
33.25	0.3150	0.2211			0.2984	0.0388	1871.48
33.75							1868.73
34.25							1866.24
34.75							1863.84
35.25	0.3171	0.2438	0.0632	0.0475	0.3163	0.0416	1861.30
35.75							1858.83
36.25							1856.38
36.75							1853.81
37.25	0.3960	0.2362	0.0903	0.0461	0.4423	0.0479	1851.37
37.75							1849.09
38.25							1846.86
38.75							1844.59
39.25							1842.39
39.75							1840.23
40.25							1838.17
40.75							1836.11
41.25							1834.04
41.75							1831.95
42.25							1829.71
42.75							1827.61
43.25							1825.70
43.75							1823.65
44.25							1821.57
44.75							1819.64
45.25							1817.63
45.75							1815.60
46.25							1813.61
46.75							1811.42
47.25							1809.10
47.75							1806.82
48.25							1804.38
48.75							1801.78
49.25							1799.26
49.75							1796.69
50.25							1793.90
50.75							1790.99
51.25							1788.17
51.75							1785.16
52.25							1782.28
52.75							1779.89
53.25							1777.21
53.75							1773.91
54.25							1770.65

54.75							1767.50
55.25							1764.73
55.75							1762.39
56.25							1759.65
56.75							1756.57
57.25							1753.42
57.75							1750.33
58.25							1747.17
58.75							1744.19
59.25							1741.55
59.75							1738.77
60.25							1735.97
60.75							1732.91
61.25							1729.69
61.75							1726.53
62.25							1723.28
62.75							1720.49
63.25							1718.10
63.75							1715.22
64.25							1711.80
64.75							1708.40
65.25							1705.40
65.75							1702.32
66.25							1699.01
66.75							1695.60
67.25							1692.01
67.75							1688.57
68.25							1685.10
68.75							1681.81
69.25							1678.47
69.75							1674.90
70.25							1671.51
70.75							1668.12
71.25							1664.69
71.75							1661.54
72.25							1658.56
72.75							1655.17
73.25							1652.04
73.75							1649.37
74.25							1646.40
74.75							1643.24
75.25							1640.25
75.75							1637.32
76.25							1634.27
76.75							1631.34
77.25							1628.13

Table B2: Total dry mass sedimentation rates for the SK 31 sediment core.

Midpoint depth (cm)	Midpoint depth CRS dates	Total dry mass sedimentation (g/cm ² yr)	Total dry mass sedimentation error (1 std. dev.)
0.25	2022.60	0.0433	0.0050
0.75	2022.37	0.0357	0.0040
1.25	2022.04	0.0257	0.0023
1.75	2021.58	0.0214	0.0017

2.25	2020.91	0.0208	0.0015
2.75	2020.19	0.0213	0.0021
3.25	2019.31	0.0218	0.0015
3.75	2018.10	0.0215	0.0019
4.25	2016.73	0.0211	0.0012
4.75	2015.33	0.0209	0.0017
5.25	2013.83	0.0208	0.0012
5.75	2012.20	0.0210	0.0016
6.25	2010.45	0.0213	0.0011
6.75	2008.73	0.0217	0.0018
7.25	2007.10	0.0223	0.0015
7.75	2005.58	0.0225	0.0020
8.25	2004.09	0.0229	0.0014
8.75	2002.32	0.0258	0.0022
9.25	2000.55	0.0292	0.0019
9.75	1998.87	0.0330	0.0031
10.25	1997.35	0.0377	0.0028
10.75	1995.96	0.0496	0.0062
11.25	1994.67	0.0674	0.0078
11.75	1993.58	0.0880	0.0176
12.25	1992.74	0.1193	0.0219
12.75	1991.82	0.0796	0.0097
13.25	1990.69	0.0699	0.0070
13.75	1989.22	0.0378	0.0028
14.25	1987.95	0.1301	0.0245
14.75	1987.09	0.0895	0.0179
15.25	1985.95	0.0630	0.0073
15.75	1984.37	0.0545	0.0078
16.25	1982.55	0.0462	0.0045
16.75	1980.40	0.0412	0.0054
17.25	1977.77	0.0357	0.0035
17.75	1974.93	0.0309	0.0038
18.25	1971.64	0.0264	0.0024
18.75	1967.66	0.0179	0.0018
19.25	1962.74	0.0120	0.0009
19.75	1957.61	0.0175	0.0021
20.25	1953.07	0.0292	0.0037
20.75	1949.66	0.0482	0.0137
21.25	1947.78	0.0990	0.0426
21.75	1946.37	0.0772	0.0365
22.25	1943.92	0.0602	0.0165
22.75	1941.02	0.0545	0.0208
23.25	1938.53	0.0504	0.0140
23.75	1935.81	0.0470	0.0188
24.25	1932.64	0.0430	0.0134
24.75	1929.58	0.0413	0.0184
25.25	1926.66	0.0405	0.0137
25.75	1923.39	0.0330	0.0138
26.25	1919.47	0.0266	0.0075
26.75	1915.36	0.0255	0.0118
27.25	1910.80	0.0248	0.0095
27.75	1906.33	0.0269	0.0177
28.25	1902.12	0.0313	0.0175
28.75	1898.21	0.0326	0.0291
29.25	1894.88	0.0363	0.0266

Table B3: Measured ^{210}Pb , ^{137}Cs and ^{226}Ra values and CRS dates for the SK 26 sediment core.

Midpoint depth (cm)	Total ^{210}Pb (dpm/g)	^{210}Pb error (1 std. dev.)	^{137}Cs (dpm/g)	^{137}Cs error (1 std. dev.)	^{226}Ra (dpm/g)	^{226}Ra error (1 std. dev.)	Midpoint depth CRS dates with linear extrapolation
0.25	6.0959	2.6438	0.8651	0.2258	0.5477	0.3257	2022.60
0.75	6.2283	2.5241	1.0843	0.2420	0.8171	0.2110	2022.45
1.25	5.3635	2.1193	0.9301	0.2007	0.9091	0.2152	2022.35
1.75	4.5601	1.7565	1.1162	0.1837	0.8629	0.1893	2022.24
2.25	5.6510	1.2086	1.1441	0.1535	1.1924	0.1766	2021.95
2.75	4.7899	1.2119	1.4200	0.1703	0.8817	0.1638	2021.46
3.25	6.9586	1.0172	1.4028	0.1578	0.8952	0.1353	2020.73
3.75	5.5401	0.9582	1.4632	0.1619	1.0287	0.1393	2019.88
4.25	4.9038	0.9732	1.4328	0.1607	0.9177	0.1361	2019.15
4.75	4.9511	0.7817	1.6911	0.1661	1.2562	0.1273	2018.35
5.25	4.6149	0.9016	1.5939	0.1693	1.0350	0.1369	2017.49
5.75	4.8463	1.2638					2016.72
6.25	5.0853	0.8856	1.8036	0.1968	1.0278	0.1326	2015.73
6.75	5.1063	1.1734					2014.76
7.25	5.1274	0.7698	1.8224	0.1800	0.9264	0.1144	2013.81
7.75	5.0884	1.0963					2012.70
8.25	5.0496	0.7806	1.7769	0.1762	1.0380	0.1191	2011.66
8.75	5.0039	1.0692					2010.53
9.25	4.9584	0.7306	1.9758	0.1872	1.3537	0.1242	2009.24
9.75	4.5614	1.0306					2008.02
10.25	4.1863	0.7269	1.7047	0.1699	1.0637	0.1162	2006.91
10.75	4.1727	1.0680					2005.74
11.25	4.1591	0.7824	1.7258	0.1715	1.5250	0.1389	2004.61
11.75	4.0881	1.0386					2003.33
12.25	4.0179	0.6830	1.8333	0.1792	1.4215	0.1243	2001.93
12.75	3.9963	1.1067					2000.60
13.25	3.9748	0.8708	2.2320	0.2201	1.0519	0.1771	1999.31
13.75	3.7419	1.0875					1997.88
14.25	3.5182	0.6514	2.2876	0.2142	1.2646	0.1146	1996.35
14.75	3.7896	1.0433					1994.84
15.25	4.0746	0.8150	2.0870	0.2016	1.3562	0.1374	1993.37
15.75	3.0538	1.0594					1992.18
16.25	2.2196	0.6768	1.3376	0.1390	1.0264	0.1143	1991.15
16.75	2.5670	0.9388					1990.29
17.25	2.9489	0.6507	2.1146	0.2039	1.4187	0.1217	1989.33
17.75	3.1864	0.9000					1987.95
18.25	3.4364	0.6217	3.0882	0.2838	1.5295	0.1202	1986.23
18.75	3.3439	0.8851					1984.47
19.25	3.2531	0.6300	2.5981	0.2408	1.7983	0.1301	1982.77
19.75	3.1533	0.8585					1981.16
20.25	3.0557	0.5832	1.8738	0.1778	1.8027	0.1251	1979.43
20.75	2.9722	0.8596					1977.54
21.25	2.8903	0.6315	1.4678	0.1437	1.8566	0.1331	1975.79
21.75	2.6545	0.8638					1974.39
22.25	2.4319	0.5893	1.1570	0.1179	1.9769	0.1329	1973.39
22.75	2.2361	0.8374					1972.82
23.25	2.0511	0.5949	0.8826	0.0964	2.1032	0.1387	1972.68
23.75	2.2475	0.8388					1972.53
24.25	2.4560	0.5913	0.9146	0.0993	2.0115	0.1354	1971.88
24.75	1.8948	0.8268					1971.11
25.25	1.4263	0.5778	1.1302	0.1153	1.8093	0.1277	1970.76
25.75	1.9448	0.8552					1970.28

26.25	2.5759	0.6304	1.1272	0.1162	1.6328	0.1267	1968.92
26.75	2.3003	0.8822					1967.33
27.25	2.0451	0.6172	1.1773	0.1178	1.7733	0.1308	1966.40
27.75	2.0600	0.8572					1965.65
28.25	2.0749	0.5949	1.0846	0.1131	1.7291	0.1263	1964.82
28.75	2.1241	0.8775					1964.07
29.25	2.1742	0.6451	0.6795	0.0841	1.8113	0.1355	1963.34
29.75	2.2672	0.9110					1962.45
30.25	2.3628	0.6433	0.4496	0.0679	1.9301	0.1386	1961.47
30.75	2.4906	1.1152					1960.14
31.25	2.6228	0.9110					1958.25
31.75	2.7597	1.1162					1955.63
32.25	2.9012	0.6450	0.2390	0.0574	1.8063	0.1333	1952.34
32.75	2.7034	1.0861					1949.06
33.25	2.5147	0.8738					1946.28
33.75	2.3351	1.0541					1944.03
34.25	2.1642	0.5896	0.1737	0.0498	1.9357	0.1328	1942.31
34.75	2.2345	1.0247					1940.37
35.25	2.3063	0.8381					1937.92
35.75	2.3796	1.0282					1935.12
36.25	2.4544	0.5957	0.068954	0.04073	1.8155	0.1281	1930.23
36.75	2.2845	1.0343					1925.87
37.25	2.1227	0.8455					1923.46
37.75	1.9687	1.0368					1921.26
38.25	1.8223	0.6001	0.040088	0.037872	1.7066	0.1273	1919.23
38.75	1.8162	1.0175					1916.89
39.25	1.8102	0.8217					1914.64
39.75	1.8041	0.9952					1912.50
40.25	1.7981	0.5614	-0.01421	#DIV/0!	1.9033	0.1274	1910.06
40.75	1.7223	0.9750					1907.61
41.25	1.6487	0.7972					1905.31
41.75	1.5772	0.9777					1903.04
42.25	1.5078	0.5660	0.003512	0.009746	1.7839	0.1250	1900.63
42.75							1898.14
43.25							1895.72
43.75							1893.12
44.25							1890.77
44.75							1888.33
45.25							1885.57
45.75							1883.04
46.25							1880.81
46.75							1878.53
47.25							1876.03
47.75							1873.61
48.25							1871.15
48.75							1868.62
49.25							1866.01
49.75							1863.41
50.25							1860.87
50.75							1858.06
51.25							1855.11
51.75							1852.36
52.25							1849.71
52.75							1846.95
53.25							1843.94
53.75							1840.77
54.25							1837.85
54.75							1834.82
55.25							1831.69

55.75							1828.76
56.25							1825.38
56.75							1822.16
57.25							1819.16
57.75							1815.91
58.25							1813.04
58.75							1810.27
59.25							1807.24
59.75							1804.30
60.25							1801.40
60.75							1798.16
61.25							1795.16
61.75							1792.42
62.25							1789.56
62.75							1786.74
63.25							1783.70
63.75							1780.69
64.25							1777.68
64.75							1774.79
65.25							1772.09
65.75							1768.98
66.25							1765.44
66.75							1762.07
67.25							1758.56
67.75							1755.06
68.25							1751.86
68.75							1748.47
69.25							1744.89
69.75							1741.61
70.25							1738.62

Table B4: Total dry mass sedimentation rates for the SK 26 sediment core.

Midpoint depth (cm)	Midpoint depth CRS dates	Total dry mass sedimentation (g/cm ² yr)	Total dry mass sedimentation error (1 std. dev.)
0.25	2022.60	0.0450	0.0230
0.75	2022.45	0.0439	0.0210
1.25	2022.35	0.0529	0.0258
1.75	2022.24	0.0655	0.0330
2.25	2021.95	0.0503	0.0142
2.75	2021.46	0.0611	0.0209
3.25	2020.73	0.0384	0.0076
3.75	2019.88	0.0491	0.0117
4.25	2019.15	0.0561	0.0157
4.75	2018.35	0.0547	0.0129
5.25	2017.49	0.0581	0.0165
5.75	2016.72	0.0529	0.0187
6.25	2015.73	0.0482	0.0120
6.75	2014.76	0.0462	0.0144
7.25	2013.81	0.0448	0.0101
7.75	2012.70	0.0443	0.0132
8.25	2011.66	0.0438	0.0106
8.75	2010.53	0.0434	0.0134
9.25	2009.24	0.0426	0.0105
9.75	2008.02	0.0466	0.0161

10.25	2006.91	0.0516	0.0162
10.75	2005.74	0.0507	0.0211
11.25	2004.61	0.0496	0.0169
11.75	2003.33	0.0491	0.0204
12.25	2001.93	0.0479	0.0156
12.75	2000.60	0.0455	0.0206
13.25	1999.31	0.0430	0.0163
13.75	1997.88	0.0453	0.0215
14.25	1996.35	0.0472	0.0170
14.75	1994.84	0.0405	0.0183
15.25	1993.37	0.0346	0.0124
15.75	1992.18	0.0540	0.0358
16.25	1991.15	0.0935	0.0778
16.75	1990.29	0.0697	0.0571
17.25	1989.33	0.0536	0.0271
17.75	1987.95	0.0481	0.0278
18.25	1986.23	0.0427	0.0185
18.75	1984.47	0.0443	0.0264
19.25	1982.77	0.0464	0.0242
19.75	1981.16	0.0488	0.0342
20.25	1979.43	0.0520	0.0307
20.75	1977.54	0.0539	0.0458
21.25	1975.79	0.0564	0.0425
21.75	1974.39	0.0779	0.1057
22.25	1973.39	0.1156	0.1793
22.75	1972.82	0.4083	2.9930
23.25	1972.68	3.7868	200.1342
23.75	1972.53	0.3893	2.7446
24.25	1971.88	0.1049	0.1555
24.75	1971.11	0.2008	0.7529
25.25	1970.76	0.4776	3.3152
25.75	1970.28	0.1356	0.3590
26.25	1968.92	0.0547	0.0486
26.75	1967.33	0.0797	0.1388
27.25	1966.40	0.1283	0.2818
27.75	1965.65	0.1295	0.3765
28.25	1964.82	0.1302	0.2934
28.75	1964.07	0.1184	0.3405
29.25	1963.34	0.1088	0.2302
29.75	1962.45	0.0896	0.2113
30.25	1961.47	0.0744	0.1156
30.75	1960.14	0.0582	0.1134
31.25	1958.25	0.0453	0.0616
31.75	1955.63	0.0351	0.0464
32.25	1952.34	0.0268	0.0203
32.75	1949.06	0.0321	0.0464
33.25	1946.28	0.0402	0.0672
33.75	1944.03	0.0534	0.1473
34.25	1942.31	0.0753	0.1985
34.75	1940.37	0.0566	0.1777
35.25	1937.92	0.0418	0.0894
35.75	1935.12	0.0314	0.0636
36.25	1930.23	0.0234	0.0240

Table B5: Measured ^{210}Pb , ^{137}Cs and ^{226}Ra values and CRS dates for the SK 58 sediment core.

Midpoint depth (cm)	Total ^{210}Pb (dpm/g)	^{210}Pb error (1 std. dev.)	^{137}Cs (dpm/g)	^{137}Cs error (1 std. dev.)	^{226}Ra (dpm/g)	^{226}Ra error (1 std. dev.)	Midpoint depth CRS dates with linear extrapolation
0.25	7.1944	1.4250	0.4617	0.1455	-0.0101	0.0344	2022.59
0.75	7.0863	1.8258					2022.38
1.25	6.9794	1.1414	0.4148	0.1100	-0.0536	0.0704	2022.09
1.75	8.3217	0.9385	0.7026	0.1136	0.0411	0.0526	2021.54
2.25	9.2057	0.8029	1.0346	0.1217	0.4984	0.2762	2020.67
2.75	8.2847	0.7423			-0.0016	0.0033	2019.15
3.25	9.2330	0.7006	1.1883	0.1214	0.0022	0.0015	2016.94
3.75	9.0289	0.7016	1.0386	0.1111	0.2563	0.0597	2014.57
4.25	9.2472	0.7730	0.9539	0.1118	0.2795	0.0725	2012.06
4.75	10.8598	0.8400	1.1052	0.1242	0.2839	0.0706	2009.25
5.25	11.4599	0.8419	1.1319	0.1236	0.0915	0.0301	2005.70
5.75	11.5903	1.0365	1.1424	0.1392	0.4030	0.1020	2001.75
6.25	12.4522	0.9302	1.0889	0.1238	0.0536	0.1035	1997.73
6.75	8.3010	0.7755	1.0663	0.1236	-0.0164	0.0554	1993.12
7.25	6.2477	0.6376	1.0441	0.1153	-0.0006	0.0130	1988.29
7.75	4.5289	0.6065	1.1305	0.1218	0.0404	0.1055	1983.72
8.25	3.1827	0.4948	1.1689	0.1178	-0.0014	0.0031	1979.69
8.75	2.5530	0.4652	1.1888	0.1182	0.1242	0.0364	1975.86
9.25	2.4964	0.4598	1.0960	0.1096	0.0053	0.0300	1972.29
9.75	3.5967	0.5172	1.3057	0.1298	-0.0044	0.0270	1966.71
10.25	2.2235	0.4702	1.0930	0.1092	0.2746	0.0581	1961.26
10.75	2.1379	0.4465	0.9078	0.0934	0.1516	0.0417	1956.69
11.25	1.5573	0.4453	0.8193	0.0862	0.0301	0.0118	1950.82
11.75	1.3916	0.6378					1945.22
12.25	1.2380	0.4566	0.5846	0.0692	0.1736	0.0431	1939.88
12.75	0.9954	0.6683					1934.23
13.25	0.7868	0.4879	0.3636	0.0558	0.1327	0.0475	1928.41
13.75	0.5204	0.4045	0.2816	0.0429	-0.0038	0.0014	1924.03
14.25	0.3903	0.4805	0.2307	0.0424	-0.0061	0.0025	1918.52
14.75	0.0779	1.2263					1911.75
15.25	0.5250	0.4792	0.1744	0.0431	0.0480	0.0156	1905.50
15.75	0.3770	0.7093					1899.18
16.25	0.2598	0.5229	0.1379	0.0393	0.1271	0.0337	1892.76
16.75							1885.90
17.25							1879.15
17.75							1871.06
18.25	0.2473	0.5024	0.0642	0.0342	0.3600	0.1055	1863.19
18.75							1856.44
19.25							1848.66
19.75							1839.87
20.25							1830.96
20.75							1822.62
21.25							1817.26
21.75							1811.54
22.25	0.1932	0.5367	0.0762	0.0328	-0.0031	0.0162	1802.13
22.75							1792.57
23.25							1783.24
23.75							1773.88
24.25							1764.39
24.75							1754.22
25.25							1744.34
25.75							1735.19

26.25							1725.83
26.75							1716.52
27.25							1707.24
27.75							1697.43
28.25							1687.76
28.75							1678.33
29.25							1668.87
29.75							1658.27
30.25							1647.71
30.75							1638.54
31.25							1629.25
31.75							1618.30

Table B6: Total dry mass sedimentation rates for the SK 58 sediment core.

Midpoint depth (cm)	Midpoint depth CRS dates	Total dry mass sedimentation (g/cm ² yr)	Total dry mass sedimentation error (1 std. dev.)
0.25	2022.59	0.0774	0.0158
0.75	2022.38	0.0781	0.0207
1.25	2022.09	0.0788	0.0136
1.75	2021.54	0.0651	0.0078
2.25	2020.67	0.0575	0.0062
2.75	2019.15	0.0620	0.0058
3.25	2016.94	0.0521	0.0042
3.75	2014.57	0.0495	0.0043
4.25	2012.06	0.0449	0.0042
4.75	2009.25	0.0351	0.0031
5.25	2005.70	0.0303	0.0025
5.75	2001.75	0.0263	0.0027
6.25	1997.73	0.0218	0.0020
6.75	1993.12	0.0287	0.0031
7.25	1988.29	0.0329	0.0039
7.75	1983.72	0.0394	0.0064
8.25	1979.69	0.0494	0.0086
8.75	1975.86	0.0554	0.0118
9.25	1972.29	0.0501	0.0110
9.75	1966.71	0.0311	0.0054
10.25	1961.26	0.0399	0.0108
10.75	1956.69	0.0380	0.0099
11.25	1950.82	0.0439	0.0145
11.75	1945.22	0.0417	0.0220
12.25	1939.88	0.0397	0.0179
12.75	1934.23	0.0433	0.0325
13.25	1928.41	0.0464	0.0346
13.75	1924.03	0.0646	0.0612

Appendix C – Sediment core loss-on-ignition

Table C1: Results of loss-on-ignition analysis for the sediment core of SK 31 including water content, organic matter content, mineral matter content (including and excluding carbonate) and carbonate content.

Midpoint depth (cm)	Water (%)	Organic matter (%)	Mineral matter (%)	Mineral matter-carbonate free (%)	Carbonate (CaCO ₃) (%)
0.25	99.36	36.79	63.21	52.94	10.28
0.75	97.79	54.30	45.70	37.59	8.11
1.25	98.26	63.21	36.79	32.94	3.85
1.75	97.29	60.00	40.00	29.47	10.53
2.25	96.90	60.56	39.44	30.38	9.07
2.75	96.98	57.14	42.86	31.85	11.01
3.25	95.69	50.50	49.50	31.43	18.07
3.75	94.62	50.74	49.26	31.08	18.18
4.25	94.45	48.97	51.03	31.71	19.32
4.75	94.28	50.00	50.00	30.62	19.38
5.25	93.27	34.48	65.52	39.72	25.79
5.75	93.26	43.03	56.97	35.60	21.38
6.25	91.78	40.07	59.93	33.81	26.12
6.75	92.82	48.51	51.49	34.92	16.58
7.25	93.46	45.37	54.63	33.96	20.67
7.75	93.03	46.54	53.46	34.65	18.81
8.25	92.89	43.75	56.25	36.70	19.55
8.75	91.03	41.61	58.39	40.31	18.07
9.25	91.82	41.64	58.36	42.18	16.18
9.75	89.64	33.44	66.56	49.25	17.31
10.25	90.51	35.30	64.70	47.90	16.80
10.75	85.89	27.03	72.97	57.07	15.90
11.25	87.00	26.85	73.15	58.13	15.02
11.75	84.31	22.59	77.41	66.69	10.72
12.25	85.92	25.40	74.60	60.26	14.34
12.75	84.55	24.15	75.85	61.81	14.04
13.25	87.81	29.49	70.51	53.48	17.03
13.75	85.71	25.37	74.63	61.19	13.43
14.25	81.76	21.27	78.73	65.21	13.52
14.75	83.78	23.03	76.97	64.12	12.85
15.25	86.99	28.02	71.98	54.57	17.41
15.75	82.81	21.58	78.42	65.64	12.78
16.25	84.50	23.43	76.57	60.35	16.22
16.75	82.13	21.42	78.58	65.03	13.55
17.25	80.84	21.26	78.74	61.91	16.82
17.75	83.65	24.73	75.27	60.07	15.19
18.25	83.99	25.02	74.98	59.53	15.45
18.75	85.62	27.76	72.24	54.71	17.54
19.25	89.61	36.34	63.66	47.33	16.34
19.75	84.64	25.34	74.66	58.55	16.11
20.25	79.80	20.09	79.91	67.02	12.89
20.75	79.70	19.21	80.79	67.54	13.25
21.25	79.16	18.51	81.49	70.54	10.95
21.75	78.13	16.44	83.56	73.90	9.66
22.25	74.20	15.63	84.37	75.63	8.74
22.75	76.73	18.05	81.95	70.70	11.25
23.25	77.49	18.66	81.34	68.16	13.18
23.75	78.36	19.77	80.23	66.92	13.31

24.25	77.98	21.52	78.48	64.31	14.17
24.75	77.69	19.88	80.12	66.32	13.80
25.25	79.15	21.64	78.36	60.91	17.46
25.75	79.70	21.63	78.37	61.12	17.25
26.25	80.16	22.24	77.76	62.90	14.85
26.75	79.93	22.13	77.87	60.93	16.94
27.25	79.06	22.29	77.71	63.21	14.51
27.75	81.77	26.16	73.84	57.76	16.08
28.25	78.05	22.69	77.31	63.31	14.00
28.75	80.45	27.16	72.84	58.24	14.60
29.25	80.57	27.47	72.53	57.85	14.67
29.75	80.74	25.89	74.11	60.36	13.75
30.25	82.12	30.30	69.70	55.04	14.66
30.75	80.11	28.50	71.50	56.09	15.41
31.25	81.02	29.25	70.75	52.06	18.69
31.75	81.42	27.29	72.71	56.59	16.12
32.25	80.99	31.39	68.61	53.94	14.68
32.75	83.39	33.62	66.38	50.40	15.98
33.25	83.11	33.63	66.37	48.91	17.46
33.75	82.47	31.39	68.61	48.43	20.18
34.25	85.46	37.26	62.74	45.90	16.84
34.75	82.26	35.45	64.55	47.98	16.56
35.25	84.53	35.87	64.13	45.36	18.76
35.75	85.18	37.63	62.37	44.33	18.04
36.25	82.98	33.30	66.70	46.51	20.19
36.75	84.36	36.22	63.78	38.97	24.81
37.25	83.68	37.67	62.33	39.79	22.53
37.75	85.26	39.35	60.65	40.95	19.70
38.25	85.08	40.55	59.45	36.15	23.29
38.75	84.75	41.56	58.44	36.33	22.10
39.25	85.58	40.44	59.56	36.55	23.01
39.75	86.40	41.50	58.50	35.20	23.30
40.25	86.09	41.47	58.53	35.12	23.40
40.75	86.39	43.22	56.78	32.50	24.28
41.25	86.63	45.44	54.56	31.73	22.83
41.75	84.84	47.14	52.86	31.68	21.19
42.25	87.49	45.61	54.39	33.07	21.32
42.75	86.09	42.74	57.26	35.37	21.89
43.25	87.21	45.06	54.94	33.96	20.98
43.75	86.52	47.44	52.56	30.49	22.07
44.25	85.74	46.32	53.68	33.30	20.37
44.75	86.94	49.37	50.63	30.34	20.29
45.25	85.77	47.91	52.09	30.94	21.15
45.75	87.17	49.53	50.47	29.92	20.55
46.25	85.60	48.00	52.00	32.16	19.85
46.75	84.99	45.27	54.73	32.06	22.67
47.25	85.02	48.36	51.64	33.81	17.82
47.75	84.02	46.73	53.27	35.68	17.59
48.25	84.23	45.47	54.53	37.39	17.14
48.75	84.04	44.88	55.12	39.17	15.95
49.25	82.83	41.40	58.60	41.60	17.00
49.75	82.88	42.29	57.71	41.95	15.76
50.25	82.63	44.61	55.39	40.34	15.05
50.75	82.20	42.37	57.63	42.46	15.17
51.25	80.69	41.60	58.40	42.52	15.89
51.75	83.02	43.39	56.61	38.26	18.36
52.25	82.42	42.34	57.66	42.21	15.45
52.75	81.36	42.76	57.24	42.21	15.02
53.25	80.48	41.38	58.62	43.02	15.61

53.75	80.91	43.02	56.98	41.48	15.50
54.25	80.60	41.28	58.72	43.05	15.67
54.75	81.42	43.10	56.90	42.59	14.31
55.25	81.11	45.71	54.29	39.55	14.74
55.75	81.04	43.71	56.29	41.94	14.35
56.25	80.73	45.04	54.96	39.25	15.71
56.75	80.93	45.89	54.11	38.81	15.30
57.25	80.35	50.06	49.94	33.76	16.18
57.75	81.88	49.38	50.62	32.63	17.99
58.25	81.61	47.31	52.69	36.82	15.87
58.75	80.43	50.18	49.82	33.62	16.20
59.25	81.33	46.55	53.45	35.38	18.07
59.75	81.04	45.16	54.84	38.12	16.72
60.25	81.18	45.85	54.15	36.75	17.40
60.75	80.74	55.31	44.69	30.11	14.58
61.25	80.08	50.47	49.53	34.16	15.37
61.75	80.29	46.72	53.28	36.95	16.34
62.25	80.84	54.84	45.16	31.84	13.31
62.75	80.54	51.44	48.56	31.41	17.15
63.25	80.62	54.24	45.76	31.25	14.51
63.75	79.87	53.60	46.40	31.72	14.68
64.25	80.23	55.63	44.37	30.35	14.02
64.75	80.10	56.93	43.07	29.14	13.94
65.25	77.94	48.99	51.01	35.71	15.30
65.75	79.63	55.52	44.48	30.33	14.14
66.25	77.85	55.66	44.34	30.42	13.92
66.75	78.56	59.14	40.86	29.33	11.53
67.25	78.68	55.53	44.47	30.70	13.77
67.75	78.93	63.55	36.45	26.41	10.04
68.25	79.21	61.25	38.75	25.14	13.61
68.75	77.66	61.20	38.80	25.83	12.97
69.25	77.80	63.55	36.45	25.47	10.98
69.75	77.59	74.47	25.53	17.06	8.48
70.25	77.70	69.01	30.99	21.26	9.73
70.75	79.48	74.16	25.84	21.66	4.17
71.25	80.17	73.61	26.39	20.83	5.56
71.75	78.73	65.75	34.25	24.53	9.72
72.25	79.98	76.67	23.33	19.52	3.82
72.75	80.11	72.02	27.98	21.86	6.12
73.25	80.15	73.55	26.45	21.12	5.33
73.75	80.78	75.34	24.66	20.15	4.50
74.25	79.38	75.58	24.42	20.53	3.89
74.75	79.51	76.47	23.53	19.81	3.72
75.25	78.83	76.97	23.03	20.25	2.78
75.75	77.26	77.05	22.95	19.78	3.17
76.25	79.86	70.40	29.60	21.55	8.05
76.75	78.41	69.35	30.65	21.94	8.71

Table C2: Results of loss-on-ignition analysis for the sediment core of SK 26 including water content, organic matter content, mineral matter content (including and excluding carbonate) and carbonate content.

Midpoint depth (cm)	Water (%)	Organic matter (%)	Mineral matter (%)	Mineral matter-carbonate free (%)	Carbonate (CaCO ₃) (%)
0.25	99.15	41.66	58.34	52.99	5.36

0.75	98.88	46.51	53.49	49.27	4.22
1.25	99.02	41.57	58.43	50.24	8.19
1.75	98.06	53.06	46.94	41.39	5.55
2.25	95.17	49.32	50.68	43.74	6.94
2.75	93.10	45.86	54.14	46.25	7.89
3.25	93.45	50.11	49.89	42.45	7.44
3.75	91.71	48.29	51.71	45.51	6.21
4.25	91.64	48.64	51.36	44.16	7.20
4.75	90.04	45.62	54.38	45.62	8.76
5.25	90.89	53.31	46.69	40.08	6.61
5.75	91.26	51.22	48.78	43.62	5.17
6.25	90.46	49.06	50.94	45.20	5.74
6.75	90.84	48.33	51.67	46.52	5.15
7.25	90.36	47.47	52.53	45.05	7.47
7.75	91.71	48.77	51.23	46.20	5.04
8.25	90.38	48.50	51.50	45.38	6.13
8.75	89.67	48.25	51.75	45.46	6.29
9.25	88.72	48.26	51.74	46.09	5.65
9.75	88.84	50.53	49.47	44.53	4.94
10.25	88.58	48.22	51.78	45.11	6.66
10.75	88.87	56.23	43.77	39.19	4.58
11.25	87.28	49.95	50.05	45.02	5.03
11.75	87.73	50.60	49.40	43.48	5.91
12.25	87.47	49.35	50.65	45.21	5.43
12.75	87.55	49.13	50.87	45.89	4.98
13.25	88.15	48.40	51.60	45.64	5.96
13.75	87.29	48.01	51.99	43.52	8.47
14.25	88.44	50.07	49.93	42.08	7.85
14.75	86.97	49.33	50.67	46.04	4.63
15.25	89.18	51.89	48.11	42.82	5.29
15.75	88.76	51.32	48.68	42.46	6.22
16.25	86.98	51.96	48.04	41.37	6.67
16.75	87.05	50.16	49.84	44.08	5.76
17.25	88.11	50.24	49.76	43.98	5.78
17.75	85.44	49.65	50.35	43.30	7.05
18.25	85.45	50.08	49.92	42.99	6.93
18.75	85.17	49.67	50.33	44.83	5.50
19.25	85.44	51.45	48.55	43.05	5.50
19.75	86.01	50.47	49.53	44.09	5.45
20.25	82.02	49.01	50.99	45.32	5.67
20.75	80.91	48.53	51.47	46.45	5.02
21.25	83.60	49.13	50.87	44.95	5.92
21.75	81.85	47.94	52.06	45.66	6.40
22.25	82.13	46.69	53.31	47.04	6.27
22.75	81.13	48.65	51.35	45.29	6.05
23.25	80.90	47.78	52.22	45.90	6.32
23.75	80.42	49.06	50.94	45.84	5.10
24.25	80.34	50.24	49.76	45.08	4.68
24.75	81.62	51.45	48.55	44.26	4.29
25.25	80.91	49.84	50.16	44.61	5.55
25.75	81.73	49.30	50.70	44.59	6.11
26.25	80.84	50.64	49.36	42.08	7.28
26.75	82.30	50.85	49.15	42.37	6.79
27.25	82.28	51.81	48.19	41.47	6.72
27.75	80.94	49.74	50.26	45.57	4.69
28.25	82.98	52.17	47.83	41.57	6.26
28.75	83.36	51.27	48.73	40.94	7.79
29.25	83.57	55.05	44.95	38.09	6.86
29.75	83.31	52.21	47.79	42.56	5.23

30.25	84.05	57.37	42.63	34.22	8.41
30.75	83.77	53.59	46.41	40.37	6.04
31.25	82.53	53.33	46.67	40.70	5.96
31.75	81.91	51.60	48.40	41.87	6.53
32.25	81.10	50.52	49.48	43.36	6.13
32.75	81.28	47.01	52.99	42.99	10.00
33.25	82.64	50.40	49.60	42.67	6.93
33.75	80.98	59.27	40.73	26.70	14.03
34.25	80.21	51.42	48.58	42.32	6.26
34.75	77.94	47.52	52.48	47.30	5.17
35.25	80.38	49.40	50.60	44.54	6.05
35.75	80.18	47.96	52.04	45.03	7.00
36.25	78.14	51.78	48.22	43.39	4.84
36.75	78.32	49.44	50.56	45.99	4.57
37.25	77.17	50.39	49.61	46.09	3.52
37.75	78.89	52.84	47.16	41.56	5.60
38.25	76.27	47.27	52.73	47.72	5.01
38.75	76.76	48.88	51.12	46.06	5.06
39.25	78.14	48.98	51.02	44.64	6.37
39.75	78.46	48.78	51.22	45.07	6.15
40.25	75.41	47.59	52.41	45.86	6.55
40.75	76.69	49.04	50.96	44.52	6.44
41.25	75.95	46.52	53.48	48.12	5.36
41.75	76.58	47.30	52.70	46.69	6.01
42.25	75.27	47.42	52.58	45.87	6.71
42.75	76.47	47.38	52.62	44.99	7.63
43.25	76.41	48.40	51.60	44.57	7.03
43.75	75.05	46.72	53.28	47.26	6.03
44.25	78.53	48.74	51.26	44.30	6.96
44.75	74.42	48.13	51.87	45.83	6.04
45.25	75.27	50.15	49.85	42.10	7.76
45.75	76.11	55.53	44.47	37.26	7.21
46.25	74.90	50.41	49.59	40.04	9.55
46.75	78.58	48.08	51.92	44.96	6.96
47.25	76.22	48.58	51.42	44.64	6.78
47.75	75.11	47.19	52.81	46.38	6.43
48.25	74.08	47.34	52.66	45.42	7.24
48.75	75.89	53.71	46.29	38.84	7.45
49.25	74.34	47.54	52.46	44.78	7.69
49.75	74.70	47.34	52.66	45.22	7.44
50.25	72.24	48.16	51.84	45.27	6.57
50.75	73.69	47.47	52.53	44.89	7.63
51.25	73.30	48.96	51.04	44.33	6.71
51.75	71.88	48.33	51.67	46.85	4.82
52.25	75.05	50.07	49.93	42.98	6.95
52.75	73.63	49.66	50.34	43.25	7.09
53.25	70.91	46.63	53.37	47.89	5.48
53.75	69.97	45.48	54.52	48.06	6.46
54.25	72.90	49.22	50.78	43.45	7.33
54.75	70.64	45.31	54.69	46.94	7.74
55.25	69.58	45.79	54.21	46.61	7.61
55.75	70.59	45.31	54.69	47.25	7.44
56.25	70.79	46.94	53.06	43.86	9.20
56.75	71.70	45.03	54.97	47.30	7.67
57.25	70.80	44.64	55.36	48.45	6.91
57.75	71.50	47.72	52.28	45.36	6.92
58.25	71.58	45.61	54.39	47.08	7.31
58.75	71.01	44.52	55.48	48.27	7.21
59.25	71.18	45.59	54.41	46.33	8.08

59.75	72.76	47.27	52.73	45.07	7.66
60.25	71.97	46.43	53.57	45.70	7.87
60.75	72.06	47.01	52.99	45.66	7.33
61.25	72.07	48.86	51.14	41.94	9.19
61.75	71.53	48.37	51.63	45.18	6.45
62.25	71.99	47.68	52.32	45.94	6.37
62.75	72.37	47.61	52.39	45.33	7.06
63.25	72.26	46.88	53.12	45.78	7.34
63.75	71.96	46.56	53.44	45.58	7.86
64.25	72.17	49.23	50.77	44.00	6.77
64.75	71.63	47.38	52.62	44.85	7.77
65.25	72.14	49.56	50.44	43.11	7.33
65.75	69.51	47.75	52.25	45.48	6.76
66.25	67.08	47.83	52.17	48.69	3.48
66.75	67.03	44.75	55.25	47.41	7.84
67.25	67.37	44.27	55.73	50.36	5.37
67.75	68.83	49.53	50.47	46.71	3.76
68.25	67.13	46.73	53.27	45.78	7.49
68.75	69.88	48.81	51.19	47.36	3.83
69.25	68.27	49.73	50.27	47.33	2.94
69.75	68.99	50.91	49.09	45.59	3.50
70.25	68.63	50.32	49.68	46.46	3.22

Table C3: Results of loss-on-ignition analysis for the sediment core of SK 58 including water content, organic matter content, mineral matter content (including and excluding carbonate) and carbonate content.

Midpoint depth (cm)	Water (%)	Organic matter (%)	Mineral matter (%)	Mineral matter-carbonate free (%)	Carbonate (CaCO ₃) (%)
0.25	99.02	38.98	61.02	42.58	18.44
0.75	96.13	33.66	66.34	38.48	27.86
1.25	94.47	36.43	63.57	31.94	31.63
1.75	90.87	35.69	64.31	32.31	32.00
2.25	89.56	34.01	65.99	33.56	32.43
2.75	79.42	26.79	73.21	34.36	38.86
3.25	78.56	28.09	71.91	33.89	38.02
3.75	81.21	28.61	71.39	33.40	37.98
4.25	80.22	28.99	71.01	34.52	36.49
4.75	81.40	29.90	70.10	34.45	35.65
5.25	80.71	31.34	68.66	32.81	35.85
5.75	83.62	29.21	70.79	33.86	36.93
6.25	83.33	29.40	70.60	32.69	37.91
6.75	79.18	26.97	73.03	34.45	38.57
7.25	75.68	24.45	75.55	35.70	39.85
7.75	71.96	22.31	77.69	35.76	41.93
8.25	69.81	21.27	78.73	36.25	42.48
8.75	69.31	21.64	78.36	35.93	42.43
9.25	71.91	22.70	77.30	37.02	40.29
9.75	67.45	22.01	77.99	35.63	42.37
10.25	88.50	21.29	78.71	35.91	42.80
10.75	68.23	21.32	78.68	35.89	42.79
11.25	64.58	22.69	77.31	36.15	41.15
11.75	65.11	21.91	78.09	36.37	41.72
12.25	67.83	22.09	77.91	36.17	41.74
12.75	65.16	21.17	78.83	38.35	40.48

13.25	61.73	20.45	79.55	45.25	34.30
13.75	62.19	19.48	80.52	43.41	37.11
14.25	57.46	17.65	82.35	49.35	32.99
14.75	64.98	21.22	78.78	39.11	39.67
15.25	58.88	19.73	80.27	54.32	25.96
15.75	58.18	18.34	81.66	48.24	33.42
16.25	59.14	18.65	81.35	53.48	27.87
16.75	55.45	16.59	83.41	47.92	35.49
17.25	58.32	20.47	79.53	53.71	25.82
17.75	55.64	17.31	82.69	48.65	34.04
18.25	55.21	18.33	81.67	49.93	31.73
18.75	55.92	18.20	81.80	48.65	33.14
19.25	51.80	15.57	84.43	49.79	34.65
19.75	50.47	15.23	84.77	52.92	31.86
20.25	48.66	15.92	84.08	51.48	32.60
20.75	50.50	15.56	84.44	49.68	34.76
21.25	49.27	15.40	84.60	50.01	34.59
21.75	49.40	15.84	84.16	49.87	34.28
22.25	50.24	16.40	83.60	47.94	35.66
22.75	49.99	16.38	83.62	47.77	35.85
23.25	49.14	15.87	84.13	46.44	37.68
23.75	49.86	16.40	83.60	45.51	38.09
24.25	48.23	15.02	84.98	50.93	34.05
24.75	46.13	14.04	85.96	50.16	35.80
25.25	48.13	14.38	85.62	50.89	34.73
25.75	46.25	14.09	85.91	51.87	34.04
26.25	47.99	14.85	85.15	50.17	34.98
26.75	47.10	16.41	83.59	46.40	37.19
27.25	47.36	15.97	84.03	46.21	37.82
27.75	47.44	14.94	85.06	49.84	35.23
28.25	48.68	16.16	83.84	47.79	36.05
28.75	48.27	15.64	84.36	48.92	35.44
29.25	49.07	16.17	83.83	50.20	33.62
29.75	43.85	16.71	83.29	53.19	30.11
30.25	49.20	18.84	81.16	45.59	35.57
30.75	48.20	17.08	82.92	45.85	37.07
31.25	47.93	16.25	83.75	47.64	36.11
31.75	47.75	16.24	83.76	50.52	33.24

Appendix D – Standard Operating Procedure (SOP)

SOP for evolving and measuring the isotope composition (^{18}O , ^{13}C) of pond/lake sediment carbonate

1.0 Introduction

Purpose: This standard operating procedure (SOP) provides detailed methods for evolving and measuring the oxygen isotope composition of carbonate ($\delta^{18}\text{O}_{\text{carb}}$) from pond/lake sediment. Changes in the oxygen isotope composition of endogenic carbonate that forms in isotopic equilibrium can reflect the temperature and oxygen isotope composition of pond/lake water at the time of mineral precipitation (Kim and O’Neil, 1997; Leng and Marshall, 2004). In paleolimnological applications, the oxygen isotope composition of endogenic carbonate ($\delta^{18}\text{O}_{\text{carb}}$) in pond/lake sediment can provide information on changes in water balance (Anderson et al., 2005; Kelts and Talbot, 1990; Steinman et al., 2010, 2013; Steinman and Abbott, 2013; Talbot, 1990). Methods for preparing pond/lake sediment samples for carbonate oxygen isotope analysis closely follow those of Leng and Marshall (2004).

2.0 Safety Precautions

Always wear a lab coat and gloves, closed-toe shoes and long pants when processing samples, especially when handling phosphoric acid (see section 4.5). Read entire procedure carefully before beginning and ask questions if there are uncertainties. Below are some brief guidelines for working with phosphoric acid; please refer to the Material Safety Data Sheet for a full overview. Prior to the handling of phosphoric acid please be aware of nearest eye wash station.

Phosphoric acid

Hazards and first aid measures: may cause eye and skin burns upon contact; immediately flush affected area with water for at least 15 minutes and contact medical aid. May cause digestive and respiratory tract burns if ingested. Do not induce vomiting, drink milk or water and seek medical aid immediately.

Handling and storage: wash thoroughly after handling and store in a tightly closed container in a cool, dry and well-ventilated area away from incompatible substances. Do not store in metal containers; may be corrosive.

3.0 Materials

- Falcon tubes
- Sharpie for labelling
- Plastic scoopula
- Deionized water
- Kim wipes
- Elastics
- Glass mortar and pestle
- 5 ml exetainer vials with screw caps and pre-baked septa
 - Provided by UW-EIL

- Foil boat
- Metal scoopula
- 22-gauge needles (~12)
 - Provided by UW-EIL
- Purified phosphoric acid
 - Provided by UW-EIL
- 100 ml syringe
 - Provided by UW-EIL

4.0 Procedure

4.1 Loss-on-ignition

1. Loss-on-ignition (LOI) must be completed first to have estimate of carbonate (CaCO_3) content (expressed as a percentage) for each sub-sample.

4.2 Freeze-drying and homogenizing

1. Subsample wet sediment into falcon tubes.
2. Remove caps from falcon tubes and cover each tube with a Kimwipe secured by an elastic band. Freeze subsamples overnight; ensure they are placed in the freezer on a 45° angle.
3. Once samples are fully frozen, freeze-dry sediment.
4. Homogenize freeze-dried sediment with a glass mortar and pestle. Rinse the mortar and pestle thoroughly with deionized water and dry completely with Kimwipes between samples to avoid cross-contamination.

4.3 Weighing

1. Determine the amount of sediment needed for each sample using Equation 2 (see below).
 - Use CaCO_3 content ('x') measured through loss-on-ignition analysis to determine amount of sediment (in mg) needed for each subsample ('y').
 - Note: it is better to underestimate the amount of sediment needed than to overestimate.

$$y = 20.327X^{-1.005} \quad (1)$$

1. Label each 5-ml glass extainer vial with sample number (#1-60) and sample identification. Standards should be prepared for the beginning, middle and end of each run. It is recommended to prepare standards according to Table 2. Prepare duplicates every 5-10 samples.

Table 2. Template for sample numbers, sample identification (ID), target weights (mg) and actual weights (mg). A total of 60 vials (44 samples and 16 standards) can be processed at a time.

Sample #	Sample ID	Target wt. (mg)	Actual wt. (mg)
1	EIL-21	0.10	
2	EIL-21	0.10	
3	IAEA-CO-1	0.10	
4	IAEA-CO-1	0.10	
5	IAEA-CO-8	0.10	
6	IAEA-CO-8	0.10	
-			
31	EIL-21	0.20	
32	EIL-21	0.15	
33	EIL-21	0.10	
34	EIL-21	0.05	
-			
55	EIL-21	0.10	
56	EIL-21	0.10	
57	IAEA-CO-1	0.10	
58	IAEA-CO-1	0.10	
59	IAEA-CO-8	0.10	
60	IAEA-CO-8	0.10	

2. Weigh freeze-dried homogenized sediment samples and standards using a small foil weigh boat on the microbalance (Mettler Toledo MX5, max: 5,1g, d=1µg) to 0.05 decimal places. Once the target weight is reached, carefully place the samples into respective vials and cap them.
3. Replace septa in exetainer caps with pre-baked septa (baked for 24 hours minimum at 90°C, to remove impurities).
 - Note: this will be done at the UW-EIL laboratory immediately prior to helium flushing (see section 4.4). Here, you will have access to pre-baked septa and drying oven.
 - Place unbaked septa in drying oven set to 90° Celsius.
4. Screw caps on tight enough to ensure a seal but not overly tight, just until there is resistance. You want to avoid an excess build up of pressure (the septa will expand above the caps outer ring if there is too much pressure and look like a bellybutton).

4.4 Helium Flushing

5. Set up helium flushing system: Attach 10 vials at a time to dual needle gas flushing system (Figure 1). Each exetainer must be connected to the helium gas tank via tubing and a 22-gauge needle. A second needle must be placed in each exetainer to allow gases to flush their headspace. Connect the gas flow meter to the top left sample instead of an open needle to measure the speed of flushing.



Figure 1. Image of dual-needle gas flushing system at the Environmental Isotope Laboratory (University of Waterloo). Gas flow meter is pictured on the left-hand side, with tubing connecting the meter to the vial through a secondary dispensing needle. Vials are attached to dispensing needle connected to the helium tank.

6. Open helium tank (red lever found at the top of the tank, found to the left of the flushing system) and flush samples at a target flow rate of 100-200 ml/min for 5 minutes.
 - Note: You can adjust the helium flow rate via tightening and loosening the valve found on the top of the helium tank and monitor the rate via the flow meter.
7. Carefully remove vials from needle system by holding the blue section of both needles and pulling each vial downwards. The top row of vials should be detached first to avoid needle pokes.
8. Repeat steps 6-8 for remaining samples. Close helium tank with red lever once all samples have been flushed.

4.5 Evolving (with acid)

9. Purify phosphoric acid. This is done through boiling the acid to remove any water entered by air vapour.
 - Note: The UW-EIL provides already purified phosphoric acid.
10. Attach a 22-gauge needle head to a 100 ml syringe and pull up ~80-100mL of purified phosphoric acid. Insert the needle through each exetainer septa and add 12 drops (roughly 100 micro liters) of phosphoric acid to each sample.
 - Note: If there is lots of resistance when inserting the needle through a septa, replace the needle head as it has likely become dull. Because phosphoric acid can be highly viscous, there may be a delay in filling your syringe. Maintain resistance and be patient!

4.6 Isotope Ratio Mass Spectrometer

11. Place extainer samples sequentially into the isotope ratio mass spectrometer in specified order: Sample #1 should be placed on the left in the uppermost row and subsequent samples are placed below the previous sample. See Figure 2 for reference.
 - Note: If there are less than 60 samples in the batch/run, place an empty vial in spot numbers 56 and 60 to ensure spectrometer is well-balanced.

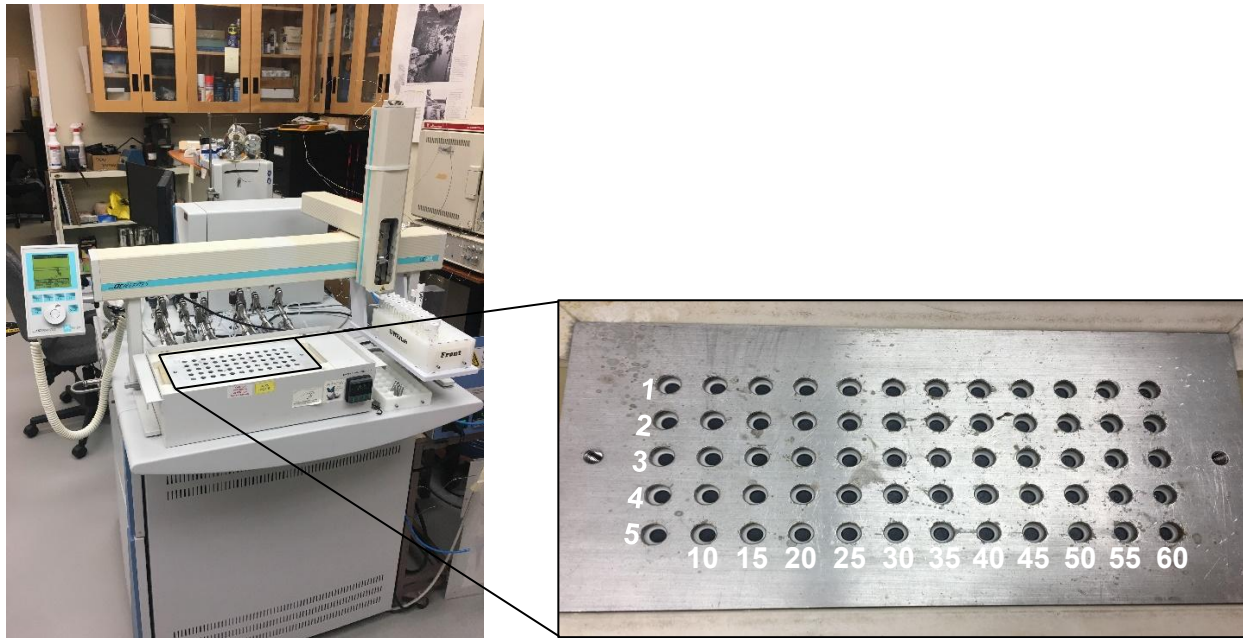


Figure 2. Delta V Plus Isotope ratio mass spectrometer (pictured on the left-hand side). Enlargement of the sample tray located within the spectrometer (pictured on the right-hand side). Samples are placed into the tray in the order noted on the picture, sample #1 is placed in the top left-hand corner and sample #60 is placed in the bottom right-hand corner.

12. Input each sample number and identification into the spreadsheet on the computer connected to the isotope ratio mass spectrometer.
13. Allow samples to rest in the heated tray of the mass spectrometer for 90 minutes before samples are run (This will be done by a technician at the UW-EIL).

Appendix E – Sediment core carbonate isotope composition

Table E1: Carbonate isotope composition ($\delta^{13}\text{C}$, $\delta^{18}\text{O}$) values (‰ VPDB) including carbonate-inferred pond water $\delta^{18}\text{O}$ (‰ VSMOW) and pond water temperature used in Equation 1 to calculate pond water $\delta^{18}\text{O}$ for the SK 31 sediment core.

Mid point depth (cm)	CRS dates	$\delta^{13}\text{C}_{\text{carb}}$ (‰ VPDB)	$\delta^{18}\text{O}_{\text{carb}}$ (‰ VPDB)	$\delta^{18}\text{O}_{\text{pw}}$ (‰ VSMOW)	Water temperature used to calculate $\delta^{18}\text{O}_{\text{pw}}$
0.25	2022.53	-0.4	-11.1	-9.8	17.59
1.25	2022.21	-2.3	-11.2	-9.9	17.59
2.25	2021.28	-1.5	-12.1	-10.8	17.59
3.25	2019.85	-0.6	-12.0	-10.7	17.59
4.25	2017.43	-0.3	-11.6	-10.3	17.59
5.25	2014.65	0.2	-11.6	-10.2	17.59
6.25	2011.38	0.0	-11.9	-10.6	17.59
7.25	2007.94	-0.5	-11.9	-10.6	17.59
8.25	2004.90	-0.6	-11.7	-10.3	17.59
9.25	2001.37	-1.0	-12.0	-10.7	17.59
10.25	1998.03	-1.2	-12.1	-10.8	17.59
11.25	1995.23	-1.4	-12.6	-11.2	17.59
12.25	1993.05	-1.3	-12.2	-10.8	17.59
13.25	1991.23	-0.9	-12.9	-11.6	17.59
14.25	1988.28	-1.1	-13.0	-11.7	17.59
15.25	1986.55	-1.7	-12.2	-10.9	17.59
16.25	1983.38	-0.8	-12.5	-11.2	17.59
17.25	1979.08	-0.9	-12.6	-11.3	17.59
18.25	1973.40	-1.0	-12.8	-11.5	17.59
19.25	1965.44	-0.8	-12.1	-10.8	17.59
20.25	1955.19	-1.3	-12.7	-11.4	17.59
21.25	1948.37	-1.4	-13.2	-11.9	17.59
22.25	1945.55	-1.6	-12.9	-11.6	17.59
23.25	1939.74	-1.6	-13.0	-11.6	17.59
24.25	1934.31	-2.0	-12.8	-11.4	17.59
25.25	1928.19	-1.8	-12.2	-10.9	17.59
26.25	1921.65	-1.6	-13.1	-11.7	17.59
27.25	1913.43	-1.9	-12.7	-11.4	17.59
28.25	1904.50	-2.6	-12.3	-11.0	17.59
29.25	1896.68	-2.0	-12.9	-11.6	17.59
30.25	1890.70	-2.4	-12.8	-11.4	17.59
31.25	1884.35	-2.3	-12.6	-11.2	17.59
32.25	1878.47	-3.5	-12.1	-10.8	17.59
33.25	1872.93	-3.1	-12.0	-10.6	17.59
34.25	1867.44	-3.3	-12.0	-10.7	17.59
35.25	1862.65	-2.8	-12.0	-10.7	17.59
36.25	1857.71	-3.3	-12.4	-11.1	17.59
37.25	1852.57	-2.6	-12.7	-11.4	17.59
38.25	1848.02	-3.1	-12.8	-11.5	17.59
39.25	1843.49	-3.6	-12.2	-10.9	17.59
40.25	1839.17	-3.0	-10.3	-9.0	17.59
41.25	1835.04	-3.6	-11.0	-9.7	17.59
42.25	1830.87	-4.4	-11.4	-10.1	17.59
43.25	1826.67	-4.6	-11.2	-9.9	17.59
44.25	1822.57	-4.9	-11.3	-10.0	17.59
45.25	1818.70	-5.2	-11.0	-9.7	17.59
46.25	1814.65	-7.2	-10.5	-9.2	17.59

47.25	1810.28	-6.2	-11.3	-10.0	17.59
48.25	1805.73	-7.6	-11.0	-9.6	17.59
49.25	1800.53	-7.9	-10.0	-8.6	17.59
50.25	1795.38	-9.0	-10.4	-9.0	17.59
51.25	1789.56	-4.9	-1.2	0.1	17.59
52.25	1783.53	-8.9	-10.6	-9.2	17.59
53.25	1778.76	-3.3	2.4	3.7	17.59
54.25	1772.17	-7.7	-10.2	-8.9	17.59
55.25	1765.88	-7.7	-10.6	-9.3	17.59
56.25	1761.21	-9.4	-10.7	-9.4	17.59
57.25	1755.05	-11.2	-10.0	-8.7	17.59
58.25	1748.85	-9.9	-10.5	-9.1	17.59
59.25	1742.90	-9.7	-10.3	-9.0	17.59
60.25	1737.34	-11.0	-10.4	-9.1	17.59
61.25	1731.23	-10.1	-10.7	-9.3	17.59
62.25	1724.91	-7.8	-5.3	-3.9	17.59
63.25	1719.33	-9.3	-8.9	-7.6	17.59
64.25	1713.57	-10.3	-11.4	-10.1	17.59
65.25	1706.78	-11.8	-10.4	-9.1	17.59
66.25	1700.62	-12.1	-10.5	-9.2	17.59
67.25	1693.80	-10.8	-10.2	-8.9	17.59
68.25	1686.91	-13.0	-11.7	-10.3	17.59
69.25	1680.34	-13.0	-13.3	-12.0	17.59
70.25	1673.21	-13.1	-13.1	-11.8	17.59
71.25	1666.43	-16.6	-16.4	-15.0	17.59
72.25	1660.12	-17.0	-14.2	-12.9	17.59
73.25	1653.34	-17.4	-16.2	-14.9	17.59
74.25	1648.01	-15.6	-16.3	-15.0	17.59
75.25	1641.70	-20.3	-20.9	-19.6	17.59
76.25	1635.83	-11.7	-14.1	-12.8	17.59

Table E2: Carbonate oxygen isotope composition ($\delta^{18}\text{O}$, $\delta^{13}\text{C}$) values (‰ VPDB) including carbonate-inferred pond water $\delta^{18}\text{O}$ (‰ VSMOW) and pond water temperature used in Equation 1 to calculate pond water $\delta^{18}\text{O}$ for the SK 26 sediment core.

Mid point depth (cm)	CRS dates	^{13}C (‰ VPDB)	$^{18}\text{O}_{\text{carb}}$ (‰ VPDB)	$^{18}\text{O}_{\text{pw}}$ (‰ VSMOW)	Water temperature used to calculate $\delta^{18}\text{O}_{\text{pw}}$
0.25	2022.60	-13.9	-18.4	-17.0	17.87
1.25	2022.35	-10.7	-17.1	-15.7	17.87
2.25	2021.95	-10.4	-17.0	-15.7	17.87
3.25	2020.73	-10.7	-16.8	-15.5	17.87
4.25	2019.15	-11.1	-15.9	-14.6	17.87
5.25	2017.49	-13.3	-17.0	-15.7	17.87
6.25	2015.73	-11.9	-16.6	-15.3	17.87
7.25	2013.81	-13.1	-15.9	-14.6	17.87
8.25	2011.66	-13.0	-16.6	-15.3	17.87
9.25	2009.24	-12.7	-17.2	-15.9	17.87
10.25	2006.91	-13.9	-17.0	-15.7	17.87
11.25	2004.61	-14.7	-17.0	-15.6	17.87
12.25	2001.93	-17.0	-17.7	-16.4	17.87
13.25	1999.31	-14.6	-17.3	-16.0	17.87
14.25	1996.35	-18.5	-18.8	-17.5	17.87
15.25	1993.37	-15.3	-18.6	-17.3	17.87
16.25	1991.15	-20.6	-20.2	-18.9	17.87

17.25	1989.33	-16.5	-16.0	-14.7	17.87
18.25	1986.23	-16.3	-18.1	-16.8	17.87
19.25	1982.77	-15.4	-16.1	-14.8	17.87
20.25	1979.43	-21.8	-20.3	-19.0	17.87
21.25	1975.79	-24.9	-20.7	-19.4	17.87
22.25	1973.39	-26.0	-22.5	-21.2	17.87
23.25	1972.68	-28.5	-22.5	-21.1	17.87
24.25	1971.88	-26.5	-22.3	-21.0	17.87
25.25	1970.76	-30.1	-21.7	-20.4	17.87
26.25	1968.92	-29.4	-21.7	-20.4	17.87
27.25	1966.40	-30.1	-21.8	-20.5	17.87
28.25	1965.65	-30.0	-22.4	-21.1	17.87
29.25	1964.07	-30.1	-21.7	-20.4	17.87
30.25	1962.45	-30.2	-23.2	-21.9	17.87
31.25	1960.14	-30.5	-23.1	-21.8	17.87
32.25	1955.63	-30.2	-22.6	-21.3	17.87
33.25	1949.06	-30.4	-22.6	-21.3	17.87
34.25	1944.03	-30.1	-22.9	-21.6	17.87
35.25	1940.37	-30.1	-22.7	-21.4	17.87
36.25	1935.12	-28.8	-22.5	-21.1	17.87
37.25	1925.87	-29.6	-23.1	-21.7	17.87
38.25	1921.26	-29.7	-23.6	-22.3	17.87
39.25	1916.89	-29.5	-23.7	-22.4	17.87
40.25	1912.50	-29.5	-23.9	-22.5	17.87
41.25	1907.61	-29.8	-23.3	-22.0	17.87
42.25	1903.04	-29.6	-23.5	-22.2	17.87
43.25	1898.14	-29.3	-23.3	-22.0	17.87
44.25	1893.12	-29.7	-23.5	-22.2	17.87
45.25	1888.33	-29.4	-23.4	-22.1	17.87
46.25	1883.04	-29.5	-25.0	-23.7	17.87
47.25	1878.53	-29.6	-24.4	-23.1	17.87
48.25	1873.61	-29.7	-24.7	-23.4	17.87
49.25	1868.62	-29.6	-24.2	-22.9	17.87
50.25	1863.41	-29.2	-24.3	-23.0	17.87
51.25	1858.06	-29.5	-25.2	-23.9	17.87
52.25	1852.36	-29.9	-24.6	-23.3	17.87
53.25	1846.95	-29.5	-24.9	-23.6	17.87
54.25	1840.77	-29.6	-24.9	-23.6	17.87
55.25	1834.82	-29.3	-24.1	-22.7	17.87
56.25	1828.76	-28.7	-24.2	-22.9	17.87
57.25	1822.16	-29.1	-24.0	-22.7	17.87
58.25	1815.91	-29.2	-24.5	-23.2	17.87
59.25	1810.27	-29.3	-23.8	-22.5	17.87
60.25	1804.30	-29.0	-25.1	-23.8	17.87
61.25	1798.16	-29.3	-25.0	-23.7	17.87
62.25	1792.42	-29.3	-25.2	-23.9	17.87
63.25	1786.74	-29.1	-25.4	-24.1	17.87
64.25	1780.69	-29.4	-25.2	-23.9	17.87
65.25	1774.79	-29.4	-25.4	-24.0	17.87
66.25	1768.98	-29.2	-25.4	-24.1	17.87
67.25	1762.07	-29.0	-24.7	-23.4	17.87
68.25	1755.06	-29.0	-24.3	-23.0	17.87
69.25	1748.47	-28.6	-24.7	-23.4	17.87
70.25	1741.61	-29.1	-26.2	-24.9	17.87

Figure E1: Graphs showing stratigraphic variation of carbonate-inferred pond water $\delta^{18}\text{O}$ (‰ VSMOW), carbonate $\delta^{13}\text{C}$ (‰ VPDB), and ^{226}Ra activity (Bq/g) for the sediment core of SK 26. Also shown is red dashed line at ~1980 CE to highlight notable shift in data.

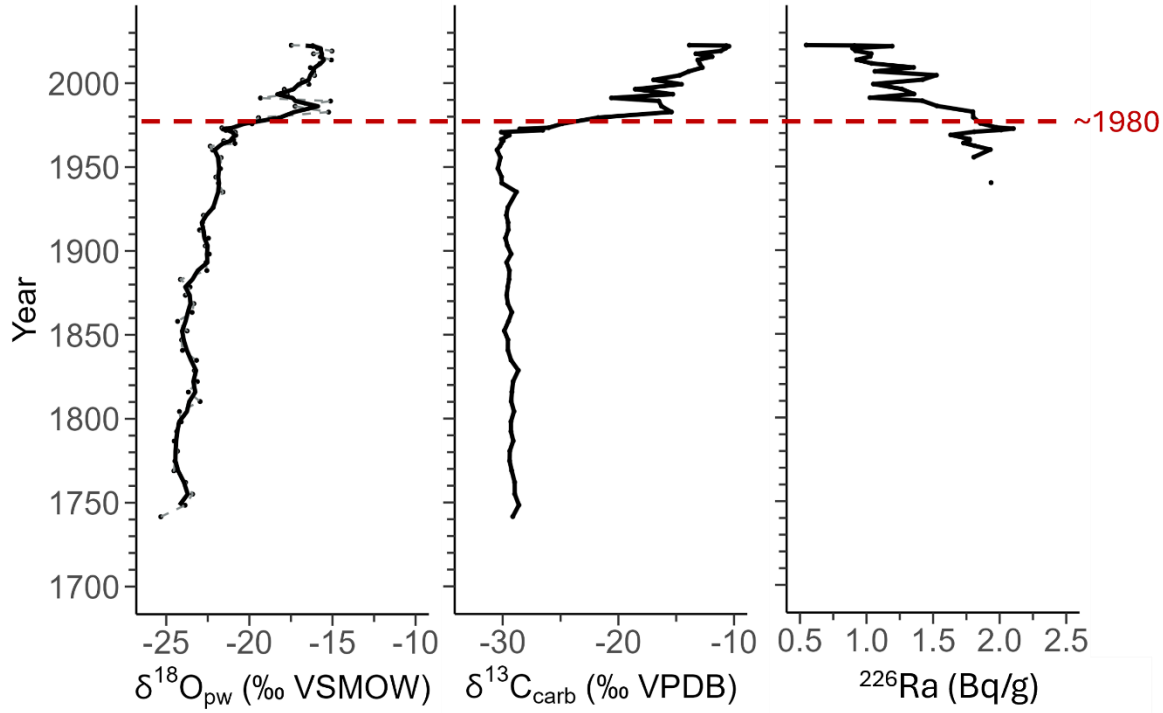


Table E3: Carbonate oxygen isotope composition ($\delta^{18}\text{O}$, $\delta^{13}\text{C}$) values (‰ VPDB) including carbonate-inferred pond water $\delta^{18}\text{O}$ (‰ VSMOW) and pond water temperature used in Equation 1 to calculate pond water $\delta^{18}\text{O}$ for the SK 58 sediment core.

Mid point depth (cm)	CRS dates	^{13}C (‰ VPDB)	$^{18}\text{O}_{\text{carb}}$ (‰ VPDB)	$^{18}\text{O}_{\text{pw}}$ (‰ VSMOW)	Water temperature used to calculate $\delta^{18}\text{O}_{\text{pw}}$
0.25	2022.49	-3.5	-15.7	-14.4	20.09
1.25	2022.28	-4.2	-18.7	-17.4	20.09
2.25	2021.18	-3.2	-15.4	-14.1	20.09
3.25	2018.13	-3.0	-14.0	-12.7	20.09
4.25	2013.38	-3.2	-13.2	-11.9	20.09
5.25	2007.77	-3.6	-12.9	-11.5	20.09
6.25	1999.88	-3.6	-12.8	-11.5	20.09
7.25	1990.66	-2.7	-13.3	-11.9	20.09
8.25	1981.53	-3.2	-13.5	-12.2	20.09
9.25	1973.88	-2.6	-14.3	-13.0	20.09
10.25	1962.72	-2.5	-13.7	-12.4	20.09
11.25	1953.59	-3.0	-13.4	-12.1	20.09
12.25	1942.39	-3.2	-13.4	-12.1	20.09
13.25	1931.10	-3.1	-13.0	-11.7	20.09
14.25	1922.35	-3.7	-13.6	-12.2	20.09
15.25	1908.81	-3.7	-13.5	-12.1	20.09
16.25	1896.17	-3.4	-13.5	-12.2	20.09
17.25	1882.45	-3.8	-13.5	-12.1	20.09

18.25	1866.26	-3.7	-12.9	-11.6	20.09
19.25	1852.77	-4.1	-13.0	-11.7	20.09
20.25	1835.19	-3.7	-13.2	-11.9	20.09
21.25	1818.52	-3.7	-13.1	-11.8	20.09
22.25	1807.09	-3.8	-13.4	-12.0	20.09
23.25	1787.99	-3.7	-12.5	-11.2	20.09
24.25	1769.25	-4.0	-13.2	-11.9	20.09
25.25	1748.90	-4.1	-13.1	-11.8	20.09
26.25	1730.59	-4.5	-13.2	-11.9	20.09
27.25	1711.98	-4.9	-13.7	-12.4	20.09
28.25	1692.35	-5.0	-13.2	-11.9	20.09
29.25	1673.47	-5.0	-13.7	-12.4	20.09
30.25	1652.27	-3.7	-12.6	-11.2	20.09
31.25	1633.93	-3.5	-12.6	-11.2	20.09

Appendix F – Sediment core organic carbon and nitrogen elemental and isotope composition

Table F1: Organic carbon and nitrogen elemental and isotope composition for the sediment core from SK 58.

Depth interval (cm)	$\delta^{13}\text{C}$ (VPDB \pm 0.2‰)	$\delta^{15}\text{N}$ (AIR \pm 0.3‰)	Total Carbon (%)	Total Nitrogen (%)	C/N
0-0.5	-28.65	1.77	34.76	3.77	9.73
0.5-1.0	-29.47	1.33	40.11	4.15	9.62
1.0-1.5	-29.55	0.91	41.61	4.26	9.69
1.5-2.0	-27.87	1.66	45.86	4.93	9.40
2.0-2.5	-27.27	1.81	47.23	4.94	9.55
2.5-3.0	-26.80	2.02	48.56	5.00	9.69
3.0-3.5	-26.81	1.88	48.60	4.96	9.79
3.5-4.0	-26.71	1.93	46.85	4.86	9.63
4.0-4.5	-26.95	1.78	47.31	4.62	10.24
4.5-5.0	-26.78	1.91	50.33	4.91	10.24
5.0-5.5	-26.76	1.89	48.61	5.20	9.34
5.5-6.0	-26.98	1.78	44.96	4.51	9.96
6.0-6.5	-27.00	2.06	49.43	4.19	10.73
6.5-7.0	-26.17	1.93	49.15	5.20	9.44
7.0-7.5	-26.69	2.27	50.94	5.43	9.38
7.5-8.0	-26.60	1.89	50.05	4.94	10.14
8.0-8.5	-26.37	1.89	50.18	5.09	9.86
8.5-9.0	-26.51	1.57	50.32	5.12	9.83
9.0-9.5	-26.22	1.79	49.94	5.06	9.86
9.5-10.0	-26.52	1.43	49.72	5.01	9.92
10.0-10.5	-26.47	1.39	50.21	5.11	9.83
10.5-11.0	-26.27	1.72	49.16	5.01	9.80
11.0-11.5	-26.62	1.34	51.96	5.25	10.26
11.5-12.0	-26.76	0.81	52.44	5.32	9.86
12.0-12.5	-26.78	0.49	51.57	5.22	9.88
12.5-13.0	-26.84	0.48	51.83	5.19	9.98
13.0-13.5	-26.90	0.58	50.90	5.05	10.40
13.5-14.0	-27.07	0.40	50.87	5.12	9.94
14.0-14.5	-27.34	0.49	52.07	5.27	9.88
14.5-15.0	-27.08	0.54	51.09	5.22	9.79
15.0-15.5	-27.21	0.80	52.79	4.94	11.31
15.5-16.0	-27.57	0.33	51.56	5.31	9.71
16.0-16.5	-27.22	0.54	50.97	5.14	9.92
16.5-17.0	-27.01	0.47	52.02	5.08	10.24
17.0-17.5	-27.33	0.45	51.30	5.22	9.83
17.5-18.0	-27.10	0.63	51.15	5.19	9.85
18.0-18.5	-27.39	0.27	51.25	5.22	9.81
18.5-19.0	-27.62	0.33	51.94	5.32	9.76
19.0-19.5	-27.24	0.67	51.19	5.10	10.03
19.5-20.0	-27.02	0.89	51.50	5.08	10.14
20.0-20.5	-26.88	0.81	50.46	5.11	9.87
20.5-21.0	-26.94	0.94	51.06	5.03	10.15
21.0-21.5	-27.02	0.78	49.90	5.13	9.72
21.5-22.0	-26.73	0.96	50.78	4.97	10.21
22.0-22.5	-26.96	0.79	51.24	4.96	10.33
22.5-23.0	-25.62	0.87	50.03	2.99	13.24
23.0-23.5	-26.92	0.87	48.94	4.80	10.20

23.5-24.0	-27.38	0.64	42.28	4.30	9.84
24.0-24.5	-27.38	0.71	50.47	4.86	10.39
24.5-25.0	-27.41	0.62	51.32	5.01	10.24
25.0-25.5	-27.29	0.68	49.67	4.78	10.39
25.5-26.0	-26.99	0.89	49.76	4.83	10.30
26.0-26.5	-26.78	0.97	45.38	4.49	10.11
26.5-27.0	-26.58	0.98	49.79	4.87	10.23
27.0-27.5	-26.46	1.10	50.57	4.90	10.33
27.5-28.0	-26.68	1.09	50.54	4.90	10.32
28.0-28.5	-26.92	1.05	50.35	4.81	10.47
28.5-29.0	-27.12	0.93	50.62	4.78	10.58
29.0-29.5	-26.77	0.96	50.50	4.80	10.52
29.5-30.0	-27.18	0.87	27.43	2.92	9.40

Appendix G – Sediment core dominant diatom species enumeration

Table G1: Most dominant diatom (>10%) species expressed as a percentage enumerated for the sediment core of SK 31.

Year	Mid point depth (cm)	Nitzschia amphibia	Mastogloia smithii	Navicula cryptocephala	Gomphonema angustum	Navicula oblonga
2020	2.75	45.7	14.0	9.3	0.3	3.0
2007	7.25	38.7	25.9	5.2	3.3	4.9
1993	11.75	34.0	16.3	16.7	3.0	2.0
1985	15.25	47.0	19.3	9.3	2.3	1.3
1962	19.25	31.0	14.7	16.7	3.3	1.3
1938	23.25	26.6	28.3	8.2	2.0	7.2
1906	27.75	22.1	19.8	22.8	2.6	3.3
1882	31.25	21.7	20.0	15.7	5.3	2.7
1861	35.25	19.3	15.3	12.0	9.6	5.6
1842	39.25	12.3	20.3	9.6	20.3	7.0
1823	43.75	11.0	16.2	13.6	11.4	12.3
1809	47.25	19.2	20.9	14.6	8.3	11.6
1788	51.25	13.0	31.0	18.0	3.0	14.3
1764	55.25	9.6	26.6	26.9	1.0	8.6
1741	59.25	13.0	23.0	26.7	2.0	7.7
1718	63.25	18.3	46.7	9.0	0.7	5.0
1692	67.25	16.3	34.7	6.3	1.3	2.7
1661	71.75	9.0	37.5	12.4	2.7	16.4
1637	75.75	10.7	33.3	6.7	3.3	13.7

Table G2: Most dominant (>10%) diatom species expressed as a percentage enumerated for the sediment core of SK 26.

Age	Mid point depth (cm)	Mastogloia smithii	Navicula oblonga	Nitzschia amphibia	Fragilaria construens var. construens	Fragilaria construens var. venter	Fragilaria girdle view
2021	2.75	5.3	7.0	5.0	6.0	15.0	55.0
2014	6.75	4.1	3.8	7.6	12.0	25.1	39.9
2007	10.25	3.6	5.6	5.6	10.6	7.9	53.8
2003	11.75	0.7	3.7	5.3	19.0	40.7	21.3
1997	13.75	2.6	2.3	4.9	23.6	40.3	19.7
1992	15.75	1.0	2.3	9.3	24.3	34.0	19.7
1990	16.75	3.3	1.7	6.6	20.9	46.8	14.0
1987	17.75	1.3	3.0	5.7	21.0	35.7	17.3
1984	18.75	1.3	3.0	3.3	18.7	23.3	41.7
1980	20.25	1.6	1.0	4.6	17.7	46.9	19.0
1974	21.75	0.7	0.7	1.3	6.7	25.0	53.0
1972	23.75	1.3	2.7	4.3	9.3	22.0	48.3
1967	26.75	1.3	0.7	1.0	11.0	50.0	25.7
1959	30.75	1.7	0.7	1.0	10.0	38.9	40.2

Table G3: Most dominant (>10%) diatom species expressed as a percentage enumerated for the sediment core of SK 58.

Year	Mid point depth (cm)	Nitzschia amphibia	Navicula oblonga	Mastogloia smithii
2022	1.25	1.9	0.0	26.9
2020	2.25	9.2	0.3	9.9
2011	4.25	8.8	0.7	17.1
1996	6.25	4.3	2.0	5.6
1976	8.25	5.9	7.9	9.2
1958	10.25	8.4	14.1	7.4
1938	12.25	14.0	16.7	7.7
1914	14.25	17.4	24.2	11.9